

Department of Electrical & Computer Engineering
Digital Image & Signal Processing Laboratory

Characterization of Epileptic Activity Based on Integrated Functional Network from MEG Data on a Realistic Head Model

Diploma Thesis

by

Vasileios S. Dimakopoulos

A THESIS SUBMITTED IN PARTIAL FULLFILLMENT OF THE
REQUIREMENTS FOR THE DIPLOMA DEGREE OF
ELECTRICAL & COMPUTER ENGINEERING

THESIS COMMITTEE:

Professor Zervakis Michalis, *Thesis Supervisor*
Professor Liavas Athanasios
Professor Wolters Carsten, *University of Münster*

Chania, Greece, March 2019

© Copyright by Vasileios S. Dimakopoulos 2018
All rights reserved

No part of this publication may be reproduced, distributed, or transmitted in any form or by any means, including photocopying, recording, or other electronic or mechanical methods, without the prior written permission of the publisher, except in the case of brief quotations embodied in critical reviews and certain other noncommercial uses permitted by copyright law.

Abstract

Epilepsy is a complex brain disorder which affects millions of people worldwide. A significant percentage of the cases is described by drug resistance increasing this way the need for exploiting different approaches for the treatment. Such techniques incorporate invasive methods to resect the cortical tissues that are responsible for epileptogenesis (epileptic seizures). However, these approaches require spatial accuracy in order to preserve every brain functionality. An important step prior to the operative treatment is the presurgical evaluation which aims in accurate detection of the epileptic focus utilizing the Electrocorticography (ECoG).

This thesis addresses the source localization/reconstruction problem from interictal epileptic spikes to improve presurgical epilepsy diagnosis with the ultimate goal to save patients from multiple repetitions of these invasive techniques.. Specifically, it aims to detect the epileptic activity at source level as derived from combined electroencephalography (EEG) and magnetoencephalography (MEG) Data on a realistic head model. The source reconstruction problem is focusing on disentangling the brain sources from the activity recorded non-invasively by the sensors of the neuroimaging modalities by simulating brain anatomy and conductivities. The proposed approach includes unsupervised learning methods to sort epileptic activity using adaptive features for the spikes and comparison of algorithms such as sLORETA, eLORETA and Minimum Norm Estimate (MNE) for solving the localization problem.

In the clustering model of our method we consider the problem of describing the interictal spikes with adequate features, which could be used for sorting purposes. Henceforth, we build a grid from neurons to assign each interictal spike with Self Organized Map (SOM). The topology of the spike assignment is used as a-priori knowledge for a K-Means algorithm to eliminate random initializations. In the source reconstruction, we solve the forward problem using a 6-compartment head model and compute leadfields with Finite Element Method (FEM). The inverse solution of the problem is being performed mainly with the sLORETA algorithm but MNE and other inverse methods were also evaluated utilizing the FEM head-model. The reconstruction approach takes into consideration every cluster of spikes and every combination of them both from single modality or from a Combined EEG and MEG approach.

Acknowledgements

First and foremost, I would like to thank my supervisor Prof. Zervakis Michalis for his patient guidance throughout this work with his invaluable advice. Furthermore, I would like to thank Marios Antonakakis, PhD candidate at University of Münster, for his contribution in the technical part based on his experience in the field of Computational Neuroscience.

Moreover, I would like to express the deepest appreciation to Prof. Wolters for offering me the possibility of joining his group for a 3-month internship enriching thus my background both in data acquisition and data analysis aspects in the source localization problem. Additionally, the financial support of John S. Latsis Public Benefit Foundation with scholarships, through the entire period of my studies is gratefully acknowledged.

Last but not least, I would like to express my deepest gratitude to my family for supporting me from the very first beginning of my academic steps and especially my mother and my father Aristeia and Stylianos but also my sister Eleutheria for their consistent trust in my abilities. It would be also omission not to mention my aunt Dionysia for her endless affection especially in difficult situations and my friends for standing besides me throughout the studies.

To my father

This thesis is dedicated to the fond memory of my father who passed away during my studies but throughout his life didn't stop believing in me.

Contents

Contents	vi
List of Figures	ix
1 Introduction	1
1.1 Computational Neuroscience and Epilepsy Studies	1
1.2 Related - Previous Work	2
1.3 Aim, Contribution and Innovations of this research work	3
1.4 Thesis Outline	4
2 Brain Physiology and Epilepsy	6
2.1 Central Nervous System	6
2.1.1 Synaptic Transmission	9
2.2 Brain Structure	10
2.2.1 Brain Regions & Components	10
2.2.2 Brain Lobes	12
2.2.3 Brain Compartments	14
2.3 Epilepsy and Different Types	15
2.4 Brain and Epileptic Activity	16
2.4.1 Spikes and Epileptic Focus	17
2.4.2 Epilepsy Diagnosis	18
2.4.3 Epilepsy Treatment	19
3 Magnetoencephalography - Electroencephalography	20
3.1 Introduction	20
3.2 Brain Signal Recording - Action Potentials/Magnetic Fields	22
3.2.1 Signals Physiological Basis	23
3.2.2 Evoked/Event Related Potentials and Fields	25
3.3 EEG Recording System	26
3.4 MEG Recording System	28
3.5 Interferences in the recording of the brain signals	31
3.5.1 Physiological/Internal Artifacts	31
3.5.2 External and System Artifacts	32
3.6 Differences between EEG and MEG	33
3.7 EEG, MEG and Epilepsy	33

3.8	Combined EEG and MEG	34
4	Data Preprocessing	35
4.1	Recording System and Patient	35
4.2	Data Processing with FieldTrip	35
4.3	Downsampling and Filtering	37
4.4	Correcting noisy channels' signal	40
4.5	Component Analysis	41
4.5.1	Principal Component Analysis	42
4.5.2	Blind Source Separation	44
4.5.3	Independent Component Analysis	46
4.5.4	Assumptions and Ambiguities of ICA	46
4.5.5	Mathematical Formulation of ICA	47
4.5.6	Extended Infomax Algorithm	50
4.6	Artifact Detection	51
4.6.1	Visual Inspection of Components	53
4.6.2	Kurtosis, Entropy and Thresholding	56
4.6.3	Global and Local Correlation Approach	58
4.7	Artifact Rejection and Correction	59
4.7.1	Empirical Mode Decomposition Algorithm	59
5	Clustering of Epileptic Activity	61
5.1	Spike Detection and Marking of Spike Activity	61
5.2	Clustering of Epileptic Spikes	62
5.3	Feature Extraction from Interictal Spikes	63
5.4	Self Organized Map Algorithm - SOM	66
5.5	K - Means Algorithm	68
5.6	Combining SOM and K - Means	71
5.7	Clustering and Source Localization	76
6	Source Localization	77
6.1	Forward and Inverse Problem	77
6.2	Forward Problem	78
6.2.1	Source Model	79
6.2.2	Head Model	80
6.2.3	Maxwell Equations	81
6.2.4	Poisson Equation	82
6.2.5	Solving Forward Problem	83
6.3	Inverse Problem	87
6.3.1	Assumptions of the Inverse Problem	88
6.3.2	Mathematical Formulation	88
6.4	Algorithms for the Inverse Solution	88
6.4.1	Dipole Scanning	90
6.4.2	Beamforming	90
6.4.3	Minimum Norm Estimate (MNE)	90
6.4.4	sLORETA	91
6.4.5	eLORETA	92

CONTENTS

6.5	Source Localization on Clustered Data	92
6.6	Source Localization and Combined EEG/MEG	102
7	Conclusions	105
7.1	Conclusions	105
7.2	Future Work	105
	Bibliography	106

List of Figures

2.1	CNS and PNS interaction	6
2.2	Nerve Cell Structure	7
2.3	Types of Glial Cells	8
2.4	Transmission at a chemical synapse	9
2.5	The three regions of the brain	10
2.6	Lateral View of Brain	11
2.7	Brain Components	11
2.8	The brain lobes	13
2.9	Meninges protective layers	14
2.10	Epileptic spikes states, Epileptic focus by interictal spikes	17
3.1	Action Potential morphology	23
3.2	EEG/MEG Signals Origin	24
3.3	Post-Synaptic potentials	25
3.4	The International 10-20 electrode placement system	27
3.5	EEG Setup Block Diagram	27
3.6	Magnetic Fields Strength Comparison	28
3.7	Block Diagram of a standard MEG system	29
3.8	Magnetically Shielded Room	30
3.9	Different Types of artifacts in EEG	32
4.1	FieldTrip Structures Example	36
4.2	Flowchart of Preprocessing Pipeline	36
4.3	Time Series of Random EEG and MEG channels	37
4.4	Time Series of EEG and MEG channels after Downsampling	38
4.5	Energy Spectrum Density of EEG and MEG channels before/after Downsampling	39
4.6	Filters Chosen for Data Preprocessing	39
4.7	Energy Spectrum Density Before/After Filtering of a random EEG channel visualized in Logarithmic scale	40
4.8	User Interface Window in Fieldtrip for Marking Bad/Noisy Sensors	41
4.9	Time segment of EEG Channels before/after noisy channels reconstruction	41
4.10	Visual inspection of EEG before/ after reconstruction of bad channels in the whole time range	41
4.11	BSS Network	45

4.12	BSS Standard Flow	46
4.13	PCA maximum variance directions and ICA independent components	47
4.14	Kurtosis values and non-gaussianity	50
4.15	PCA on EEG/MEG data based on PUI criterion at 95%	52
4.16	Artifact Detection Plan	53
4.17	Topographic Distributions of Independent Components at 4th state run recording	53
4.18	Suspicious EEG Independent Components	54
4.19	Suspicious MEG Independent Components	55
4.20	Possible Ocular Artifacts Time Waveform	55
4.21	Possible Cardiac Artifact Time Waveform	55
4.22	Artifact Metrics for MEG ICs that declare non-brain activity	56
4.23	Application of Metrics Approach faulty case	57
4.24	Global Cross Correlation Approach	58
4.25	Empirical Mode Decomposition Process	59
4.26	Intrinsic Mode Functions of an Ocular Artifact in a decreasing frequency order	60
4.27	Signal/Spectrum of a channel before and after Ocular Artifacts Correction . . .	60
5.1	Typical Spike Waveforms	62
5.2	Clustering Step Flowchart	63
5.3	The Haar Wavelet	64
5.4	Wavelet Packet Decomposition	65
5.5	SOM Grid and Models of Grid neurons	67
5.6	SOM Output Visualized	68
5.7	Elbow Point	70
5.8	Silhouette Plot for a sample dataset example	71
5.9	2-Stage Clustering Approach	72
5.10	Neural Network Toolbox and SOM Architecture	72
5.11	8x8 SOM clustering	73
5.12	SOM Weight Adaptation Plot	73
5.13	Weights Distribution for each Feature	74
5.14	K-Means clustering for different K's and distance metrics	74
5.15	Silhouette index for two sample K's	75
5.16	Clustering of spikes after the 2-level approach	75
5.17	Average of spikes in each EEG & MEG clusters	76
6.1	Forward and Inverse Problem Correlation	77
6.2	Equivalent Current Dipole	78
6.3	Source Model as dipole layer and single dipole	80
6.4	The progress of head-modelling	81
6.5	BEM headmodel geometry tessellation	85
6.6	FEM model for the forward problem	86
6.7	Forward Problem using the FieldTrip Toolbox	92
6.8	Brain Segmentation and Meshing	93
6.9	Minimum Norm Estimate for MEG clusters	94
6.10	Minimum Norm Estimate for EEG clusters	94
6.11	Minimum Norm Estimate for MEG clusters visualized in the Brain Mesh . . .	94
6.12	FEM headmodel various meshes (top: scalp, bottom: gray and white matter)	95

6.13 Single Dipole Scan for EEG/MEG clusters	96
6.14 MNE on EEG Cluster 1	97
6.15 MNE on EEG Cluster 2	97
6.16 MNE on EEG Cluster 3	97
6.17 MNE on MEG Clusters	98
6.18 sLORETA on EEG Clusters (a): visualized in white matter, (b): visualized in gray matter	99
6.19 sLORETA on EEG cluster 2 - Propagation Phenomenon	99
6.20 sLORETA on MEG Clusters	100
6.21 eLORETA on EEG Clusters	100
6.22 eLORETA on MEG Clusters	100
6.23 Beamforming on EEG clusters top row: source space visualization, bottom row: visualization on white matter mesh	101
6.24 Beamforming on MEG clusters top row: source space visualization, bottom row: visualization on white matter mesh	101
6.25 Signal topographies orthogonality for EEG & MEG clusters	103
6.26 sLORETA EMEG Source Reconstruction for 2nd EEG and 2nd MEG cluster for 6 different time instances	103
6.27 EMEG reconstruction leads to FCDs detection	104

Introduction

1.1 Computational Neuroscience and Epilepsy Studies

Computational Neuroscience is a rapidly evolving field with methods and techniques that allow us to understand and model the brain and its behaviour [1],[2]. An aspect in which this field is introducing novelties is the experiments design but also the interpretation of them by developing new hypotheses which could be rephrased in mathematical terms. Mathematical modelling is an essential tool for incorporating the complexity of neurobiological systems and the interaction with other elements. For this reason, these models are able to capture features of a biological system at multiple spatial and temporal scales, thereby offering the opportunity to establish for instance, links between brain networks involved in epilepsy. In general, computational neuroscience can be applied in many ways incorporating theories and approaches from electrical engineering, computer science and physics to understand how the central nervous system is processing and transferring the information.

During the last decades technological proliferation have created new gates for brain research. The neuroimaging methods which are still evolving permit us to visualize brain while in action identifying thus the regions associated to various human senses or regions correlated to epileptogenesis [3]. However, it is extremely difficult to interpret brain behaviour and make reasonable assumptions without considering brain physiology. The latter is highly demonstrated by the vast amount of recent publications which simulate brain physiology with mathematical models [4],[5],[6] to prove the neurophysiological basis of signals. The question which could arise is how these models improve epilepsy studies.

Epilepsy as a neurological disease has complex characteristics but is mainly described by seizures and abnormal brain behaviour. However, seizure symptoms could vary widely leading in many types of epilepsy requiring thus different approaches for treatment in each case. Many patients could be exempted from seizures with medication using the so - called Anti-Epileptic Drugs (AED). On the other side, a significant percentage of patients suffer from pharmaco - resistant epilepsy, refractory epilepsy, in which the use of AEDs is not advisable. Henceforth, the modern era is marked by an expansion of interest in understanding the mechanisms underlying these forms of drug-resistant seizures. Computational models aid in unravelling the complexity of epileptic activity by means of contribution in prediction, diagnosis and treatment. They considered as an efficient way to structure the neurobiological knowledge to interpret experimental findings. For instance by modelling networks of interconnected neurons it is feasible to study mechanisms and to simulate activities at the cell level [7].

For epilepsy case studies computational models could help in overcoming issues related to neuronal processes [8]. Specifically the majority of mechanisms at cellular, tissular and regional level are nonlinear and identifying their effects could be crucial for diagnosis or treatment. Furthermore, recording brain activity is only reflecting partially the neuronal responses since potentials in cortex don't encapsulate the generation of activity in main neuronal cells. Moreover, observations and recordings are over a limited time window which lead to make decisions from sparse information. Last but not least, epileptic spikes last milliseconds compared to the seizures that could last even some minutes while the frequency of seizures among patients differs increasing thus the complexity of these phenomena [9]. The aforementioned consist typical examples of situations which computational neuroscience could resolve within an innovative framework offering accurate insight of the brain mechanisms complexity to epileptologists.

In order to exploit the potential of the computational models although, it is imperative to be accurately designed preserving the brain physiology. The brain is a complex multiscale structure both from temporal and spatial perspective. This biological system is organized into modules defined by either anatomical or functionally defined cortical regions which serve as the lever motor for the cognitive functions [10]. In the spatial domain, the brain is heterogenously comprised of cells which form columns of neurons and therefore areas and lobes. Specifically, it is composed of billions of nerve cells which transmit the electrical signals and the glial cells for shaping protective layers to support and feed the nerve cells. The main parts of the brain are Cerebellum, brain stem and Cerebrum which is made up of 4 sections known as lobes each of which is correlated to a human sense or a fundamental functionality.

The temporal scaling of the brain is corresponding to brain rhythms with varying frequencies that relate to cognitive functions. The gamma band, namely is thought to be connected with conscious perception. Another key thing to highlight is the changing pattern of neuronal connections with learning and memory through timescale plasticity [11]. Furthermore, functional and structural connectivity are changing either in short term or in long term scaling, fact which needs to be taken into consideration especially in cognitive studies. Therefore, all these complexity aspects of brain should be incorporated in computational models either with mathematical terms or physics rules.

1.2 Related - Previous Work

The research towards epilepsy and its focus has been peaked during the last years with literature contributing in source localization area offering guidelines to doctors for the removal of epileptic tissues. Among the findings of these studies it is induced that the orientation of spike currents could offer insight about the areas that are involved in a seizure. Specifically according to [12], tangential patterns indicate mesial temporal involvement while radial ones are associated with temporal or frontal neocortex. Furthermore, many studies have conducted research in source localization from a non-invasive aspect using EEG or MEG and MRI (or fMRI) and they have proved that the accuracy is significant and complements significantly the presurgical evaluation.[13], [14],[15]

Moreover, in many cases different inverse approaches are being evaluated in various epilepsy studies. Typical examples are the use of sLORETA, eLORETA, Minimum Norm Estimate, beamforming each of which is suitable based on the application. With this in mind according to [16] it is shown that Minimum Norm Estimate is efficient for detecting sources

in the surface of source space while sLORETA could estimate deeper sources accurately if there is no regularization which could lead in higher localization errors. It is also proved that spike sorting of similar spikes enhance the signal to noise ratio of spike field maps and therefore allows accurate reconstruction of sources responsible for epileptic discharges [17]. Based on spike shapes a clustering approach could discriminate a group of spikes which are associated to the irritative zone reducing the localization errors focusing on the area related to the epileptogenesis.

Equally important is the study focusing on the evaluation of using combination of modalities to improve source localization. According to [18], [19] combined EEG, MEG source localization is performing better than the single modality reconstruction fact which could lead in the detection of irritative zone and could reveal propagation pathways. Simultaneous recording of EEG and MEG is exploiting the complementary information offering an interplay between these modalities mitigating their defects and increasing the accuracy of source reconstruction at the spike onset. Coupled with this, the study [20] confirms the advantage of combined EEG,MEG for source localization and using a realistic head model from high resolution MRI a focal cortical dysplasia was detected which was correlated to the seizure symptomatology in a patient with multifocal epilepsy. In addition, MRI template models are to be avoided for source localization since they might lead in erroneous localizations. While on the other hand, using patient's MRI and incorporating to the headmodel the information from anisotropy [21], [22] and multicompartement geometry [23] reconstruction of the sources could be performed in high accuracy.

1.3 Aim, Contribution and Innovations of this research work

This thesis aims at detecting the sources which are responsible for epileptogenesis for a patient with multifocal epilepsy. These areas are connected with focal cortical dysplasias that have been discovered previously for this patient using Zoomed MRI and Combined EEG/MEG source localization [20]. However, through a clustering approach this thesis intends to improve source reconstruction achieving higher accuracy. This could be accomplished by creating groups (clusters) of interictal spikes with similar features extracted adaptively. In other words, based on either spatial (shape) and temporal (time - frequency) characteristics of spikes the discrimination of them is achieved by using a novel approach with Self Organized Maps followed by K - means algorithm.

The proposed method for preprocessing of the data is performed with band pass and notch filters while the artifacts removal is implemented by means of Component Analysis. A combination of Principal and Independent Component Analysis is decomposing the data facilitating the marking of artifacts. The artifacts are detected with calculation of metrics such as kurtosis and entropy which contain indicative values for muscular, cardiac and ocular artifacts. For artifacts correction this thesis recommends Empirical Mode Decomposition (EMD) with improved conditions. The suggested clustering of the spikes is structured with extraction of the features such as Energy, Entropy and Wavelet Coefficients taken as input for the Unsupervised Learning Algorithm - Self Organized Map (SOM). The clustering step is being completed with SOM's output fed into K - means algorithm with the aim to produce clusters of similar spikes.

The information from the cluster structure is utilized by Source Reconstruction step which considers the averaged spike data from each cluster namely the Evoked Response Potentials

(ERP) and Evoked Response Fields (ERF). The proposed approach for the source reconstruction is founded on using either a single modality approach or a combined EEG and MEG one utilizing the ERPs or ERFs either from a single EEG/MEG cluster or from their combinations. The forward problem is solved with a headmodel using Finite Element Method composed of 6 compartments according to patient's MRI. On the inverse problem this thesis aims at evaluating and comparing different algorithms such as sLORETA, eLORETA and Minimum Norm Estimate.

1.4 Thesis Outline

In **Chapter 2 - Brain Physiology and Epilepsy**, the theoretical background of brain physiology is presented. Specifically anatomical aspects of brain regions and compartments are analyzed for the better understanding of the results but also the principles of central nervous system are explained to obtain a thorough image of the brain functionality. Furthermore, the epilepsy disorder is being introduced focusing on its characteristics, different types and the effects on the brain functionality. Epilepsy diagnosis and treatment are also described in this chapter offering a direction towards grasping how this thesis could contribute to augment the medical dimension of these fields.

Chapter 3 Magnetoencephalography - Electroencephalography firstly, illustrates the principles of Magnetoencephalography (MEG) and Electroencephalography (EEG). Secondly, the origin of the brain signals is examined and how MEG and EEG recording systems are able to capture them. Thirdly, it marks the important structural points of an EEG and MEG recording system, the conditions under which a corresponding examination is being performed and the differences between those modalities. In the final section of this chapter it is explained how the combination of these modalities offers better results but also when it is advisable to record simultaneously from these modalities.

In the **Chapter 4 Data Preprocessing** the data preprocessing procedure is depicted. This step is composed of many steps of which the first is the downsampling and the filtering of the raw data. The toolbox used for data processing is briefly inspected in section 4.2. The sections following are focusing on techniques to remove noisy components of data. Specifically, noisy channels correction and component analysis are presented in details. Firstly, the metrics used for detecting noisy channels are listed. Secondly, Principal and Independent Component Analysis are described deriving their mathematical formulations while evaluating their assumptions and ambiguities. Coupled with this, the artifact detection plan is determined explaining each of the three approaches followed. To mark a component as an artifact it is required to visually inspect the topography of the signal which represents, to calculate universal metrics such as kurtosis setting adequate thresholds and to correlate either locally or globally the timeseries signal of the component with the correspondent sensors which record non brain activity. This chapter concludes with the artifact correction technique using the EMD algorithm.

Chapter 5 Clustering of Epileptic Activity, investigates the spike clustering and the methods - algorithms used to achieve it. Initially, it briefly introduces the transition from clean and preprocessed data to spike events with the marking of interictal timepoints. It proceeds with the feature extraction from epileptic spikes and the methods to select the more representative features. The analysis of Self Organized and K-means algorithms follows with thorough analysis of their steps. Both of these algorithms belong to unsupervised learning

methods for clustering and since they don't require training set it is recommended to evaluate them with performance metrics, namely the silhouette value. According to section 5.6 the combination of those two methods could profit from the spike sorting for source localization studies while the section 5.6 is describing how the source localization step could utilize this information.

In the **Chapter 6 Source Localization**, the forward and inverse problem and their solutions are defined. In more details, for the forward problem the head model anatomy and conductivities are expressed through mathematical equations for the boundary conditions and dipole moments with analytic approaches such as Boundary Element Method or Finite Element Method. Consequently, the different geometry types of headmodels are introduced while the effect of each model on the solution is shown deriving the mathematical expression with numerical analysis. The next section of this chapter contains more complex mathematical formulations since it involves the inverse problem and its solution. First of all, it formulates the assumptions and limitations of this ill posed problem while analyzing the Maxwell equations which serve critically to forge the mathematical expression of inverse problem for different headmodels. The different algorithms used for solving the inverse problem are reported extensively. The last sections of this chapter incorporate all the results from the various solutions on clustered data in either single modality or in combination of EEG and MEG. The sources located are visualized in a three dimensional representation of a headmodel and specifically on either gray or white matter.

Finally, the **Chapter 7 Conclusions** retrospects the results extracting important conclusions for the epilepsy and for related studies. At the same time it encapsulates plans and ideas for the future work to advance further this work and to complement related neuroscientific research projects. The suggestions offered are mainly focused on clustering step with the use of modern techniques of supervised learning to ameliorate the sorting performance.

Brain Physiology and Epilepsy

2.1 Central Nervous System

The nervous system is a system which regulates the activity of the other organ systems in the human body [24]. It consists of billions of neurons which are interconnected in complex networks linking this way the body to the external environment through the sensory organs. Specifically, nervous system expresses the number of neuron interconnections which distinguish an area of the brain from another, the brain from another organ or the structure of the brain among different individuals. Moreover, it is an accurate mechanism of processing and transferring information since every minute it receives millions of bits of information and decodes this amount of information to determine responses from different parts of the body.

It is divided into central and peripheral systems which consist two distinct anatomical regions. The Central Nervous System (CNS) is composed of the brain and the spinal cord. The Peripheral Nervous System (PNS) is made up of pairs of nerves that branch from the spinal cord and cranial nerves that arise from the brainstem. These nerves are responsible for carrying the information from the CNS to the rest of the body controlling thus, vital functions and human senses. To grasp the function of the nervous system one should focus on the structural components of individual nerve cells, the mechanisms utilized by these cells to produce signals but also the connections between the nerve cells and the modifications of those throughout the experience [3].

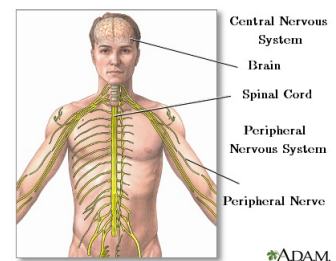


Figure 2.1: CNS and PNS interaction

There are two main classes of cells in the nervous system, namely the nerve and glial cells. The former are the information processing units while the latter are responsible for supporting and feeding the nerve cells. Generally, the neurons come in a variety of sizes and shapes but they share features to permit their intercommunication [25]. A typical neuron is comprised of four regions: **the cell body, the dendrites, the axons and the presynaptic terminals**, *figure: 2.2*. First of all, the **cell body** contains all the genetic information and therefore it is the metabolic center since it synthesizes the cell's proteins. Moreover, it enables two processes the dendrites and the axons. **Dendrites** are branches in tree shapes which are the main source of handling the incoming signals from other nerve cells. The role of dendrites is to receive the information from other cells and transfer it to the cell body for completing its processing. They correspond to the receiving information by increasing the cell's surface

area and thus improving its incoming signal capacity. The axon is a long extension of the neuron cell body which originates from a thickened area called **axon hillock**. An axon can convey electrical signals in distances ranging from the scale of *mm to m*. The signals which it transfers are known as **action potentials** and they initiated in a trigger region near the axon hillock called **initial segment** from which they reach the axon with high speeds without loss of the information.

It is important to highlight that the brain interprets the signals received not by their geometrical shapes such as form or the amplitude but by the pathway which follow. Specifically, brain analyzes the patterns of incoming signals and it conveys responses to specific parts of the body creating in this way our sensations. The nerve cells are also increasing the speed by which action potentials are conducted since the large axons are wrapped with a substance called **myelin**. In the PNS myelin forms when a **Schwann cell** wraps its membrane around an axon. The myelin is located in specific shaped sheaths which are interrupted at regular intervals by nodes known as **nodes of Ranvier** which facilitate the conveying of the signals by increasing the speed of the ions. Finally, in axon's end there is a division into zones which shape branches for contact with other nerve cells for communication. These branches are known as **synapses**. When a cell receives information it is called postsynaptic cell while the one which emits and send the corresponding signal is the presynaptic cell. The two different types of cells are separated by a narrow space. The presynaptic terminals of each cell ends in a number of knobs called terminal buttons. These knobs contain granules or vesicles that store the synaptic transmitters secreted by the nerves.

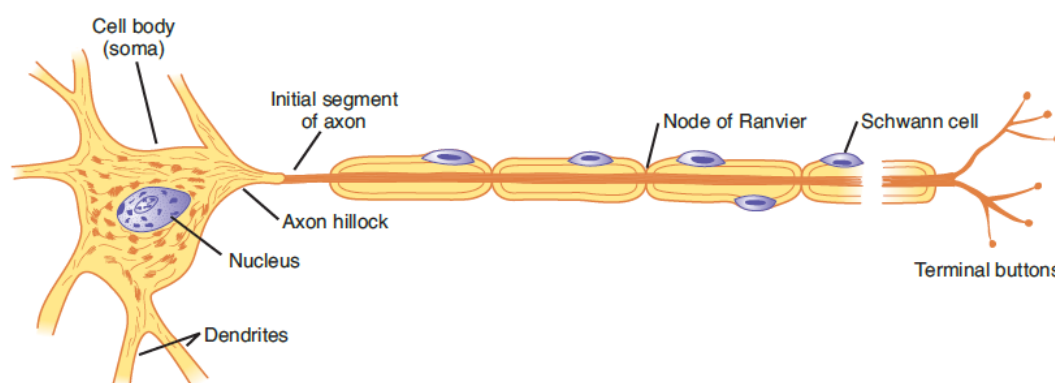


Figure 2.2: Nerve Cell Structure

Medical Physiology - Raff

Important components of the nervous system are the **glial cells**. Their name stems from the Greek word for glue. However, they don't hold the nerve cells together but they surround nerve cells either on dendrites or on cell bodies and axons. They are most commonly recognized for their role in the communication within the CNS [25]. These type of cells outnumber the neurons especially in the vertebrate CNS [3]. There are several types of glial cells which are morphologically and functionally different compared to the neurons. Coupled with this, among glial cells they exist two main types of cells, namely microglia and macroglia. **Microglia** are scavenger immune cells which are removing the debris during an injury or a disease by becoming phagocytes. Regarding **Macroglia** it could be separated into three main divisions: oligodendrocytes, Schwann cells, and astrocytes. **Oligodendrocytes and**

Schwann cells are involved in myelin formation by wrapping their membranous processes around the axon. Oligodendrocytes are found in CNS while Schwann cells form the myelin in sheaths of PNS neuron cells.

Astrocytes are star-shaped having large number of processes. It could be found either in gray or white matter either as protoplasmic astrocytes or as fibrous astrocytes respectively. Astrocytes in general, participate in four main ways of supporting the neurons. First of all, they insulate groups of neurons and synapses from each other since they separate cells. They also help in maintaining the concentration of ions and neurotransmitters by taking up K^+ and neurotransmitters. Furthermore, they form tight junctions with blood vessels called *blood brain barriers* which prevent the diffusion of e.g proteins into the cerebrospinal fluid and the brain. Last but not least, they serve as feeding mechanisms since they help surrounding neurons to nourish by releasing adequate growth factors. As an illustration of the aforementioned, glial cells are crucial for the communication within nervous system but also for supporting and feeding the neurons.

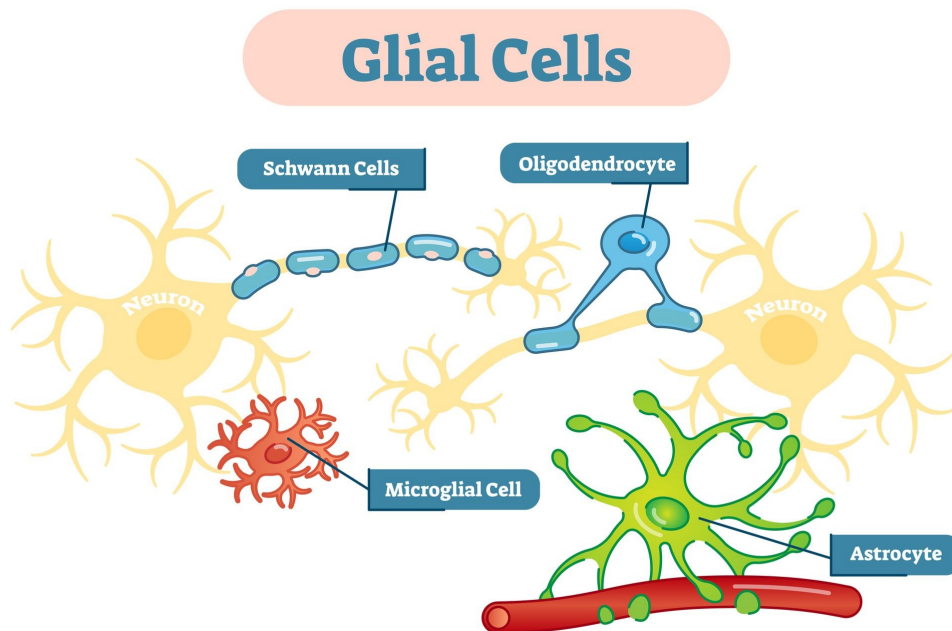


Figure 2.3: Types of Glial Cells

verywellhealth-Adriane Dellwo

After analyzing the structure of a neuron or glial cell the importance will be attached to the function of a neuron. Neuron is an information processing unit and it communicates with another cell either in an incoming or outgoing way by means of an electric impulse. A neuron may end up in a muscular cell or another type of neuron. The connections between the cells are being performed through synapses where the presynaptic cell conveys the electric signal towards synapse whereas postsynaptic cell guides the impulse away from synapse. Since this thesis is addressing neuroscientific aspects the neuron to neuron synapses will be evaluated. In the interaction between two neurons the axon terminal of presynaptic neuron comes into contact with the cell body or dendrites of the postsynaptic neuron. In this way activity from

presynaptic neuron affects the activity and the behaviour of postsynaptic neuron.

2.1.1 Synaptic Transmission

As already mentioned previously, a synapse is the area at which an electrical response is transmitted from one cell to another. Synapses are divided into two types: **electrical** and **chemical**. The latter is the common form of synapses in the nervous system where the neurons which communicate are not in complete contact but they rather separated by a small narrow gap called **synaptic cleft** (as shown in figure 2.4).

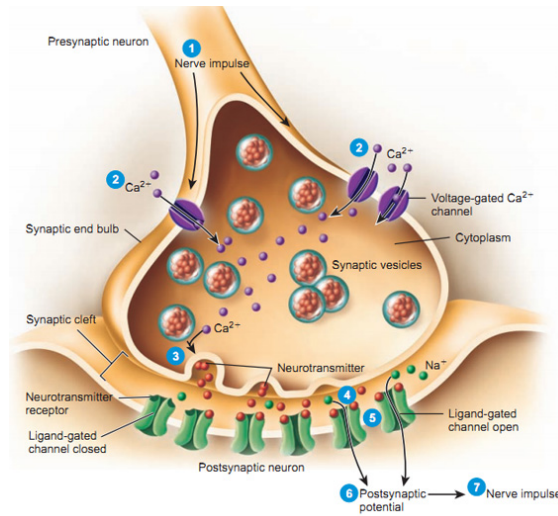


Figure 2.4: Transmission at a chemical synapse

source: Antranik

This space prevents the direct flow of the electrical impulse from one cell to another. The axon of the presynaptic neuron ends in the axon terminal known also as **synaptic knob** which stores the **synaptic vesicles** that contain the neurotransmitter. Within the synaptic knob there are several mitochondria that provide the necessary energy for the conduction of the communication and synaptic function. On the surface of the synaptic knob **voltage-gated Ca^{++} channels** could be found. These channels are open according to the following mechanism: when the action potential reached the axon terminal is accompanied by changes in voltage or depolarization which enable the gate opening. Henceforth, since calcium is highly concentrated in the external fluid (outer part of the cell) it increases the permeability of the knob allowing ions to enter the cell which force the neurotransmitter to be released from the vesicles to the synaptic cleft with the process of exocytosis. The neurotransmitters released are received by postsynaptic neuron in special receptors. By investigating the transmission mechanism it could be summarized that, since the presynaptic neuron contains the neurotransmitters and receptors are in postsynaptic side, the impulse transmission flow is unidirectional. In addition, understanding the synaptic transmission mechanism therapies for certain disorders and diseases could be advanced. For instance, in Parkinson's disease a set of neurons are using the same neurotransmitters in many places leading in problematic conditions which affect anatomic pathways. Therefore, therapies which include better signaling of the neurotransmitters are applied to counteract the abnormal transmission [26].

2.2 Brain Structure

Brain is a complex organ which controls all functions of the body, interprets information and handles emotions and senses. It is divided into several anatomical and functional regions. It is composed of billion of neurons which are connected in a unique way and the development of them is performed throughout the life of an individual. It is surrounded by many bones which together form the skull. Additionally, it is composed of many layers some of which are supportive layers to protect this valuable organ of the human body. The **brain** along with the **brainstem** and **spinal cord** consist the main functional components of CNS. First of all, the spinal cord has two major functions. It transmits nerve impulses from and to the brain while serving at the same time as a reflex center which integrates the sensory and motor pathways. Brainstem serves as lever of information flow between the cerebrum (see [2.2.1. Brain Regions](#)) and the spinal cord. It regulates fundamental body functions and it is involved with the alertness and sleep. Brainstem also forms along with clusters of neurons a control center for the respiratory, cardiovascular and other basic systems of human body. Even though brainstem is considered as one of the oldest and primitive regions of the brain and of the CNS a malfunction or disorder could be fatal [27].

2.2.1 Brain Regions & Components

The brain could be divided into three regions: **the forebrain the midbrain and hind-brain** (figure: 2.5). The forebrain consists of the **cerebrum** and the **diencephalon** (basal ganglia, thalamus, hypothalamus). The larger component of the forebrain is the cerebrum which is divided into two lateral regions, the left and the right **hemispheres**. These hemispheres consist of the **cerebral cortex** which is an outer shell made up of cell bodies giving it a gray appearance (**gray matter**). Correspondingly, in the inner area there are myelinated fiber tracts which offer a white tint to this layer which is also known as **white matter**. The midbrain along with the **pons** and **medulla oblongata** of the hindbrain compose the functional region of brainstem. Last but not least, hindbrain consists of the medulla, pons and **cerebellum**, figure 2.6, whose functions are distinct from the brainstem.

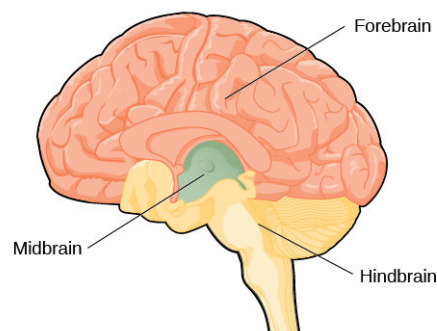


Figure 2.5: The three regions of the brain

Since brain has components which play crucial role it is important to evaluate and inspect each of these, figure: 2.7. First of all, cerebrum as mentioned above has the two hemispheres and shells which are made up of different parts of nerve cells offering different hue to each of those. However, there is also formation of cell clusters which are gray matter and

they called **subcortical nuclei**. The fiber tracts are responsible for carrying information into the cerebrum or they transfer the flow out but they also connect the two hemispheres allowing the communication between them. Although, hemispheres are separated by a long division they are connected with a bundle of fibers known as **corpus callosum**. One of its roles is to associate functional pathways by linking the two hemispheres allowing the simultaneous interaction and it permits the one part to know the processes the other is controlling.

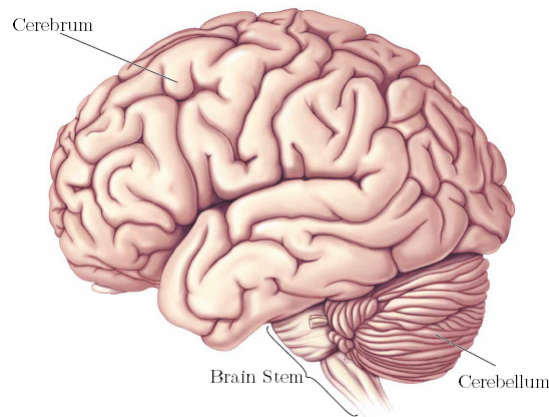


Figure 2.6: Lateral View of Brain
source: Neuroscience exploring the brain

The cerebral cortex is not a smooth area but is is mainly folded by surfaces called **gyrus**. Each gyrus is separated from another one by a **sulcus** which is a deep fissure. The functionality of these surfaces is to pack more nerve cells into a limited space.

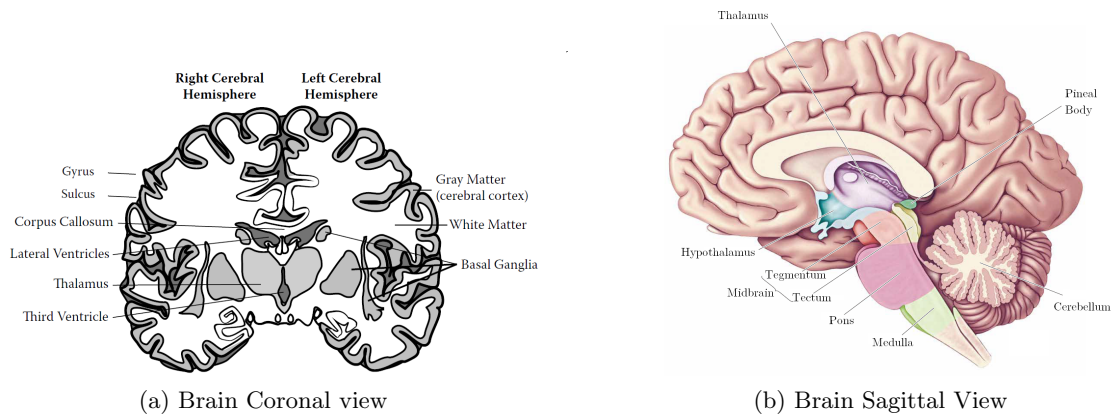


Figure 2.7: Brain Components

Source: Essential Principles of Human Physiology, Neuroscience exploring the brain

One component of utmost importance is the *thalamus*. It is located in a central point of the brain, namely between cerebrum and brainstem. It consists of a collection of nuclei and it is responsible for handling the sensory information, except the smell, before forwarding it to the cerebrum. It performs information filtering by either enhancing or preventing the gateway for this specific package of information depending its significance [24]. For example it could discard environmental sound noise while someone is sleeping.

Coupled with this *hypothalamus* plays a vital role. It is located beneath thalamus and is a tiny region but is a command center for coordinating neural and endocrine activity. Moreover, it regulates homeostasis for the body in an internal environment. Hypothalamus regulates physiological parameters, such as blood pressure and temperature, by a process which includes negative feedback mechanism. Initially, hypothalamus accesses the sensory information from the entire body. Second, it compares this information with biological options set for optimal cell function. Last step is to separate the information which deviates from these parameters and it acts by enabling behavioral and endocrine responses for resetting the parameters to the optimal point and it reestablishes the homeostasis.

Basal ganglia is also a collection of several nuclei or gray matter masses which handle the movement and some complex aspects of behaviour and motor learning. It send impulses to the brainstem, which also transmits impulses to the correspondent neurons of the spinal cord and to the thalamus and it receives back responses from the motor areas of the cerebral cortex. The components of diencephalon(hypothalamus, thalamus) along with the corpus callosum and some of the forebrain areas such as amygdala and hippocampus are part of the **limbic system**. The interconnected group of these components is associated with learning, emotional experience and behaviour but also a variety of endocrine functions.

One of the components of brain stem is the *medulla*, which extends the spinal cord including cluster of neurons that regulate the respiration, cardiovascular activity and swallowing. On the other hand the other portion of brainstem, *pons* are the relay center between cerebrum and cerebellum. Specifically, they convey information about sensation and movement between these components. The last component of brainstem, midbrain which is also the smallest one, links the components of motor system. It contains components of the auditory and visual system as well and it gives rise to pathways of muscular activity that controls eye movements.

Last but not least, *cerebellum* is situated in posterior surface of the brain and it is comprises a miniature version of the cerebrum. It is covered in sulcu and guri and although is the 10% of the total volume of the brain, it contains more than half of all its neurons [24]. The function of the cerebellum is to coordinate movement by means of interaction of skeletal muscles. However, since it is interconnected with the cerebral cortex is also involved in cognitive tasks and language processes. Fibers from cerebrum are connected to the pons by some branches and these neurons are also projected in cerebellum. Consequently, they provide copies of motor commands and signals of spinal cord to cerebellum. As mentioned also above, sensory information are copied to medulla fibers which enter the cerebellum in which a comparison between those and the descending commands from cerebrum is performed. Therefore, if the movement is not coordinating because of weather conditions, for instance, cerebellum sends a corrective command to restore equilibrium. Henceforth, a damage to cerebellum could lead in muscle contractions and loss of equilibrium.

2.2.2 Brain Lobes

Another division stems from functional regions in each hemisphere of cerebral cortex (Functionality is summarized in table 2.1). Specifically, there are four lobes in each hemisphere which are named according to the bone of skull which lie above them. These regions are **frontal**, **parietal**, **temporal** and **occipital** lobes which are divided by sulci such as central sulcus. *Frontal lobe* is situated at the front part of the cerebrum above the temporal lobe and in front of parietal lobe. It is the largest of the four lobes and is separated from parietal by a group of tissues called the central sulcus (see figure: 2.8). At the back of the frontal

lobe, the primary motor cortex lies which controls the voluntary movements. Generally, the role of this lobe is to predict future outcomes from current actions, to separate good and bad actions and to eliminate morally and socially unacceptable decisions. Another role which lobe has a significant impact is the integration of long term memories which are derived from limbic system into emotions to produce social and moral rules and norms. Last but not least, it is an important component for understanding the language and speaking. Impairment of frontal lobe could lead in changes of socialization, attention deficits and depression or anxiety.

The *temporal lobe* is located on the bottom section of the brain. It consists of components that are essential for long term memory. Involving hippocampus it classifies memory into facts and events. Additionally, it has a fundamental role in auditory processing. This functionality includes sounds understanding coupled with language understanding since hearing is crucial for recognizing language rules. Moreover, it generates visual memories in combination with hippocampus and amygdala which they form also conscious memories. A damage to temporal lobe could lead in memory, speech perception and language problems.

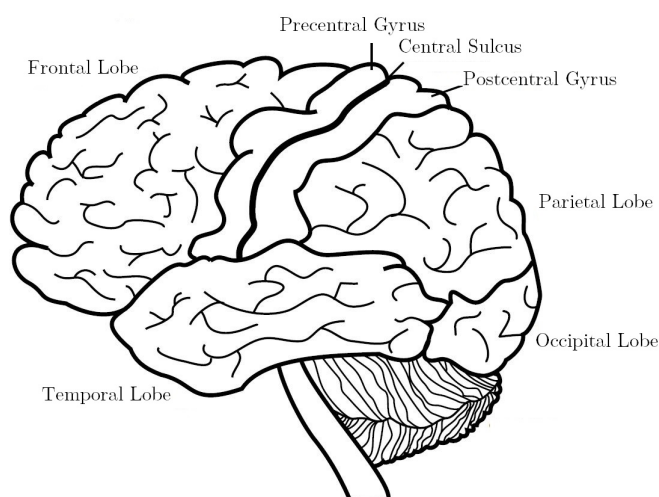


Figure 2.8: The brain lobes

The *parietal lobe* is located in the middle section of the brain and it integrates tactile sensory information. The main inputs from the skin such as touch and pain relay from thalamus to parietal lobe. Coupled with this it is also concerned with visuospatial navigation such as determining where the body is located within a space or how to avoid an obstacle. Another key functionality of this lobe is assessing the three dimensional representation of the visual objects but also the numerical relations of them while it is coordinating the attention as well. If the parietal lobe is damage the patient could have writing, language and perception struggling or visual attention could be diminished.

Finally yet importantly, *occipital lobe* is located at the back portion of the brain and it is associated with visual information. The primary visual cortex which receives and interprets information from the eyes is located in occipital lobe. Occipital lobe receives information from thalamus and its fibers and it processes this information by translating the stimulation or the visual perception. With the primary visual cortex embedded in this area occipital lobe is the main area of brain capacity for sight, size, motion, color and dimension recognition.

LOBES	FUNCTIONS
Frontal	Behaviour, Emotion Speaking, Writing Voluntary movement of skeletal muscle Intelligence, concentration
Parietal	Understanding of spoken and written language Sense of touch and pain Processing of somatosensory information Spatial and visual perception
Temporal	Understanding language Memory, Hearing Sequencing, Organization
Occipital	Processing of visual information Color, Light

Table 2.1: Lobes functionality

2.2.3 Brain Compartments

The CNS (brain and spinal cord) is covered by three protective layers (see figure 2.9 which depicts every protective layer) which are commonly known as **meninges**. These covering membranes are protecting CNS from direct contact with the bones of the skull that they encase it. The meninges is composed of the **dura matter**, **arachnoid matter** and **pia matter** each of which has a specific functionality for preserving the CNS and aiding its functionality.

The dura matter is the outermost layer and is composed of tough and fibrous connective tissue. This layer connects meninges to the skull and vertebral column. Dura matter is made up of two membrane layers. The outer layer of dura, **periosteal** lies close to the periosteum while the **meningeal** layer is closer to the brain. In many areas of the brain these two layers are fused but in other regions they enclose blood vessels and veins which are called *dural venus sinuses*. Moreover, meningeal layer forms folds which divide cranial cavity into different compartments.

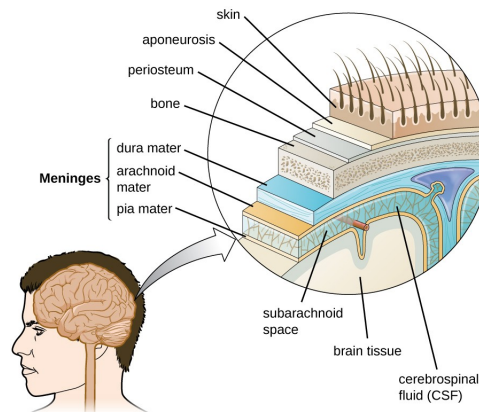


Figure 2.9: Meninges protective layers

The arachnoid matter is a thin membrane that surrounds the brain and encloses a space which separates it from the dura known also as subdural. It is connected to the pia matter with tiny extensions that span the space between the two layers in an area called subarachnoid space. The arachnoid space is filled with **Cerebrospinal Fluid (CSF)** while at the same time provides pathways for the blood vessels to the brain.

The pia matter is the layer of meninges which is closest to the cerebral cortex being in contact with it. This thin layer is full of blood vessels which could reach deep into the brain providing the necessary nutrition to the nerve cells. Furthermore, pia matter contains a network of capillaries which produce the CSF. However the part of pia matter which covers the spinal cord is less vascular but more thick and the region protecting the cerebral cortex.

Another key thing to highlight is the functionality of CSF. CSF is part of the system called ventricular system which is divided into four cavities called, *ventricles*. They are embedded in the brain and they are responsible for producing the fluid. In each of these ventricles there are some capillaries which are known as choroid plexus which are the main production source of CSF. This fluid's role is to protect the brain as a filter from harmful metabolites while minimizing also the potential damages from blows to the head and the neck. It circulates between the pia matter and arachnoid matter through the ventricles flowing downward through spinal cord and then upward towards brain through the subarachnoid space. It is secreted at a constant rate but there is much less fluid in the system forcing the CSF to turn over multiple times per day.

2.3 Epilepsy and Different Types

Epilepsy is a brain disorder which is characterized by the involuntary recurrent occurrence of synchronous discharges in cerebral cortical neurons, called epileptic seizures. These seizures could be highly connected with disruption of consciousness, impairment of mental function and disturbance in sensation and movement [28]. Epilepsy is manifested in one of every ten people during a normal lifespan and occurs in one or two percent of children. Symptoms of epilepsy could vary from person to person but the most common ones are uncontrollable jerking, losing awareness, collapsing and strange sensations. However, epilepsy is not a specific disease or a single syndrome but rather a broad category of symptoms which arise from the areas of the brain which are abnormally functioning [29]. Epilepsy is characterized by the uncontrolled excessive activity of either part or all of the CNS. It could be classified into three major categories/types, namely the **grand mal epilepsy**, **petit mal epilepsy** and **focal epilepsy**.

Grand Mal Epilepsy is characterized by generalised neuronal discharges causing abnormal electrical activity throughout all the areas of the cerebral cortex or deep parts of cerebrum and of brain stem. These discharges could be transmitted into the spinal cord causing tonic seizures with either sudden or rhythmic muscle contractions. On this specific type of epilepsy the patient usually presents symptoms such as scream in the beginning of the seizure, severe headache but also disorientation. The seizures associated with grand mal epilepsy last from few seconds to 4 minutes while the electric signals have high amplitude and frequency which means that they span over the entire cortex. Most people who have similar seizures have hereditary predisposition or traumatic lesions which could transmit signals and elicit grand mal seizures.

Petit Mal Epilepsy most commonly affects children from 5 to 9 years old but they could

also occur to adults. This type of epilepsy involves the thalamocortical activating system. The seizures last some seconds and they are characterized by loss of awareness, stop of talking, confusion, twitching contractions of muscles and restoration of the consciousness after the seizure. This sequence is called absence seizures and they could be multiples in a row. The electric wave of this seizure type have frequency between three and four Hz with slow complexes recorded in EEG.

Just as importantly, *Focal Epilepsy* could involve any local part of the brain or deeper structures of brain stem as well. They usually start in confined brain regions and remain restricted to these or they spread to other brain areas. Most often focal seizures arise because of localized organic lesions due to a brain injury or brain infection or functional abnormalities such as a tumor region. These abnormal tissues could promote rapid discharges in the local neurons. This electric activity spreads to adjacent areas which could be either in the scale of few millimeters or of few centimeters. If the electric wave traverses the motor cortex it could cause contractions throughout the other side of the body. For instance it could start from the mouth and continue downward to the legs. The semiology of these seizures vary depending on brain region in which the synchronous discharges are enabled.

2.4 Brain and Epileptic Activity

Epilepsy is mainly characterized by seizures and by corresponding semiology according to the area of the cerebrum or brain stem which provokes the neurons' synchronous discharges in a process called **epileptogenesis**. According to clinical studies this process is dynamic and evolving causing establishment of critical interconnections [29]. Consequently, there is an area of cerebral cortex which is responsible for initiating seizures and the resection of which could result in seizure control (see 2.4.4 *Epilepsy Treatment*). This area is known as **epileptogenic zone**. It is worth mentioning that there are several examples of this zone to spread along subcortical pathways such as *corpus callosum* where the activity is transferred from one hemisphere to another.

From the definition of this area a significant need for detecting this part of the brain arises since this is the abnormal region in terms of functionality. Upon it is successfully detected recent studies claim that the resection of it could lead in seizure freedom. However, there is a notable percentage of unsuccessful seizure handling with this method or operations which their treatment properties are accompanied by side effects for patient's behaviour, emotions and social life. According to *Jerome Engel and Timothy Padley*, surgical therapeutic intervention could be optimal only when the multiple medical, psychological and environmental factors are addressed.

To optimally detect this zone the epileptologist and neuroscientist firstly should classify the seizure type in which the patient belongs. In general, the seizures could be classified into two broad categories, focal and generalized. *Focal seizures* originate in a small group of neurons which could result from a brain infection or stroke/tumor. The symptoms of this type could be divided into simple and complex. This subdivision is based on the alteration of the consciousness, namely the former doesn't lead to consciousness loss while the latter is mainly responsible for that. The onset zone of these seizures is most commonly called *auras*.

On the contrary, *Generalized seizures* are associated with widespread electric activity and involve both hemispheres while they could be further divided into convulsive or non-convulsive types. This classification is depending on whether the seizure is correlated with tonic or clonic

movements. For instance, absence seizure is considered as one of the nonconvulsive form since the consciousness loss which they provoke are momentary.

2.4.1 Spikes and Epileptic Focus

An indicative characteristic of epilepsy are the synchronized bursts from a group of neurons which result in a discharge which is called **spike** [30]. Specifically the presence of discharges which are caused between seizures, **interictal spikes** could reflect the epileptic seizure onset zone or the propagation patterns to the seizure activity, **ictal activity**. These spikes, known also as interictal epileptiform discharges are used to diagnose epilepsy, localize the zone which causes changes in the period between the onset of seizures, the irritative zone and provide a further insight on the epileptic network. In general, the interictal spikes have high amplitude, they are followed by a slow wave while their duration is in the scale of milliseconds. However interictal spiking isn't the only case for epileptic activity since it may occur before (**preictally**), during (**ictally**), after (**postictally**) a seizure or between seizures (**interictally**), *see figure 2.10*.

Epileptic seizures may appear frequently or infrequently or at specific patterns which are still under investigation in order to be predicted. However, epileptogenic focus generates spikes at maximum mean spiking rate while a related study [31] showed that the distribution of interictal spikes is becoming less Gaussian prior to a seizure. Moreover, there are many environmental and physiologic factors which could modulate the seizures' occurrence such as fever and alcohol consumption. Apart from interictal to ictal transmission there are research interests on the detection of epileptic focus by interictal activity. Despite the fact that the common belief is that epileptic focus has the most high spiking activity, this area is highly correlated to the synchronization of interictal spikes which they are not considered the main epileptic activity.

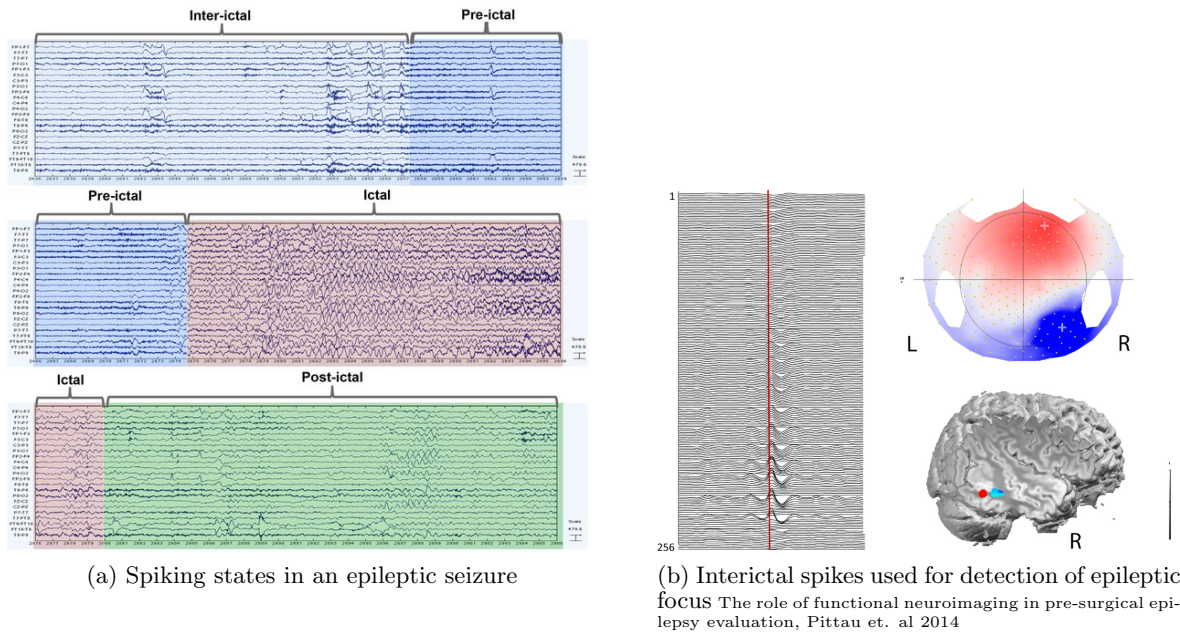


Figure 2.10: Epileptic spikes states, Epileptic focus by interictal spikes

2.4.2 Epilepsy Diagnosis

Although epilepsy is the brain disorder which is highly correlated with recurrent unprovoked seizures, there are other disorders or human's health states which could result in same symptoms. Consequently, accurate epilepsy diagnosis require many steps and thorough series of examinations. Faulty brain function could be spotted with many tests, most of which include use of imaging modalities. However, a simple test could give a first insight and better clues since it involves some questions and inspection of brain functionality through cognitive tasks. **Neurological Exam** includes methods of detecting abnormalities or malfunctionalities within the brain. It often starts with questions along with mental tasks to determine if there is a damage to the brain . At the majority of the cases it incorporates memory tests to investigate how the subject could remember words or simple math calculations while it also embeds senses and muscles functionality evaluation. This step comprises one of the very first, though important, stages of epilepsy diagnosis since it guides the doctor in the way of solving the puzzle to detect epileptic symptomatology on a patient.

Doctor needs complementary information and tests to decide if the patient is suffering from epilepsy and in that case there should be the classification of epileptic seizures type. Another type of test which the doctor decides to proceed is the **Blood Test**. A blood test could detect increased levels of *prolactin* that is rising after an epileptic seizure. This test should be performed almost right after a seizure for accurate result, namely after 10 to 20 minutes. Furthermore it could be a marker of infections or other conditions which are associated with seizures. In this way, it could rule out epilepsy as possible disorder since low glucose levels could also be associated with seizures episodes or inversely it could confirm epilepsy since prolactin is only a sign of epileptic seizures. Along with the blood test the doctor inspects also the **medical history** which could give further insight about possible epilepsy manifestation. For instance, history of family seizures could be an indication of hereditary predisposition in epilepsy or previous psychological problems could trigger epileptic statuses.

Coupled with these steps doctors use **Electroencephalography - EEG & Magnetoencephalography - MEG** to detect abnormal behaviour on brain signals. These modalities measure electrical signals and magnetic fields accordingly produced by the brain with the ultimate to goal to determine areas which are causing this behaviour. The main advantage of these modalities is that they could capture abnormal behaviour even after a seizure with the high temporal resolution which could achieve. The process of recording these signals is by attaching either a set of electrodes or gradiometers on the scalp which are able to capture activity from deep structures of the brain. A common strategy applied to increase the levels of certainty regarding the epilepsy manifestation is to combine these modalities with brain scans modalities such as **Magnetic Resonance Imaging - MRI** which have high spatial resolution. In this way a doctor could identify abnormal behaviour on signals and possibly find a region of the brain with lesions or injury which triggers the epileptic seizures.

Last in order but not of importance, other modalities used to detect epileptic activity is the **Positron Emission Tomography - PET** to identify areas of lower metabolism that they are indicative markers after a seizure. The information extracted by PET could be supplementary to the results of **Single photon emission computed tomography - SPECT** comparing thus the blood flow during or between seizures. It is worth mentioned that all these tests could not easily apply to every age group and one of the most characteristic examples are the subjects in childhood. Specifically, children are more prone to develop epilepsy because of the development of the brain networks. Therefore, in some cases they might be also sensitive

to specific tests and the doctor should decide carefully which tests to select to claim that a patient is affected by epilepsy.

2.4.3 Epilepsy Treatment

Having discussed what a correct and secure diagnosis incorporates, the treatment of epilepsy addresses ways of improving both the patient's quality of life and eliminating seizures and abnormal brain functionality. The key aspects of epilepsy treatment can be listed as follows: **Anti-Epileptic Drugs - AEDs, Ketogenic Diet, Vagus Nerve Stimulation, Epilepsy Surgery** and **Deep Brain Stimulation** [32]. *Anti-Epileptic Drugs* are most commonly used to treat epilepsy. According to research of these drugs' efficiency, they could control seizures in about 70% of the cases. AEDs are modifying chemicals in the brain by alternating the excessive electrical activity of neurons by means of ions flow. The drug of choice depends on an accurate diagnosis of the epileptic syndrome based on a variety of groups of anticonvulsant mechanisms such as Gamma-aminobutyric acid (GABA). *Ketogenic Diet* is a high fat, low carbohydrate protein diet is often applied to children with seizures after at least two unsuccessful medications. This specific diet is suitable for limited seizure types and epileptic syndromes, namely myoclonic seizures. The mechanisms underlying the diet treatment plan stems from the energy source of the body. The body usually absorbs glucose from carbohydrates for its energy source but when a patient is on this diet the ketones are used as energy source while the production of decanoic acid could help reducing the seizures. *Vagus Nerve Stimulation* is a procedure of a device implantation which stimulates vagus nerves with electrical impulses. These types of nerves are the message center of the human body since they receive and send messages from brain and the body. Vagus Nerve Stimulation could be an option for seizure frequency control after a failed medication plan. The device implanted is responsible to send signals to help the nerves calm down from irregular electrical activity. However, it requires maintenance, it is an expensive option and is invasive which renders it as a second choice.

Epilepsy Surgery is a technique used to eliminate the seizures after ineffective use of AEDs. Specifically, there are many types of brain surgeries which involve either the resection of tissues associated with epileptogenesis or with pathways cutdown to treat focal and generalised seizures correspondingly. Removing the areas of the brain responsible for the seizures is the most common surgery but it requires preliminary tests prior to the invasive approach. The brain surgery for epilepsy aims at removing the epileptic focus while preserving at the same time the eloquent cortex. Accurate marking of the epileptic focus is thereby of utmost importance. The doctors are proceeding to a step called **Presurgical Epileptic Evaluation** which aims at detecting the actual region of epileptogenesis using intracranial electrodes with a test called **Electrocorticography - ECoG**. ECoG is a test where a small array of electrodes is placed on the top of the area which is considered as the abnormal one to evaluate the exact portion of the tissue to be removed. This is performed by a scalp opening procedure which needs to be guided by a previous EEG or MEG test that give the first insight on the area width. The resection of tissues is mainly beneficial for focal types of seizures while for instance **corpus callosotomy** is usually reserved for people with generalized seizures. The ultimate goal is to split the connection pathway between the hemispheres to cut down the flow of abnormal activity from one part to another. Considering everything, *Deep Brain Stimulation* is applied to patients who can't undergo a surgery and it aims at handling the frequency of excess and abnormal activity by stimulating specific brain areas.

Magnetoencephalography - Electroencephalography

3.1 Introduction

Modern medicine applies variety of imaging techniques to inspect human body and detect abnormalities. It is believed that from the very early stages of one's life the electrical signals generated by the brain represent the status of whole body apart from the brain function. Henceforth this assumptions led to a series of attempts to record brain activity which revolutionized the field of what we know today as Neuroimaging Technologies. The first known neurophysiologic measurement was performed in animals by *Richard Canton* whereas *Hans Berger* in 1929, pioneered the **Electroencephalography (EEG)** in humans since he recorded brain signals from human scalp. The emergence of EEG contributes to understanding the underlying mechanisms and functions of human's brain which is vital for diagnostic and treatment purposes in various disorders.

EEG is a non invasive technique to record brain activity from the scalp generated by neurons and underlying structures by means of electrical signals. The principle behind EEG machine depends on the fact that the nerve cells are producing constantly electrical signals. However, this constant activation is being performed synchronously by groups of neurons which in turn transmit these signals throughout the body in the form of electrical impulses. Specifically, the neurons diffuse chemicals across cells' membranes when a person is thinking, reading or in general when the brain is stimulated. Consequently the sensors which this modality is using are able to capture and monitor this behaviour offering a signal representation which incorporates the activity in each sensor position.

The sensors that this neuroimaging technology, as it is commonly called, has electrodes in fixed positions of the scalp and they can pick up the electrical brainwaves in an exquisite temporal resolution. The signals recorded have first undergone an amplification and digitization process in order to be visible and understandable. On the question of grasping the signals recorded and their neurophysiological origin one should take into consideration that EEG has different display styles according to various mind states such as alertness, rest, sleep and dreaming which are expressed in frequency rhythms and amplitude that are associated with the brain condition in these states. The brain rhythms can be treated under four distinguished types as follows: **delta** - (0.5-4Hz), **theta** - (4-8Hz), **alpha** - (8-13), **beta** - (13-30Hz) and **gamma** ($> 30Hz$), [33]. A notable example of delta rhythm association with

mind state is that it is predominant during deep sleep with strong coherence all over the scalp. Coupled with this, theta is characteristic of rodents but when is appearing in humans it might correlate to emotional behaviour. Contrary to the delta rhythm, alpha is dominating during wakefulness and it is best observed when the eyes are closed while beta activity is an indication of increased alertness and focused attention. Last but not least, gamma activity is connected with information processing and complex calculations. Having all these mentioned and counting on its ability to measure activity even in subsecond scales, EEG is particularly useful in evaluating if a subject is suffering from a brain disorder or even if he is prone to develop one contributing both in diagnosis and prevention. However it can also mitigate issues related to localization of abnormal areas of the brain either because of a brain injury or a tumor but a disorder focus as well.

Although EEG comprises a way of evaluating brain behaviour and functionality, achieving the full understanding of the mechanisms underlying the organization of the human brain is still a complex and major challenge. For this reason, *David Cohen* in 1972 introduced a new way of measuring the brain activity by means of detecting magnetic fields generated by the brain electrical activity using sensitive superconducting quantum interference devices known as **SQUIDS**. This new innovation launched a new era in neuroscience and in neuroimaging modalities since it was the first predecessor of **Magnetoencephalography (MEG)** which comprises a very effective modality nowadays for brain research and for controlling brain disorders.

MEG is a technique which records the magnetic fields produced by currents of electrical signals. It is worth noted that MEG is completely non invasive since it doesn't require injection of various isotopes or exposure to magnetic fields while at the same time records the fields using a specific cavity with the sensors attached on it placed on top of a subject's head. The main principle of Magnetoencephalography is that the sensors of this modality are capturing varying magnetic fields by neuronal electric currents that are generated in underlying pyramidal cells. However, similar to EEG, it can detect simultaneous depolarizations of pyramidal cells in same direction that are producing 'visible' magnetic fields. Furthermore, the coils used in SQUIDS are able to measure magnetic fluxes if they cross the coil surface and thus MEG could detect activity perpendicular to sulci and fissures. In general, MEG has excellent temporal resolution while at the same time could provide spatial accuracy comparable to other imaging modalities exclusively used for their spatial resolution. Moreover, it provides information which could be exploited in a complementary way with other modalities thereby offering a thorough insight of the sources activation in an area of the brain. The fields measured by MEG are weak and therefore it is important to satisfy the requirements, namely the noise suppression and the exploitation of the sensitive devices. First of all, when a magnetic field is applied to the pickup coil of SQUIDS, a current is generated from a flux transformer circuit which in turn is converted into a magnetic flux able to measured by SQUID loop. Regarding the noise reduction magnetic shield techniques are applied such as a magnetic shielded room and also online noise filtering approaches. Last but not least, cooling of the superconductive devices/sensors secures the operation and provide reliable results.

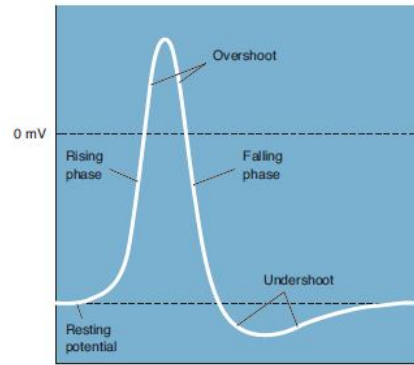
According to *Epilepsy Foundation*, MEG could be helpful in detecting the sources of seizures revealing the exact location or in mapping the exact locations of normally functioning areas near lesions such as tumor, guiding thus doctors in an accurate removal without loss of a brain function. Furthermore, for patients who had undergone surgery the electrical fields measured by EEG might be distorted by changes in brain and anatomy while MEG could identify if a further surgery is required providing the required information non invasively.

3.2 Brain Signal Recording - Action Potentials/Magnetic Fields

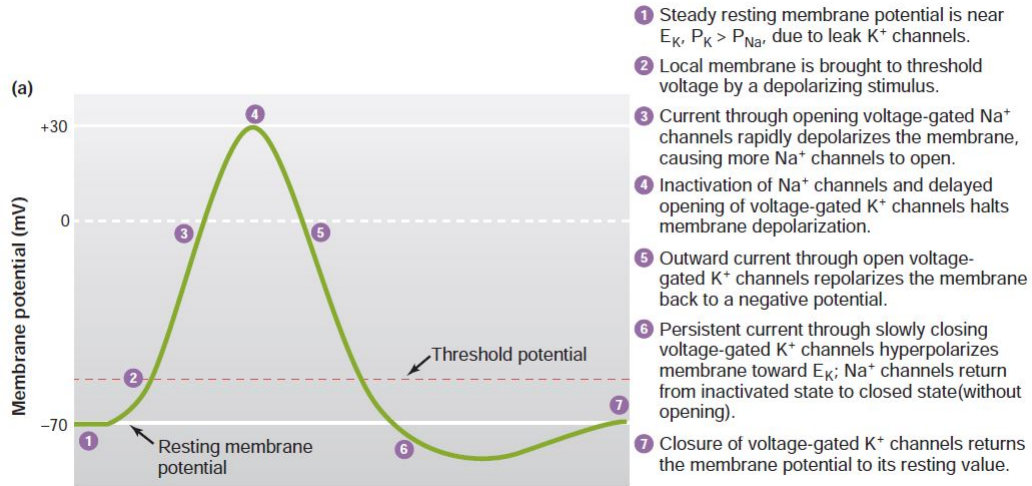
Electrical currents are crucial in a variety of roles within a living tissue. These currents produce an electric potential which can be spanned on the surface of the scalp and thereby being measurable by EEG. Also these potentials are accompanied by some magnetic field which are distinguishable by MEG. The activities in the Central Nervous System are associated with the currents that are transferred between the synapses of axons and dendrites or between dendrites. The amplitude of a potential which could be recorded is 70 mV with negative polarity under the membrane of the cell body but it could change based on the variations in synaptic activities. For instance if a potential travels along a fibre and ends in a neuromuscular junction there is high probability of the action to be occurred in the neuron following the junction and this potential is known as Excitatory Postsynaptic Potential (EPSP). On the other hand, if the potential travels along the same fibre there will be a summation of the excitatory post synaptic potentials and the likelihood of the potential to be occurred in the postsynaptic cell will be decreased. The latter is called Inhibitory Post Synaptic Potential (IPSP).

The information carried and transferred by a nerve cell is called **action potential**. It is caused by exchange of ions across neuron membranes making a temporary change in the potential of the membrane while it usually travels in one direction. Action Potentials cause a change in membrane potential between -70 and 30 mV at a rate of 250-1000 Hz. Although action potentials have short duration they are characterized by certain identifiable parts. First of all there is the **rising phase** (see Figure: 3.1) which is characterized by the rapid depolarization of the membrane. Specifically, during an action potential membrane permeability is changing allowing sodium and potassium ions to move down to its concentration materials. Therefore prior to the the rising phase, there is a potassium equilibrium till the action potential begins with a depolarization stimulus allowing for voltage gated channels to open and thus sodium is entering towards the membrane. This procedure continues since the depolarization allows more sodium channels to open leading the membrane to reach a threshold potential and thus the inner part of the neuron is positively charged while the outer part is negative. This part of the potential comprises the **overshoot**. As the membrane approaches the peak of sodium equilibrium potential the permeability declines causing blocking of open sodium channels. However at the same time this depolarized state allowing potassium gated channels to open resulting in the **repolarization** of the potential increasing again the negativity of the membrane in a phase called **falling phase**. However, the potassium channels close slow allowing the permeability to remain above resting levels thereby hyperpolarizing the membrane in a phase called **after-hyperpolarization**. Finally, there is restoration of the resting potential.

A key feature of the action potentials is that they could self propagate along a neuron if the membrane is depolarized to its threshold value. The current entering during an action potential can depolarize the membrane to the threshold . In this way membrane is depolarized every time according to the adjacent portions which result in differences inbetween the potentials leading to ions flow. Therefore, this process causes local currents and thus local action potentials setting a propagation pathway along the length of the membrane. It is worth mentioned that once a portion of the membrane is depolarized the action potential cannot return since the depolarization stimuli doesn't permit any further opening of the voltage channels rendering them unresponsive.



(a) Action Potential Phases



(b) Action Potential and changes in Membrane

Figure 3.1: Action Potential morphology

Adapted from: Vanders Human Physiology and Neuroscience: Exploring the Brain

3.2.1 Signals Physiological Basis

MEG and EEG are generated by the ionic currents flowing inside and outside neurons. In general, neurons generate electrical currents which vary in the time domain when they are activated. These currents are driven mainly by excitatory postsynaptic activity and they could be modeled as current dipoles while they are generated at the level of cellular membranes [34]. However, there are many cases in which action potentials don't produce an observable magnetic field since the currents are flowing in the opposite direction resulting in cancellation of the magnetic field. It is worth mentioned that the fields are measured by peripheral nerves and thus the current dipoles simulate the intracellular currents. The magnetic field generated by current dipoles could be computed using **Maxwell Equations** adopting a quasi-static approach. It is worth highlighted that one dendrites' flowing current is producing a weak signal which is not measurable whereas many cortical pyramidal cells have similar orientations and thus they produce magnetic fields which reinforce one another.

Moreover, the magnetic field measured by the pickup coils requires many neurons to

be activated synchronously since taking into consideration the distance of the actual source generation from the SQUIDS and given the skull and scalp thickness there is an attenuation of the field. Regarding the electrical signals, the neurons are located within a conductive medium such as Cerebrospinal Fluid which allows the current generated to flow through the skull and scalp. These volume conduction medias produce also volume currents which contribute in the EEG measurement since when they reach the scalp they produce voltage difference which is picked up by the electrodes. Both primary and volume currents produce magnetic fields (see Figure: 3.2) which are summed up and measured by the MEG sensors. If the conductive medium although, has homogeneous conductivity only the primary currents contribute to the external magnetic field. Regarding MEG signals the dipole orientation constitutes a crucial part of the measurement since radial dipoles produce negligible magnetic fields while tangential ones located in the cortical sulci have detectable magnetic fields (Hamalainen et al. 1993).

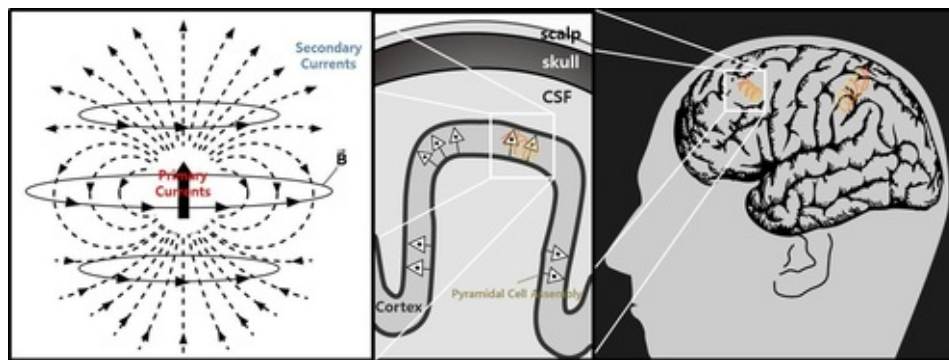


Figure 3.2: EEG/MEG Signals Origin

In the first plot the magnetic fields produced by primary currents are shown. The middle one illustrates the location of the sources generation in the sulci along with the orientation of the dipoles generated by pyramidal cells. The last one displays the position of a source in a macroscopic view on a brain sulcus.

As was pointed out before, an EEG signal is a measurement of currents that flow during synaptic excitations of the dendrites of pyramidal neurons. At the level of synapse, the transmembrane current is flowing by positive ions inwards such as Na^+ in the EPSPs while in the IPSP it is carried by negative ions inwards such as Cl^- or by positive ions outwards (K^+). Henceforth, the positive current is directed to the extracellular part of the cell regarding the EPSP while in the IPSP the current flows from the inside of the neuron to the outside, as shown in Figure: 3.3. Due to the presence of these currents, an active sink is produced by the extracellular medium in the excitatory synapse and an active source in an inhibitory synapse. Regarding the Excitatory Post Synaptic Potentials there is no accumulation of charge in the extracellular medium and thus the currents that flow either inwards or outwards apart from an active sink they generate passive sources along the membrane. On the contrary, in the case of Inhibitory Post Synaptic Potential the situation is completely reversed since apart from the active sources there are also passive sinks that they are formed on the membrane. Consequently, the activity produced in the cellular level along with the specific geometrical topology of the neurons produce open fields(electric/magnetic) that they are 'visible' by the EEG & MEG.

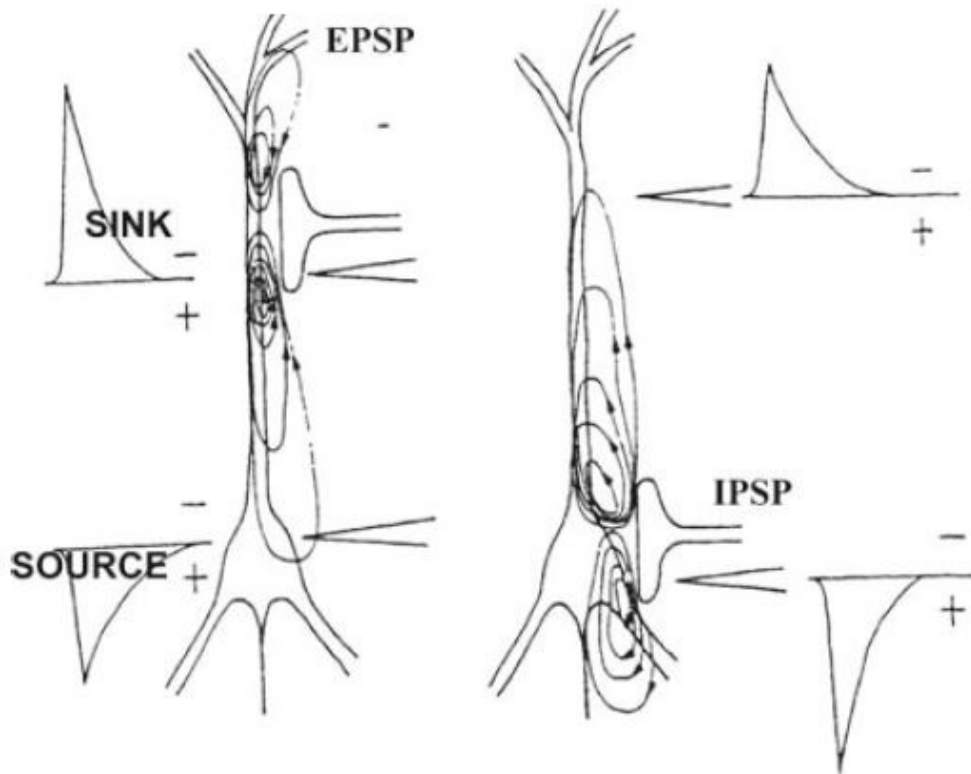


Figure 3.3: Post-Synaptic potentials

Adapted from Fernando Lopes da Silva et.al. 2010

3.2.2 Evoked/Event Related Potentials and Fields

Electroencephalography & Magnetoencephalography provide excellent ways to understand the neurobiological abnormalities and evaluate the brain networks. Time locked or evoked activity could capture neural behaviour in both cognitive and sensory processes. **Event Related Potentials (ERPs)** are small voltage fluctuations according to spontaneous electric activity related to a specific event or stimuli. The trigger condition of this potentials could derive from visual, auditory or somatosensory stimuli which are known as **Evoked Potentials**. The ERPs are generated by specific number of neurons in a time-locked way but there are issues in the accurate detection of these events. One common approach applied is the averaging which reduces the background noise and amplifies the activity at the time point which occurred since it is recognisable by many electrodes on the scalp surface. They reflect the summed postsynaptic potential and they are described by latencies and amplitudes.

The synchronous fire of a group of oriented cortical pyramidal neurons could be divided into two groups. The first one is the early ERPs which have a latency below 12 ms and they are associated with the peripheral nervous system. On the other hand, late ERPs are above 100 ms and they are correlated to brain cognitive processing. In general, ERPs provide a noninvasive means to evaluate brain functionality in a variety of disorders and they are widely used for testing the sensory pathways and for spotting brain dysfunctions. Regarding the **Event Related Fields (ERFs)** they share the same principles with the ERPs but they record summed postsynaptic magnetic fields which serve complementary to the ERPs for the diagnostic tests.

3.3 EEG Recording System

The first attempts to record electrical activity was performed using galvanometers. Coupled with this instrument a mirror was also used to magnify variations of the pointer by the light projected to the galvanometer. This technology consists the ancestor of modern EEG since the galvanometers led to the invention of electrometers and consequently of the electrodes. The recent EEG systems incorporate a number of **electrodes**, a set of **amplifiers**, **filters** and **needle registers** [35]. However, with this setup the only way of visualizing the signals was on paper. Proceeding to the era of digital information many scientists decided to transform EEG signals in digital form in order to analyze it and interpret it easier using computers to perform demanding processing. The digitization procedure requires **sampling**, **quantization and encoding devices** and signal processing tools embedded in the computer systems. The conversion from analogue to the digital EEG is implemented with **Analog to Digital Converters** at specific bandwidths. The bandwidth of EEG is limited to 100 Hz thus 200 samples per second (according to Nyquist criterion) but in some applications it is feasible to record even at 2000 samples per second. In modern EEG setups the representation of each sample is performed with 16 bits maintaining thus the diagnostic information in an accurate and high level.

The EEG electrodes are fundamental elements of recording equipment and there are many types used in the EEG systems. For instance, disposable gel-less, reusable disc electrodes or headbands comprise some characteristic examples. For the multichannel recordings which are extensively used nowadays the most typical electrode setup is the electrode cap. It consists of electrodes from silver chloride disks less than 3mm that they are attached on the patient's scalp. The knowledge of the exact position of the electrodes is of utmost importance for both interpretation and analysis. For this reason there are some standardized strategies for the electrodes placement such as the 10-20 system (see Figure: 3.4) or the corresponding 10-10 one. The former places 21 electrodes at positions measured at 10% and 20% of the head circumference using skull landmarks as reference points such as the preauricular points (A1, A2) and the nasion. The electrodes in this setup have specific name which derives from the place that they are located. The first part indexes the array row such as Fp (Frontal Pole), F (Frontal), C (Central), P (Parietal), O (Occipital) and T (Temporal). On the other hand the second part of the electrodes labelling is either the numbers depending from the side (even for the left side and odd for the right) but also the 'z' for centrally located sensors. Regarding the 10-10 International system there are more electrodes places on the scalp at every 10% of the medial-lateral contours and it is an extension of the 10-20 strategy. It is mainly used for studies that they require higher density electrodes in order to investigate with more spatial accuracy a region of interest.

Moreover, commercial EEG recording systems are equipped with impedance monitors since high impedance between cortex and electrodes could lead to distortion. Another approach to decrease the impedance is to fill every electrode with conductive gel which improves the data quality since it optimizes the contact between the scalp and the electrodes. At this point it is worth noted that prior to the EEG examination one should ensure that the electrodes topology is accurate and calibrated. Therefore, before starting the recording a technician passes a voltage through each electrode to guarantee that each channel handles the signal identically. After the calibration procedure one should fix the EEG **Montage**. The montage is a standardized arrangement of electrodes pairs for review and display purposes. Montages are divided into two major types, namely the bipolar and the referential. Refer-

ential montages are linking each electrode to a distant reference and usually this reference is placed on the earlobe, nose, mastoid or scalp center. In the bipolar setup each channel records potential difference between two scalp electrodes. Last but not least, the average reference is an approach which subtracts the average activity from each electrode. After these preliminary tests the actual recording is next in which the signal obtained first undergoes a real-time processing by the instrument setup of EEG system.

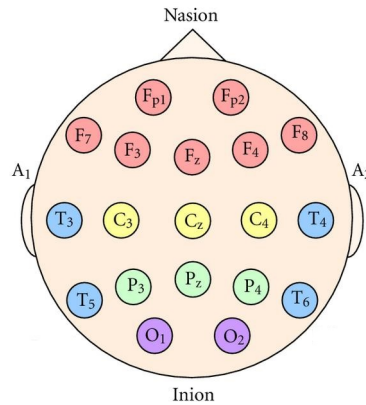


Figure 3.4: The International 10-20 electrode placement system

The initial phase is to measure potential between two electrodes with a differential amplifier which treats one signal as reference. After this step and since the sensitivity of EEG is very high there are set of waves that are contaminated by muscular, cardiac and ocular activity or by non-physiological/instrument noise, a filtering layer is applied to the signal 'online processing'. **Low Pass (LPF) and High Pass Filters (HPF)** are used to narrow down the frequency range of the signal of interest (see Figure: 3.5 below) and eliminate the noise which affects the recorded brain activity.

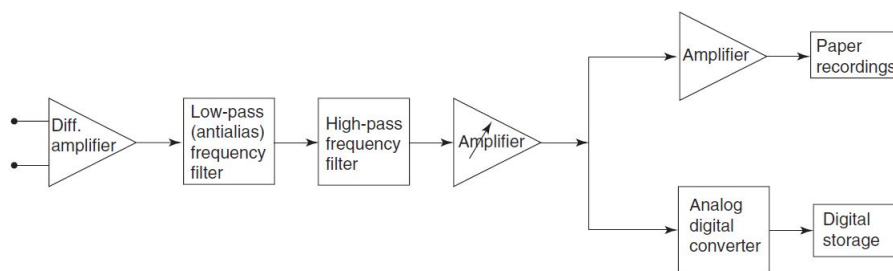


Figure 3.5: EEG Setup Block Diagram

Adapted from Blinowska, Durka at 2006

Specifically, Low Frequency Filters control the response of the instrument with a typical configuration being a frequency window of 0.5 - 1 Hz. At the same time they serve as anti-aliasing factors for the signals recorded. On the other hand High Frequency Filters attenuate the high frequencies keeping unaffected the low frequency components since its typical setting is between 35 and 70 Hz. In general, the LPF filters slow artifacts such movement artifacts while the HPF rejects electromyographic contamination. Next layer of EEG processing is an

adjustable **amplifier** prior to the analog to digital conversion. Amplifier is used to increase the magnitude or amplitude of a voltage without distorting it since the measured signals are weak and in sub scales of Volt. The **Analog to Digital Converter** digitizes the signal usually with 12-bits and with a sampling frequency ranging from 100 Hz to several hundreds. This process allows the signal to be stored in a computer system for visual inspection and data analysis in order to extract 'hidden' information out of it. Considering the pre-digitization proliferation there was just a signal fortification before printing it out on a plane paper or on a paper grid.

3.4 MEG Recording System

As previously mentioned electric currents are accompanied by magnetic fields which are measured by a complex recording setup with high accuracy. Neuromagnetic signals are spanning in the scale of the fT (50-100 fT, Hari, Hämäläinen et. al 1993) which means that their strength is really small especially when it comes to comparing with other magnetic fields. Specifically, the brain activity generates magnetic fields which are 8 orders of magnitude smaller than the Earth's magnetic field or thousand times smaller than external noise in a laboratory (as shown below).

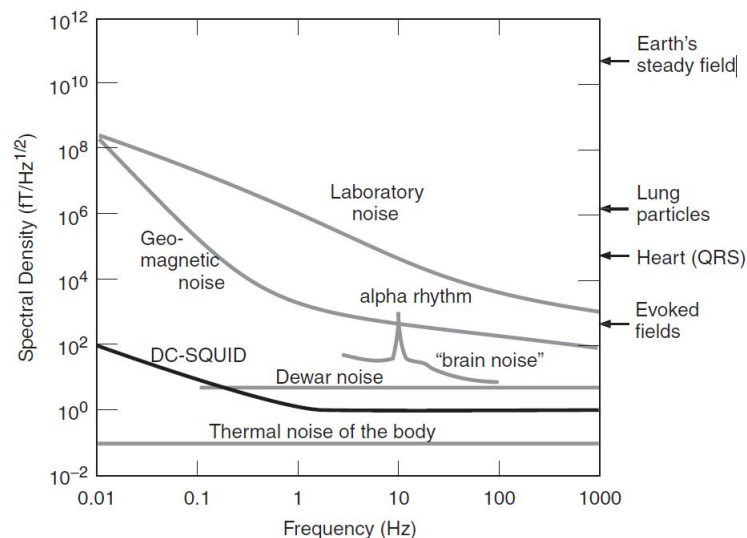


Figure 3.6: Magnetic Fields Strength Comparison

Adapted from Hämäläinen et.al. 1993

MEG recording system is comprised of many elements which suppress the external interference and focus on the optimization of acquiring the brain magnetic fields. A typical MEG system (see a block diagram of basic elements of MEG system in Figure: 3.7) consists of helmet-type sensor array inside a liquid Helium dewar, Magnetically Shielded Room, readout/control electronics, stimulus devices and signal processing tools and softwares. Recording brain magnetic activity could be performed either in lying or sitting position but the head of the subject should be as close to the sensor array. In order to evaluate the distance of the head from the sensors there is a digitization process in which three coils are placed on reference points of scalp such as preauricular points and then an instrument called **Head Po-**

sition Indicator (HPI) provides precise information about the position of the MEG system with respect to the head. The main component of the MEG system is the sensitive sensors which are able to detect weak magnetic fields generated by the brain. These sensors are based on the properties of superconductivity and their main role is to transform magnetic flux to voltage. The devices responsible for this process are known as **SQUIDS-Superconducting Quantum Interference Devices** and they function optimally when they are cooled down.

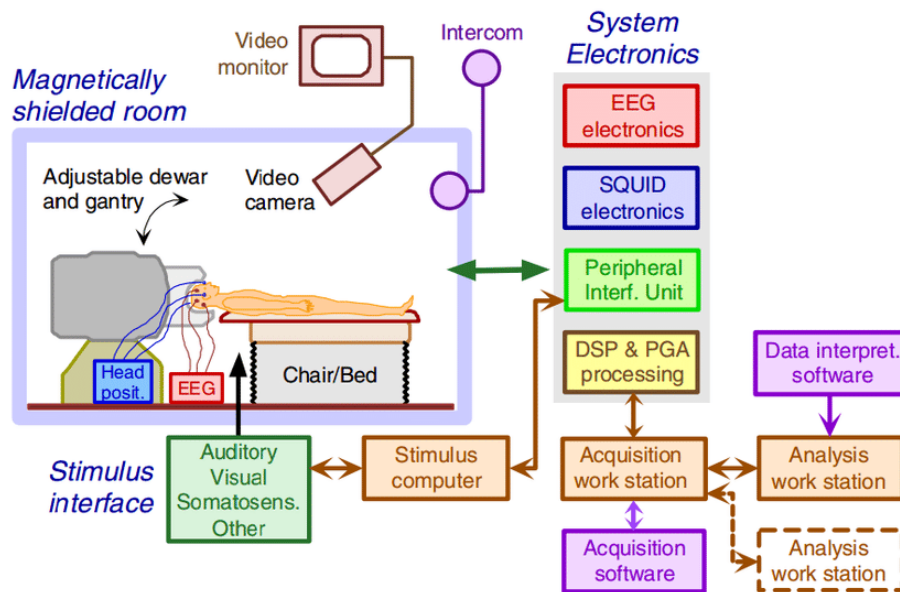


Figure 3.7: Block Diagram of a standard MEG system

Adapted from Sternickel et. al 2006

These materials lose electrical resistance when they are cooled down. Specifically, an electric current flows without friction and when they are arranged to a circulate loop the process is infinite. This perpetual flow paves the way for the generation of a magnetic field which is converted by SQUIDS inducing a shielding current on their surface cancelling out the external fields. In order for these materials to transition to the perpetual flow there is a characteristic temperature called *critical temperature* which allows the switch in superconducting state. This temperature usually achieved by specific chemical materials while the most common is **liquid Helium** whose temperature is -269°C . However, SQUIDS are not able to measure the absolute flux and hence nor the absolute magnetic field but they could capture just its variations in time.

The configuration of SQUIDS is not the best to detect directly the magnetic fields and for this reason **pickup coils/flux transformers** are used to maximize the detection efficiency. Typical pickup coils have diameter of 10mm and they could be divided into three types: **Magnetometers**, **Planar Gradiometers** and **Axial Gradiometers**. Magnetometers are the most sensitive superconductive transformers since they could detect both deep and shallow sources. On the other hand they are more prone to the external noise as well and thus they are mainly preferred when the shielding and suppression is optimal such as thick Magnetic Shield Rooms. Regarding Medium MSR the best combination is gradiometers. Axial Gradiometers have higher baselines and thus they could detect better deep sources compared to the planar ones. On the other hand planar gradiometers they are more sensitive to shallow sources

especially when the current dipole axis is perpendicular to the direction of the gradiometers.

Notwithstanding the optimization of the detection efficiency of pickup fluxes and the sensitivity of the SQUIDS it is imperative to perform measurements in an environment which combines Magnetic Shielding, High Sensitivity & Detection Efficiency. The latter is achieved by embedding the recording setup in a **Magnetically Shielded Room (MSR)**. This enclosure of the setup is reducing the external noise by guiding the magnetic fields around the room by not permitting the penetration of the external noise as shown in Figure 3.8. This room is composed of walls with layers of metal and aluminium and thus it attenuates the external noise by a factor of 100. The shielding properties of this room are associated with high permeability of mu-metal at low frequencies which provides the magnetic fields with a reluctance path along the walls while at higher frequencies it relies on eddy currents flowing on the high conductive aluminium.

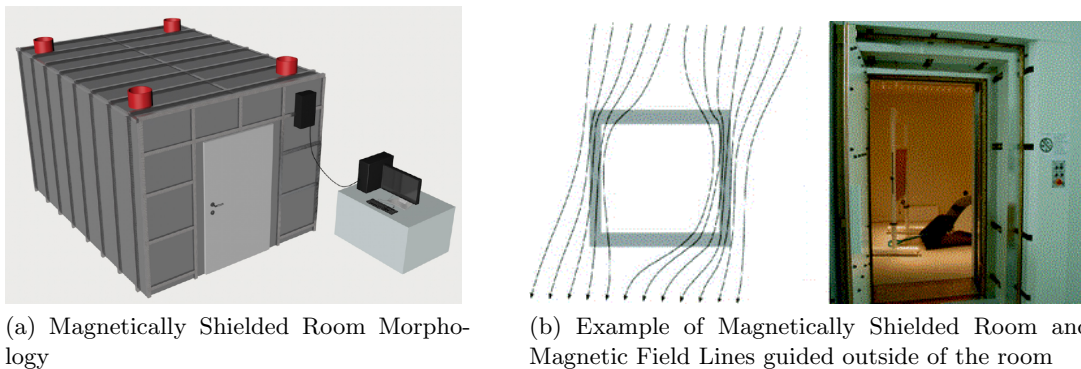


Figure 3.8: Magnetically Shielded Room

The MEG systems are associated with a cooling equipment for the superconducting sensors in order to keep them in temperatures close to absolute zero in which they operate optimally. Current commercial systems achieve cooling by placing the sensor arrays in a **dewar** filled with liquid Helium. Dewar although serves also for insulation apart from cooling purposes. Therefore, it is made of reinforced fiberglass plastic in a helmet shape and it has around 50 layers of superinsulation. Coupled with this dewar is constructed with thermal noise shielding from copper coil foil.

The output of SQUIDS is too weak to be measured directly by Analog to Digital Converters using Personal Computers. Henceforth, there is an amplification and filtering process which consists of high and low pass filtering and elimination of power line noise (similar to the EEG). However, modern MEG systems digitize this information and record using optical technologies such as optical fibres with readout electronics which profit the compactness and the increase the dynamic range. Last but not least, there are also signal processing tools incorporated in the electronics configuration of the MEG system for performing digital filtering or for rejecting various types of artifacts. Moreover, in an MEG system there are external stimuli devices for conducting experiments by triggering specific areas of the brain while at the same time it is often a recording of cardiac and ocular activity using specific electrodes for artifact rejection purposes.

3.5 Interferences in the recording of the brain signals

A significant aspect of recording brain signals is the fact that they can be hampered by unwanted sources which complicate the data analysis and affect the interpretation of brain activity. Both EEG & MEG are recording brain signals which are characterized by low signal to noise ratio and therefore since the sensitivity of their sensors is quite high they will also capture activity from other sources either external or internal. These sources are known as **artifacts** while the terms external and internal are associated with the origin of the sources (i.e by a subject itself - internal). Hence it is of vital importance to distinguish them in order to design properly the rejection strategy.

3.5.1 Physiological/Internal Artifacts

Physiological artifacts belong to the group of internal artifacts and they arise from body activities from fundamental functionalities like **cardiac**, **ocular**, **muscular** and **respiratory** activity (see Figure: 3.9). These type of artifacts could be detected in both EEG & MEG but there are several guidelines in order to reject them [36], [37].

The **eyes** can be represented as a small electrical dipole oriented from retina (charged negatively) to cornea (charged positively). When an eye movement is detected then a change in electrical field will be picked up by electrodes nearby. Specifically, in this artifact the orientation of dipole changes altering the associated electromagnetic fields in the frontal region. On the other side there is also ocular artifacts due to eye blinks which cause changes in the intensity of the dipole.

The fields generated by the activity of the **heart** are orders of magnitude higher than those of brain. First of all, a pulsating heart results in conduction of electrical activity on the scalp by means of potential changes. Moreover, a pulse artifact could contaminate a signal of an EEG electrode because of its position being on a vessel. Coupled with this, cardiac pulses which are accompanied by electrical potentials create magnetic fields which are detectable by the sensitive SQUIDS and pickup coils especially in the left hemisphere due to the heart's position in the human body. It is worth mentioned that in children the interference by cardiac activity could impact more the recordings due to shorter distance of heart with regard to the brain.

Muscle Potentials on the scalp occur in a variety of ways. This type of potentials appear due to the face/limbs movements or they are associated with other functions like swallowing, speaking or chewing. The power spectrum of muscular activity is relatively high in a bandwidth between 20 and 300 Hz which results in picking up of this activity by electrodes placed even in the center of the scalp. On the other hand muscular activity in MEG is appearing less often since the magnetic fields fell off rapidly due to the distance of dipole generators while the contribution of these secondary currents in external magnetic field is relatively low.

Respiration is producing either slow and rhythmic activity or sharp waves which occur synchronously. In the first form, this rhythmic activity affects the impedance of one electrode since it is synchronous with body movements. The other one, involves inhalation/exhalation and it is more frequent in lying positions. This type of artifacts could be identified with commercially produced sensors which measure the respiration and are attached to the recording systems.

Last but not least, **biological processes** or **body defects** may be contamination factors as well. For instance, the changes of skin potentials and resistance is one potential cause

of artifacts. Another key thing to highlight is that sweat imposes changes in impedance between skin and electrodes leading in faulty measurements. Additionally, assymetries and skull defects lead in great deviations for the sensors close to these areas.

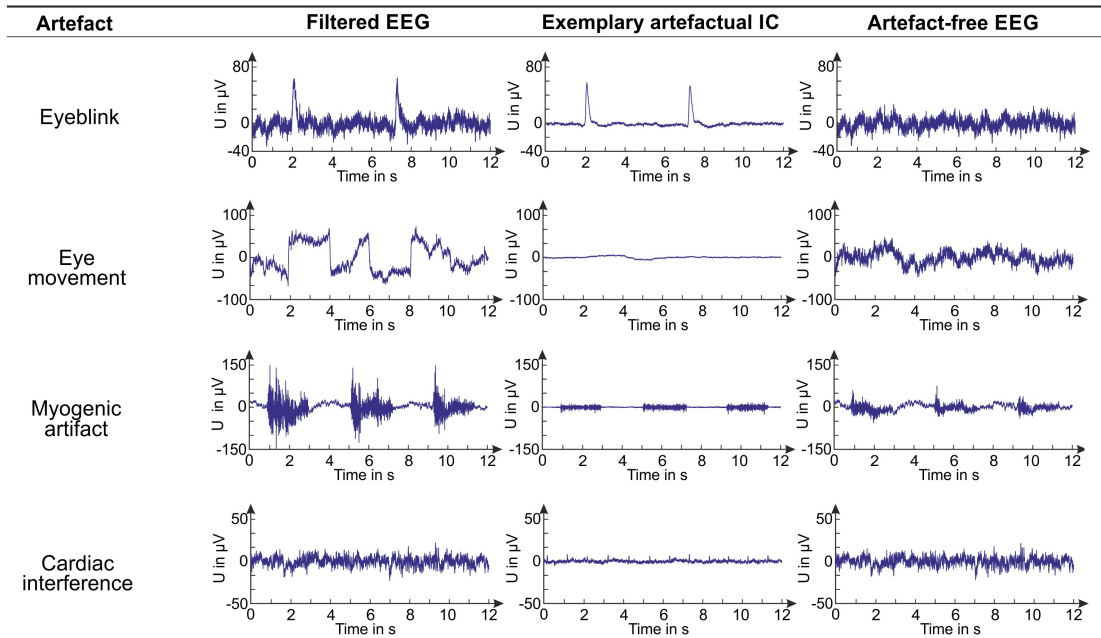


Figure 3.9: Different Types of artifacts in EEG

3.5.2 External and System Artifacts

The brain recordings are prone to the external/ non physiological factors which generate unwanted activity to the signals. Common external artifacts arise due to technology and system setup. The power supply mechanism of these setups induce artifacts known as **Power Line Noise (PLN)** at the specific frequency of 50 Hz (in Europe/60 in US) and its harmonics. The same phenomenon may appear even if the recording is being performed with battery as power supply. In addition, external electronic devices often create electric and magnetic fields which are picked up by the sensors of EEG and MEG. Movement of other persons around the patient could generate capacitive or electrostatic artifacts usually in EEG recording. Other typical artifacts are correlated with either detaching of electrodes from the scalp, which result in extremely high potential differences for a short time followed by a 'dead recording time' since there are no potential changes to capture, or by software bugs and algorithmic design.

In the case of MEG except from PLN the aforementioned are rare but MEG recordings are sensitive to metallic interference. A standard artifact which is characterized by alterations in magnetic field may come from inside the head such as implanted intracranial electrodes or from dental and other metallic prosthetics such as pacemakers. At these cases, sometimes the patients has to undergo demagnetization. However, not all metallic sources can be removed and in such cases the trained specialists make sure that the patients would avoid movements because otherwise unwanted magnetic fields would be generated which affect the whole recording process overlapping in this way the brain activity. Other external magnetic interferences such as cars or earth magnetic field are suppressed by the MSR.

3.6 Differences between EEG and MEG

Despite the fact that both EEG and MEG measure the brain activity they are characterized by some properties and features which could lead in discrimination between those two modalities. As a result there are a number of important differences between EEG and MEG. However first of all, it is advisable to underline that these modalities record electromagnetic activity generated by the same primary currents in the brain [38]. Both modalities have similarities in signals' waveforms since the distributions of potential and fields are dipolar having though a perpendicular relationship due to the rotation of 90 degrees one to another. The sensitivity of these modalities strongly depends on the dipole orientation with MEG being sensitive in **tangential sources** while EEG is able to pick up **deep and radial sources**. The ability of these modalities to identify the components of sources means that they provide complementary information.

It is commonly recognized that they share advantages and limitations and they are chosen for clinical purposes according to the use case. The biggest disadvantage is that they have relatively low spatial resolution (taking into account their exceptional temporal accuracy) compared to other imaging qualities but we could claim that MEG is slightly better than EEG on this aspect. The reason behind this is the limited number of sensors used and according to high resistive skull and conductive scalp the distortion of electrical signals is higher in EEG than MEG. Many scientists rephrased the latter sentence in source localization aspects claiming that MEG offers better accuracy on this research. Furthermore, MEG doesn't require the usage of reference channels to record a magnetic field nor it requires preparation time for the sensors such filling the electrodes with conductive gel.

On the other hand, EEG is much less complex recording system than MEG since it is not equipped with super-sensitive sensors and it doesn't require specially designed rooms for shielding purposes. Another key point which EEG outperforms MEG is when it comes to power supply since EEG could function even with battery supplies offering more flexibility. Another factor when it comes to comparing these modalities is also the cost effect of the setup and of the examination. MEG costs 20 times more than EEG with the same number of channels (high density EEG) and thus EEG is preferable in many cases. Last but not least, EEG has the advantage of the long term video recordings offering extensive temporal sampling across all mind states and cycles.

3.7 EEG, MEG and Epilepsy

As indicated previously, epilepsy is characterized by synchronized neuronal currents which either produce an electrical or a magnetic field. The so-called spikes could provide important information about the irritative zone, an area which produce abnormal functionality in an epileptic seizure, during the presurgical evaluation [39]. In this way prognosis is being improved while the monitoring of the surgery outcome is being facilitated. In order to capture these neuronal behaviour the modalities which are commonly used are the EEG & MEG. The purpose of EEG is to identify epileptiform discharges even though it is rarely used during an epileptic seizure. However, many patients suffer from epilepsy show patterns of abnormal behaviour in resting state recordings which are known as **Interictal Epileptiform Discharges (IED)**. These discharges not only indicate the presence of epilepsy but they are also markers of epileptic foci. For this reason, EEG is an essential tool in the evaluation of epilepsy since it carries prognostic information, guides epileptologists and neurologists for the medication plan

and classifies the type of epilepsy according to the features observed on the brain waveforms.

However, there are some cases that EEG is not able to capture the source of epileptic activity due to the neurogenesis of the current discharges. Specifically, electric fields are more prone to resistive properties of the skull and scalp and thus they could be distorted easily leading to misinterpretation and inability to find the epileptic focus. In these cases the MEG is used being able to capture weak magnetic fields at an excellent temporal scale even though that the amplitude of these fields are orders of magnitude weaker than the interference induced in the recording procedure. MEG recordings in several studies showed good agreement with structural lesions, atrophic areas and functionally abnormal areas which is important for planning the surgical treatment of epilepsy. Furthermore, due to the fact that these modalities complement each other a neurologist could detect components of an epileptiform discharge which is not recognizable in EEG using MEG and vice versa. MEG seems to be more sensitive for neocortical spike sources since it can detect the fast propagation of the epileptiform discharges and at the same time it is helpful for the patients with nonlesional epilepsies because it is equally accurate in the localization compared to invasive recordings which demand guiding to the specific area. Therefore, MEG defines the relationship between the lesion and the epileptogenic cortex due to its accuracy and to its exquisite sensitivity.

3.8 Combined EEG and MEG

Since MEG and EEG yield complementary information, the combined use of these two techniques enhance the localization accuracy of non invasive techniques. The reason behind claiming this is that the origin of both the bioelectric and biomagnetic signals is the bioelectric activity of the tissue. Generally, EEG is considered highly sensitive to geometrical and resistive properties of the head tissues while MEG fails to locate deep sources because of the rapid attenuation of the magnetic fields with depth. Furthermore MEG is unable to detect the radial sources fact which is enhancing the claim that simultaneous recording of these modalities could benefit the brain research. The fusion of these modalities could be proved very useful when it comes to estimating the epileptogenic sources which are measured either on scalp or in gradiometers in a form which is a superposition of activity in the sensor's range (disentangling the sources - **Inverse Problem**). In the epilepsy case studies it has been shown that the combined use of EEG and MEG could improve accuracy and efficiency of source estimation which is translated to better localization of the spike onset [18],[20]. The latter has significant impact on the clinical side of epilepsy aiding the treatment plan, the prognosis and the after-surgery monitoring. Therefore in this research the Combined EEG and MEG (EMEG) is being exploited for localization purposes by simultaneous recordings of an epileptic patient.

Chapter 4

Data Preprocessing

4.1 Recording System and Patient

In this research work the patient was undergone a recording procedure by simultaneous measurement of both EEG & MEG. The system for the MEG Data was acquired by a CTF setup from VSM MedTech Ltd. equipped with 275 axial gradiometers of which the 4 were bad sensors placed in a properly modified Magnetic Shielded Room. The setup for the MEG system has an adjustable bed at its disposal which could be modified in either sitting or supine position offering a variety of examination types. The EEG system is equipped with 72 HydroGel electrodes (along with 6 EOG and 1 ECG channels) while in both systems there are reference channels which record non brain activity such as ocular and cardiac activity ('EOG' and 'ECG' channels) and they are mainly used for regression and cleaning processes. It is worth mentioned that the patient went through a Magnetic Resonance Imaging (MRI) recording in order to obtain an image of the head for possible lesions and abnormal areas. The MRI is a 3 Tesla MAGNETOM recording setup offering a mm^3 accuracy by Siemens Medical Solutions. Data was acquired from a 49 year old female suffering from pharmacoresistant focal epilepsy [20] in six state recordings at 2440 Hz while the MRI was performed on T1, T2 and Diffusion Tensor Imaging (DTI) sequences while the subject signed all the consent forms which were approved by the ethics committee. The recording of diffusion weighted MRI was completed with 1.9 mm edge length, one flat diffusion gradient image and 20 volumes.

4.2 Data Processing with FieldTrip

FieldTrip [40] is a toolbox associated with MATLAB which was developed for data processing of mainly MEG and EEG recordings but it also supports other neurophysiological data. This software has not a user interface but it incorporates high level functions which are grouped according to their use case category (e.g preprocessing functions). It is an open source package which could be combined with other external toolboxes as well offering flexibility in data analysis. It is worth mentioned that supports a variety of recording systems from different vendors.

The FieldTrip functions are high level algorithms which are described by a set of some parameters. These parameters determine the behaviour of the algorithm and many times have default values. A FieldTrip user could change a function's parameters by modifying a configuration structure which stores the values of these parameters and at the same time

could develop new low level functions to incorporate them in the existing methods. A typical FieldTrip configuration structure and data structure is shown in the figure below.

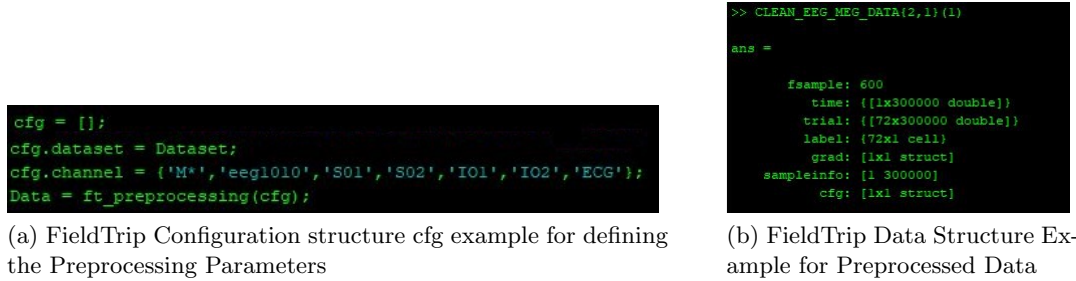


Figure 4.1: FieldTrip Structures Example

In this work the pipeline followed for preprocessing and cleaning the data is depicted in the next flowchart while the steps are explained in the next sections.

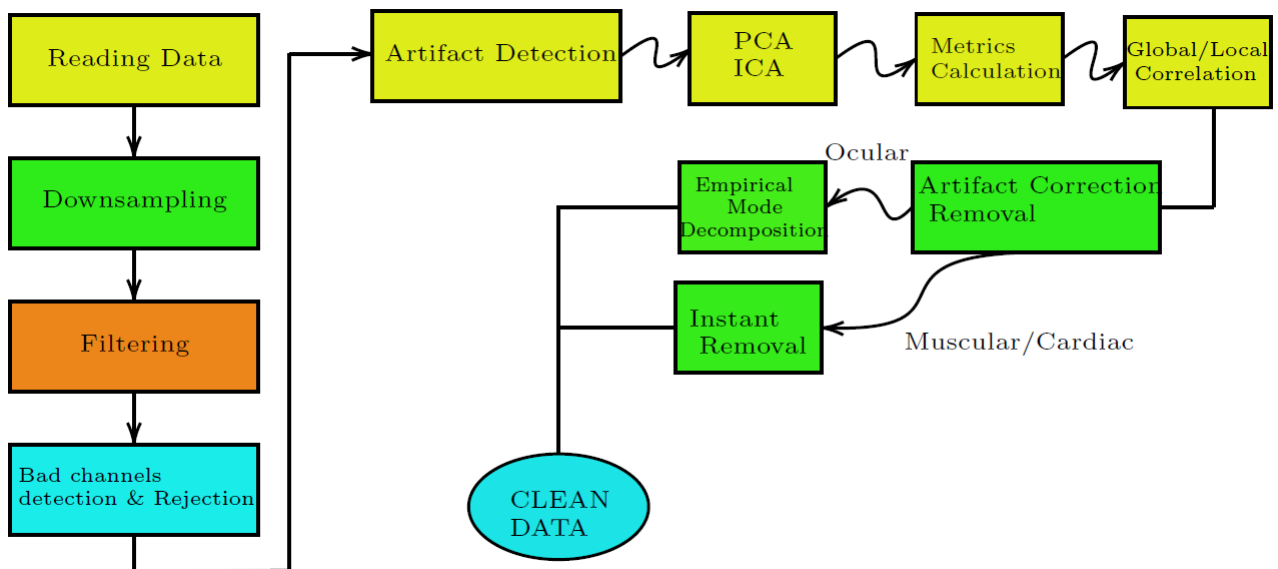


Figure 4.2: Flowchart of Preprocessing Pipeline

Initially, the data acquired by the recording setups are being transformed in Matlab data types through FieldTrip reading functions. The next steps involve the removal of unwanted components and they incorporate downsampling and filtering prior to the component analysis so that the interference from external artifacts is removed. Last but not least, the data are decomposed in Independent Components and they are evaluated by statistical metrics to mark them or not as artifactual components. A detailed procedure is followed in order to reject or to correct these components which is explained in the [section 4.7](#).

Since the data are simultaneously recorded they are stored in the same datatype which was analyzed by FieldTrip and produced a data structure containing the data in a table along with other metadata in the corresponding structure. Specifically, the data table has dimensions of recording channels (343, 271 MEG Channels, 72 EEG channels) by timebins

(approximately 1.2 millions - 2440 Hz, 500 seconds examination time).

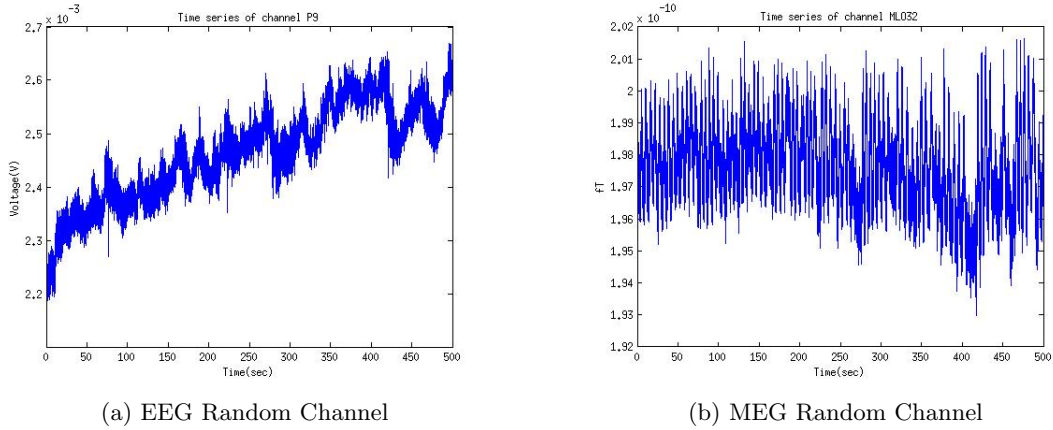


Figure 4.3: Time Series of Random EEG and MEG channels

The figure above depicts either the electrical potential or the intensity of the magnetic field recorded on electrodes and gradiometers correspondingly. In the x-axis time is displayed while on the y-axis the variation of the brain activity in time is represented. The scale of the electrical potential is in milliVolts while the intensity of the magnetic field is in femtoTesla.

4.3 Downsampling and Filtering

The recording procedure is comprised of many timesamples some of which contain redundant information and due to the multi-channel data the percentage of this unwanted information is significant. Henceforth, the preprocessing pipeline contains a downsampling step which aims at retaining the samples with the useful and important information. Moreover, reducing the size, the data processing becomes more efficient since the complexity of the algorithms used is decreasing and they are less time consuming. The original data were sampled with a frequency of 2440 Hz and they were downsampled by a factor of 4 to 600 Hz.

Observing the figure below (Figure: 4.4), we could claim that the waveform of the signals wasn't modified since the downsampling reduces only the sampling frequency. In other words, the waveform remains exactly the same with the only difference that the time axis is comprised of less time-samples, namely 300000 samples. On the question of downsampling's importance and of the optimization offered the frequency domain of the signals was evaluated.

As an illustration of the steps followed for this evaluation, the continuous time waveforms of the signals, $x(t)$ were converted using the Fourier Transform, into the Frequency Domain. The new function is a representation of the frequency spectrum, namely of the frequency distribution of the signals. The continuous Fourier transform is given by the following equation:

$$X(F) = \int_{-\infty}^{+\infty} x(t)e^{-j2\pi Ft} dt \quad (4.1)$$

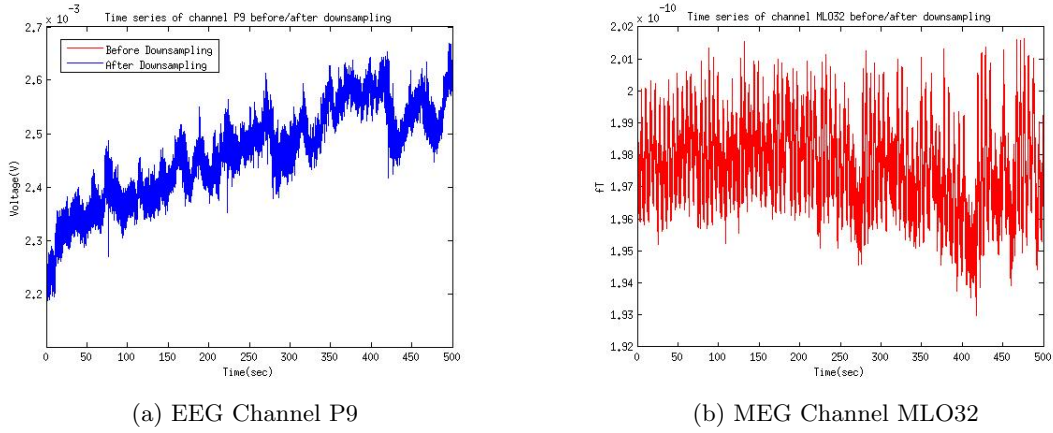


Figure 4.4: Time Series of EEG and MEG channels after Downsampling

Having the channel data in the Frequency domain the energy spectral density was calculated to inspect how the energy is distributed over the frequencies before and after the downsampling. The energy of the signal is given by the following equation:

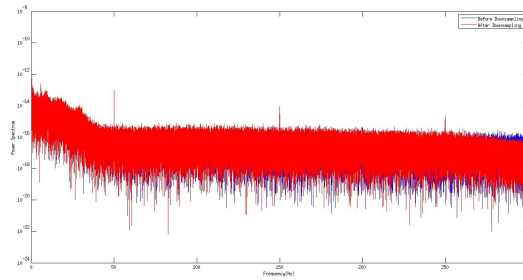
$$E_{xx} = \int_{-\infty}^{+\infty} |x(t)|^2 dt \quad (4.2)$$

Energy could be calculated also in the frequency domain as the Parseval Theorem suggests and the Energy Spectrum Density could be defined as the product of Frequency Representation of the signal with its corresponding Conjugate in the same domain as shown in equation 4.4.

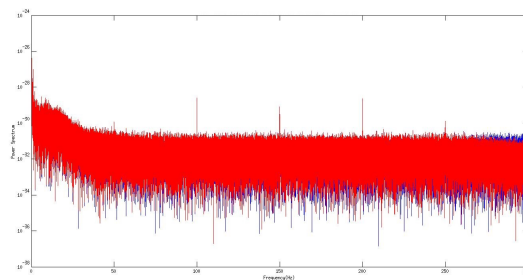
$$\int_{-\infty}^{+\infty} |x(t)|^2 = \int_{-\infty}^{+\infty} |X(F)|^2 \quad (4.3)$$

$$S_{xx}(F) = |X(F)|^2 = X(F)X^*(F) \quad (4.4)$$

The results obtained from this transformation are summarized in [Figure 4.5](#) where the Energy Spectrum Density is shown in a logarithmic scale for an EEG & MEG channel before (blue) and after (red) downsampling. The information extracted from this figure is that the energy distribution over the frequencies slightly falls which means that downsampling removes the timesamples with the negligible portion of energy. The latter is easily observed since the signals before and after the downsampling in each channel are almost identical. Moreover anyone could claim that downsampling is a useful method since it rejects redundant information and at the same time optimizes the data processing significantly.



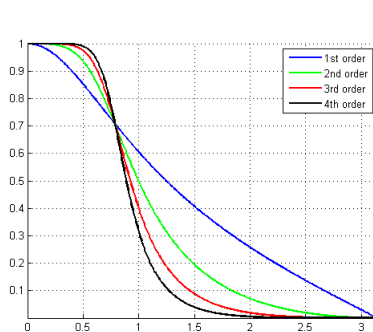
(a) EEG Channel P9



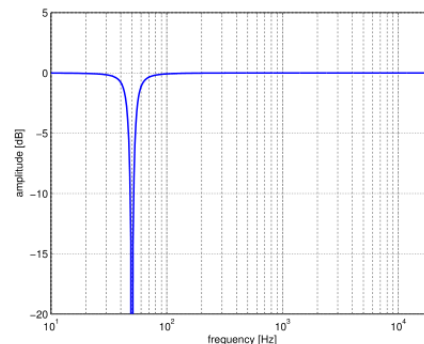
(b) MEG Channel MLO32

Figure 4.5: Energy Spectrum Density of EEG and MEG channels before/after Downsampling

The downsampling was followed by data filtering for removing the noise and for focusing on the band of interest. For epilepsy studies the band of interest is often between 1 and 100 Hz since at these frequencies the most abnormal brain states occur [41]. As a consequence of this the filters used were a **4th order (empirically defined) Butterworth bandpass filter** (see Figure: 4.6) for the band of interest and a **Notch filter** for removing the Power Line Noise Interference with a cutoff frequency of 50 Hz (The utility frequency in Europe) and its multiples. The reason why the Notch filter was applied also on multiples of 50 Hz is that PLN is being distributed in arcs and the arcs occurs twice in each cycle. In this way PLN Harmonics, as they are also known as, are restricted.



(a) Butterworth filter in 4 different design orders



(b) Notch Filter/ Cut-off Frequency 50 Hz

Figure 4.6: Filters Chosen for Data Preprocessing

The filtering procedure was implemented using the FieldTrip's `ft_preprocessing` function defining the cutoff frequencies and the type of the filters in the corresponding parameters. Regarding the filtering results Frequency Domain was once again selected to visualize the Energy Spectrum Density before and after the filtering as shown in Figure: 4.7. As illustrated in this figure, the energy spectrum density is decreased after 100Hz which confirms the cut off impact of the Butterworth filter after this specific frequency. Furthermore the narrow gaps at the red waveform (after filtering) on 50 Hz and its multiples is the Notch Filter effect.

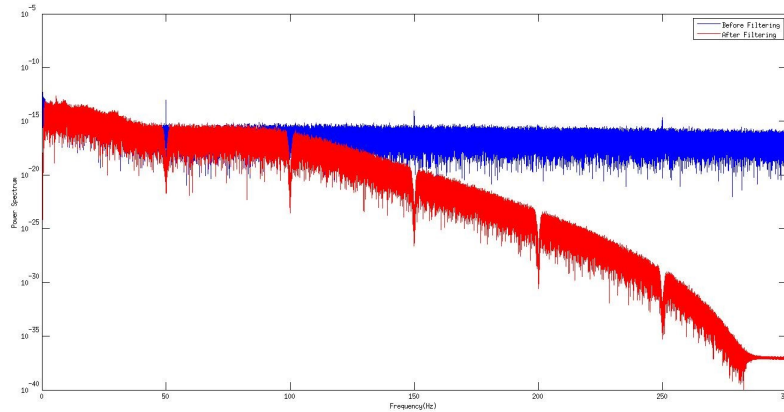


Figure 4.7: Energy Spectrum Density Before/After Filtering of a random EEG channel visualized in Logarithmic scale

4.4 Correcting noisy channels' signal

The next step of the preprocessing was to detect if there were channels with noisy data in order to reject them since they are comprised of information which is outlier compared to the other sensors. During a recording procedure some sensors could produce faulty measurements due to bad friction or due to several misfunctionalities. In order to proceed in such evaluation process the first task was to split the data structure into two, one for MEG and one for EEG to inspect the data separately. Another important thing to highlight is the plan followed to detect the bad channels. To give an illustration of that, we considered the use of some metrics. The reason behind this is that since these channels are outliers they cause high variance in their distribution and possibly this noisy behaviour is also reflected on **kurtosis and z-value**. The former evaluates the gaussian behaviour of a distribution while the latter calculates the deviation of the mean of the bad channels from the mean of the rest of the channels. With this in mind we exploited the `ft_rejectvisual` function and we calculated the aforementioned metrics for each channel of the two data structures. The values of these metrics were illustrated as a scatter plot and we marked the outlier values by visual inspection (as shown in an example at Figure: 4.8). The results of this marking led to the following bad channels: 'Pz', 'F2', 'P6', 'TP9', 'TP10', 'C5'. All these bad sensors are EEG channels while for MEG no channel was marked as artifactual one confirming the opinion of physiologists that all MEG channels are properly recording the brain activity.

However, the noisy sensors were not rejected but they instead were repaired. In order to correct the outlier signals of these sensors a reconstruction approach was considered using the activity measured by the neighbour sensors. Regarding the finding of the neighbours of faulty channels a triangulation method was used which constructs triangles based on 2D projections of the sensor location. After detecting the neighbours, the signals were reconstructed by using the weighted average of neighbours' signals. This was achieved with the `ft_channelrepair` function which determined the distances as the weights and the results were inspected with the `ft_databrowser` as the next figures portray:

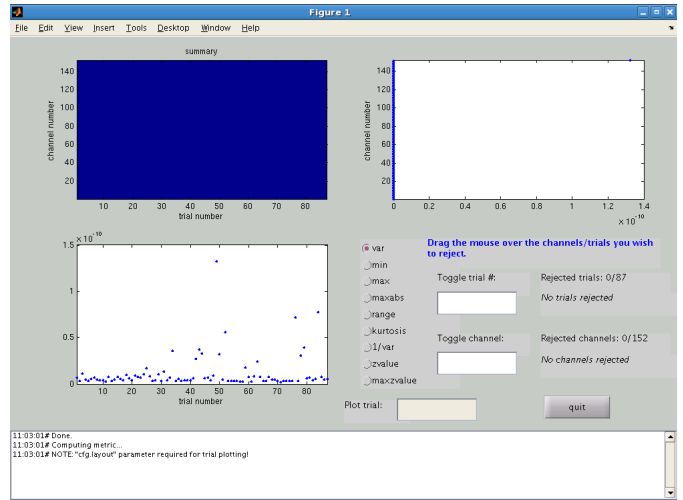


Figure 4.8: User Interface Window in Fieldtrip for Marking Bad/Noisy Sensors

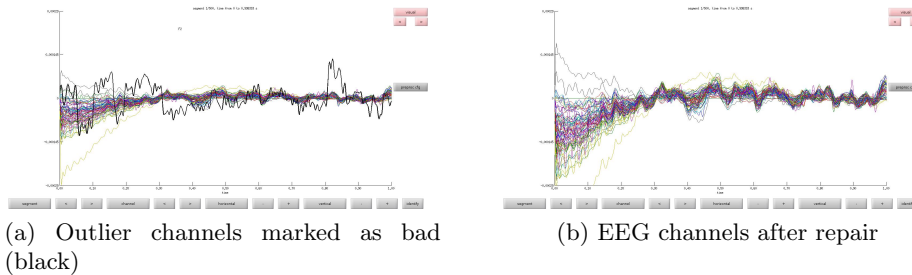


Figure 4.9: Time segment of EEG Channels before/after noisy channels reconstruction

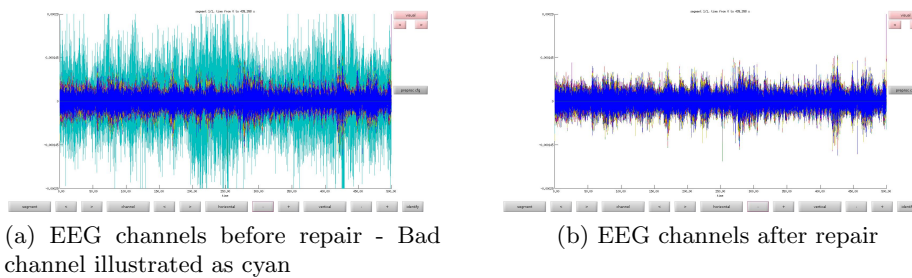


Figure 4.10: Visual inspection of EEG before/ after reconstruction of bad channels in the whole time range

4.5 Component Analysis

Multichannel recordings of electrophysiological data generate vast amount of data and there are several times that they cause overlapping of brain activity with external sources

and biological processes. In order to explore the electrophysiological underpinnings of brain networks and to interpret the brain behaviour at several states a data reduction and decomposition technique is compulsory. In computational neuroscience and in several other scientific disciplines **Component Analysis** is being adopted to perform a means of data cleaning by reducing the dimensionality and thus their size but also by decomposing the information in components which are different (**uncorrelated or independent**, see next sections) one another. These components often carry the most useful percentage of information and in this way they are distinctive characteristics of the data. The two renowned techniques which prevail in this field are **Principal** and **Independent** Component Analysis and most of the times are combined for optimal results.

4.5.1 Principal Component Analysis

Principal Component Analysis (PCA) is the one of the most popular multivariate statistical techniques which identifies patterns and expresses the data in a way of pointing out their similarities and the differences. These patterns are difficult to be discovered in multichannel and therefore multidimensional data since the graphical representation of them is not available. This technique is appropriate when there are recordings on observed variables and wish to develop a smaller set of variables, called **Principal Components**, that will account for the largest possible portion of the data variance [42],[43]. The new variables are derived by a linear transformation of the data to a set of coordinates that are represented by an orthogonal axis while the extracted points have a declining order regarding the value of variance. Therefore, the first Principal Component encompasses more information compared to the second one. At this point it is worth mentioned that the components are uncorrelated, meaning that there is no linear relationship between them. Overall, this method allows the reduction of the total amount of data of at least 90% because of the fact that the first components contain more than this percentage of the initial data.

PCA tries to uncorrelate the information from the initial complex data that they have multiple dimensions. In the simple case of two dimensional data the redundant data could be found by the slope of the line which expresses the data points. In order to perform reduction of the data size in multidimensional data PCA utilizes the covariance matrix of the observed mixture vector. The recording data is composed of m row vectors of n dimensions with the m expressing the channels (sensors) and n the time samples. In order to proceed with the PCA technique the covariance matrix needs to be calculated. In the matrix case their covariance c is defined by their inner product as follows after subtracting the mean to place the vector in the center (important step for PCA to work properly):

$$c_{\chi_1\chi_2}^2 = \frac{1}{n-1}(\chi_1 - E[\chi_1])(\chi_2 - E[\chi_2])^T = \frac{1}{n-1}\chi_1\chi_2^T \quad (4.5)$$

On the other hand for multidimensional data the covariance C_X is defined as shown below:

$$C_X = \frac{1}{n-1} \sum_{i=1}^m \sum_{j=1}^n (\chi_i - E[\chi_i])(\chi_j - E[\chi_j])^T = \frac{1}{n-1} X X^T \quad (4.6)$$

The covariance matrix is normalized by the factor of $1/n-1$. In a 3-Dimensional example of data with x,y,z being the dimensions the covariance matrix values are:

$$\begin{bmatrix} \text{cov}(x, x) & \text{cov}(x, y) & \text{cov}(x, z) \\ \text{cov}(y, x) & \text{cov}(y, y) & \text{cov}(y, z) \\ \text{cov}(z, x) & \text{cov}(z, y) & \text{cov}(z, z) \end{bmatrix}$$

PCA aims at finding an orthonormal matrix P so that the covariance matrix of Y is diagonal where Y is expressed as :

$$Y = PX \tag{4.7}$$

In fact Y comprises the new compressed representation of the data while P contains the Principal Components in its rows. The PCA relies on the eigenvalue decomposition method by calculating the eigenvalues from the covariance matrix. PCA diagonalizes the covariance matrix following the steps described below using linear algebra properties:

The covariance matrix of P is determined as:

$$C_Y = YY^T \stackrel{(a)}{=} PX(PX)^T = PXX^T P^T = PC_X P^T \tag{4.8}$$

where, the equality (a) is derived by equation (4.7).

Since C_X is symmetric it could be decomposed according to **Eigen Value Decomposition (EVD)**:

$$C_X = EDE^T \tag{4.9}$$

where E : is the eigenvector matrix and D is the diagonal matrix of eigenvalues. At this point we assume that P is orthogonal meaning that $P^{-1} = P^T$. Also we know that PCA aims at solving the equation (4.7) by choosing the P as the matrix that contains the eigenvectors in each row of P . Therefore $P = E^T$. Replacing this equation in (4.9) we obtain

$$C_X = P^T D P \tag{4.10}$$

Last but not least, covariance of compressed representation of initial data Y is expressed as:

$$C_Y = P(P^T D P)P^T = P P^T D P P^T \stackrel{(a)}{=} P P^{-1} D P P^{-1} = D \tag{4.11}$$

where the equation (a) is true due to the fact that P is orthogonal. Henceforth, from the last equation it is clear that P diagonalizes the covariance matrix of Y which is the initial goal of PCA.

After proving that choosing P diagonalizes the C_Y the steps need to be followed at a PCA procedure could be summarized in the following bullets:

- Subtract the mean

This process centers the data and produces a set of zero-mean signals

- Calculate the covariance matrix
- Calculate the eigenvectors and eigenvalues

These features are calculated by solving the equations $Ax = \lambda x$ and $\det(A - \lambda I) = 0$ correspondingly

- Reduce the dimensionality and form the feature vector

The eigenvector with the highest eigenvalue is the principle component of the dataset. The next step is to order them by highest eigenvalue to the lowest. At this point the number of these components are chosen according to the desired percentage of information to be retained. This criterion is known as Percentage of useful information (PUI) and is user defined as explained below.

- Deriving the new data

The final step of PCA is to express the initial data in a compressed form using the feature vector of retained eigenvectors (based on PUI) multiplied by the transposed original data as also the equation (4.7) suggests. Therefore **FinalData= RowFeatureVector x RowDataTranspose**

One of the most important steps of PCA is to select the number of the components which best express the data and reduce their dimensionality. In order to decide which is the appropriate number of Principal Components one should consider that Principal Components are ordered according to the value of eigenvalues and therefore of the percentage of the information they carry. The user therefore defines a percentage above 90% since the components that PCA retains contain more than this amount. The criterion for taking such decision is the Percentage of Useful Information or also known as PUI and is defined as the fraction of eigenvalue of one channel to the total amount of the eigenvalues [44].

$$PUI_i = 100 \frac{\lambda_i}{\sum_{k=1}^n \lambda^k} \quad (4.12)$$

4.5.2 Blind Source Separation

Another popular method in the field of Decomposition into components for optimizing either multidimensional data processing or image processing is the **Blind Source Separation (BSS)**. This is a problem that finds the Independent Component Analysis background. Turning now to the BSS technique, as the name suggests it aims to extract original source signals from mixed ones. This could be achieved by estimating a mixing function using only the available observed mixed signals. The term 'Blind' is justified by the fact that the mixing function is unknown and that the only a-priori knowledge we have is that the signals are statistically independent [45]. An important application of this method is a situation where there are a number of signals emitted by physical objects or sources such as different brain areas emitting electric signals; people speaking at the same time in the same room or mobile phones emitting radio waves [46].

Let us now assume that there are sensors in different positions in order to record the mixture of the signals with different weights though and that there are 3 sources (s_1, s_2, s_3) which produce an observed matrix of signals x at different time points. The mathematical formulation of the mixing procedure is shown below having some weights $a_{i,j}$ multiplied with the sources that point out the distance from the sensors.

$$\begin{aligned} x_1(t) &= a_{1,1}s_1(t) + a_{1,2}s_2(t) + a_{1,3}s_3(t) \\ x_2(t) &= a_{2,1}s_1(t) + a_{2,2}s_2(t) + a_{2,3}s_3(t) \\ x_3(t) &= a_{3,1}s_1(t) + a_{3,2}s_2(t) + a_{3,3}s_3(t) \end{aligned} \quad (4.13)$$

The BSS problem consists of finding the original signals from the mixed ones or in other words to estimate a matrix W which unmixes the observed signals such that the sources could be separated. The unmixing of the recorded signals entails that the weight matrix A (composed of all weights $a_{i,j}$) are different so that the inverse matrix of W exists and could be defined.

$$\begin{aligned} s_1(t) &= w_{1,1}x_1(t) + w_{1,2}x_2(t) + w_{1,3}x_3(t) \\ s_2(t) &= w_{2,1}x_1(t) + w_{2,2}x_2(t) + w_{2,3}x_3(t) \\ s_3(t) &= w_{3,1}x_1(t) + w_{3,2}x_2(t) + w_{3,3}x_3(t) \end{aligned} \tag{4.14}$$

However due to the restriction of the a-priori knowledge of the weight coefficients $a_{i,j}$ the calculation of W matrix as the inverse of A is not feasible. To estimate the matrix W one should consider and assume that the signals y are statistically independent or in other words that the signals x are not gaussian.

$$\begin{aligned} y_1(t) &= w_{1,1}x_1(t) + w_{1,2}x_2(t) + w_{1,3}x_3(t) \\ y_2(t) &= w_{2,1}x_1(t) + w_{2,2}x_2(t) + w_{2,3}x_3(t) \\ y_3(t) &= w_{3,1}x_1(t) + w_{3,2}x_2(t) + w_{3,3}x_3(t) \end{aligned} \tag{4.15}$$

In such situation the signals y and sources s are identical. Summarizing the BSS problem could be depicted in the figure below which represents the unmixing network.

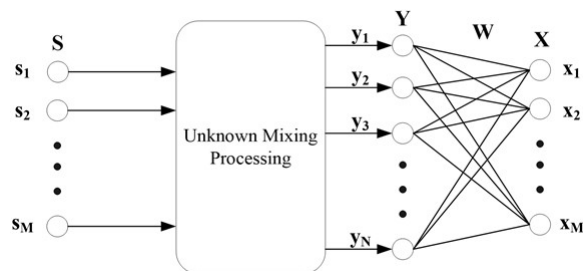


Figure 4.11: BSS Network

Adapted from Jing Wang, Qing Zhang et. al. 2013

A typical example of BSS application is what is known as **Cocktail Party Effect**. This phenomenon refers to human ability to selectively recognize one auditory source in a noisy environment [47]. This problem suggests the multiple disturbances such as loud speaking and music in a crowded place where a person filters out this information to focus on the conversation with another one. Similarly BSS separates the mixed signals by following a standard flow as shown below (Figure: 4.12) having a filtering procedure (Whitening) at the beginning which estimates the mixing coefficients and then it calculates the unmixing matrix to separate the input signals.



Figure 4.12: BSS Standard Flow

Adapted from PathPartnertech.com

4.5.3 Independent Component Analysis

Independent Component Analysis (ICA) is an extension of PCA and the goal of this technique is to find projections of the data that maximize their independence. As previously stated ICA is founded on the basis of BSS and unlike PCA which tries to perform an uncorrelation of the data, ICA uses higher-order statistics to decompose the data into independent, non-gaussian components. ICA was originally developed to deal with problems such as Cocktail Party Problem while nowadays is mainly used on fields such as electrophysiological data processing revealing activity which is not observable from the mixed signal. An illustration of such use case is the brain activity measured by either EEG or MEG where the observed signals are a mixture (superposition) of brain electrical potentials/magnetic fields from a sensor's neighbour. Exploiting ICA a physician could examine the underlying brain sources discovering thus, the actual brain activity which indicates abnormal or not states and behaviour. Moreover, unlike PCA, ICA's Components (Independent Components) are equally important and they are not orthogonal one another.

ICA is a generative model which describes the mixing procedure of the observed data. It is evident that Independent Components (sources) cannot be observed since the mixing coefficients weights are unknown and this comprises the goal of this method. Specifically it is focusing on estimating both the sources and the mixing weights. Let us denote X a vector of the observed signals with n elements while A is the matrix with the mixing weights with the $n \times m$ rank and s the source vector with m values. At this point it is worth mentioned that $m \leq n$. The mathematical formulation of ICA could be explained by the following equation which aims at estimating both A and s .

$$X = As \quad (4.16)$$

Since only X is known the A, s have to be estimated blindly from the observed signals. As a consequence ICA model is transformed and it is focusing in finding an unmixing matrix W which will approach more the unknown sources:

$$S = WX \quad (4.17)$$

In order to solve the aforementioned equation ICA makes some assumptions since only X is known.

4.5.4 Assumptions and Ambiguities of ICA

ICA demands some conditions to be fulfilled in order to estimate properly the matrix W which reestablishes the statistical independence. Therefore, certain assumptions have to be made. The most important is that **the sources are statistically independent**. In

order for a condition like this to be true the joint probability density function of the sources need to be examined. If this function is equal to the product of sources' probability densities function then the sources are independent. This point is where the PCA & ICA differ since independence is stronger than uncorrelatedness. The figure below highlights this difference. It is clear that independence doesn't mean orthogonal components as in PCA's case while at the same time ICA finds the original coordinates.

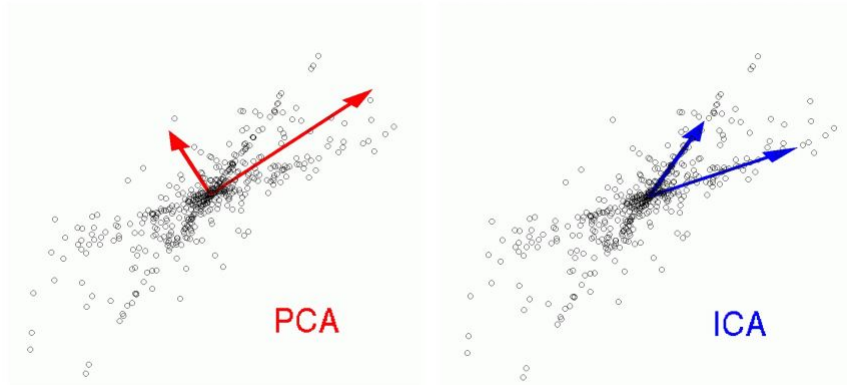


Figure 4.13: PCA maximum variance directions and ICA independent components

Another important aspect of ICA's assumptions is that the **Independent Components should not be Gaussian**. Gaussian properties are strongly connected with dependence properties since sum of two or more Gaussian variables lead to Gaussian distribution. Therefore ICA cannot estimate independent components under such circumstances. The basic idea behind ICA is the maximization of nongaussianity but also allows at only one source to be Gaussian in order to be separable. Last but not least, an optional assumption that ICA follows is that **the unknown mixing matrix is square** or in other words **number of independent components is equal to the number of observed variables**. This assumption simplifies the solution because if mixing matrix is square then it is also invertible and thus the unmixing matrix exists. However in many cases prior to ICA, PCA is applied to reduce the dimensionality and thus mixing matrix A is no longer square. In this case the unmixing matrix is estimated by the Pseudo-inverse of A ($W = A^+$).

Having defined the ICA's assumptions there are also some ambiguities when it comes to the solution. Specifically, the **energies of independent components is unknown** since the sources are scalarly multiplied by unknown weights that they can be easily cancelled out. Henceforth, the magnitude of the sources is also unknown. Last but not least, the estimated sources may be recovered **in different order** which is a consequence of the lack of knowledge for mixing matrix A and sources s .

4.5.5 Mathematical Formulation of ICA

Taking into consideration all the assumptions for the ICA model the steps of solving the unmixing problem involve some procedures called **centering and whitening**. An important aspect of ICA preprocessing steps is the mean subtraction (zero mean-centering) which simplifies the algorithm and the next steps. In this way the mixing matrix doesn't change

and thus the estimation process is not affected. The centering process is followed by the whitening which transforms the mixing matrix in a new one B of which its components are uncorrelated with unit variances. The uncorrelation is being achieved with PCA which uncorrelates the data and maximizes their variance. The whitening problem is defined as given an observed matrix the goal is to find a linear transformation B which transforms the data to a new set Z .

$$Z = BX \quad (4.18)$$

In order to perform the whitening the EVD technique is adopted again similar to the PCA. First of all the covariance matrix C_z can be expressed as follows because of the previous equation:

$$C_Z = ZZ^T = BXX^TB^T = BC_XB^T \quad (4.19)$$

The matrix Z will be white if its covariance is equal to the identity matrix.

$$C_Z = BC_XB^T = I \quad (4.20)$$

Applying the EVD decomposition, similarly with PCA, on covariance matrix we will obtain :

$$C_Z = EDE^T \quad (4.21)$$

However this equation can be rewritten as:

$$C_Z = ED^{1/2}D^{1/2}E^T \quad (4.22)$$

Replacing the X with $X = B^{-1}Z$ which result from (4.18) we obtain:

$$C_X = B^{-1}Z(B^{-1}Z)^T = B^{-1}ZZ^T(B^{-1})^T = B^{-1}C_Z(B^{-1})^T \quad (4.23)$$

Combining the (4.22) and (4.23) we obtain:

$$B = D^{-1/2}E^T \quad (4.24)$$

The last step is to prove that whitening is performed correctly (Unit Covariance) we replace (4.24) to (4.20)

$$BC_XB^T = D^{-1/2}E^T C_X (D^{-1/2}E^T)^T \quad (4.25)$$

C_X is symmetric and thus it can be decomposed according to EVD ($C_X = EDE^T$). For this reason, (4.25) is transformed as:

$$\begin{aligned} BC_XB^T &= D^{-1/2}E^T EDE^T (D^{-1/2}E^T)^T = D^{-1/2}E^T EDE^T (ED^{-1/2}) = \\ &= D^{-1/2}DD^{-1/2} = D^{-1}D = I \end{aligned} \quad (4.26)$$

where $D^{-1/2}$ is a simple computational componentwise operation and is a diagonal matrix [46]. Since covariance matrix is equal to the identity matrix the whitening procedure is succesful and we could claim that the estimation parameters are less fact which can be proven on the following equation where the estimated sources are equal to the new mixing matrix multiplied by the initial sources.

$$Z = BX = BAS = \tilde{B}S \quad (4.27)$$

where \tilde{B} is the transformed mixing matrix with which ICA estimates just $n\frac{n-1}{2}$ parameters instead of n^2 which is equivalent with the parameters of A. The reason behind this is that we restrict the search for the mixing matrix in the orthogonal space (covariance of the mixing matrix is equal to identity. Thus, the new mixing matrix is orthogonal) [46]. However, the whitening (orthogonality) is not enough but it solves half the problem. The rest of the parameters are being estimated by methods which are **minimizing or maximizing high order independence statistic metrics**.

The orthogonal principal components identified with PCA in the whitening procedure are uncorrelated which means that their covariance is zero. Uncorrelated vector doesn't imply that they are also independent. The independence is defined if their joint probability density function is factorisable on its marginal probability densities.

$$p(s) = p(s_1, \dots, s_k) = \prod_{i=1}^k p(s_i) \quad (4.28)$$

In other words, independence of the sources means that their marginal distribution contain no information on each other. The aforementioned guides ICA for approximating statistical independence which implies also uncorrelation. The latter, is the reason why whitening doesn't affect the independent components. In order to approximate statistical independence ICA measures high order statistic metrics such as **Mutual Information, Negative Entropy** and **Non-Gaussianity** which are introduced below.

The mutual information measures how much information is shared among variables. To define mutual information another important definition should be conducted. **Entropy H** of a discrete random variable s measures the amount of information contained in the random variable s or the levels of uncertainty for this specific random variable. It could be defined as:

$$H(s) = - \sum_i p(a_i) \log p(a_i) \quad (4.29)$$

where a_i are the possible values of s. Mutual information therefore, is defined using entropy.

$$I(s_1, \dots, s_k) = \sum_{i=1}^k H(s_i) - H(s) \quad (4.30)$$

It is clear that mutual information should be zero between independent components. Having said that, independence between components could be approximating by minimizing the mutual information between them.

A similar metric which is rephrasing the previous plan for approximating independence is **Negentropy**. Gaussian variables have the largest entropy among all random variables of equal variance. Negentropy J is defined as:

$$J(s) = H(s_{gauss}) - H(s) \quad (4.31)$$

where s_{gauss} is a Gaussian random variable. The significance of negentropy is founded on the fact that it differs from mutual information only by a constant C.

$$I(s_1, \dots, s_k) = C - \sum_{i=1}^k J(s_i) \quad (4.32)$$

Consequently, maximizing negentropy is associated with the minimization of mutual information thereby estimating the independence. Last but not least, since negentropy measures the difference between gaussian distribution and of the sources' distribution, independence could be approximated directly by estimating the **non-gaussianity**. Some metrics used to measure non-gaussianity are **skewness and kurtosis**. Kurtosis is the most popular and it defined as:

$$kurt(s) = E[s^4] - 3E[s^2]^2 \quad (4.33)$$

However, s is assumed to have unit variance thus kurtosis is simplified to : $E[s^4] - 3$. The values of kurtosis define the non-gaussianity. Particularly, gaussian distributions have zero-value in kurtosis whereas super-gaussians have positive values and sub-gaussians have negative kurtosis as shown in figure below.

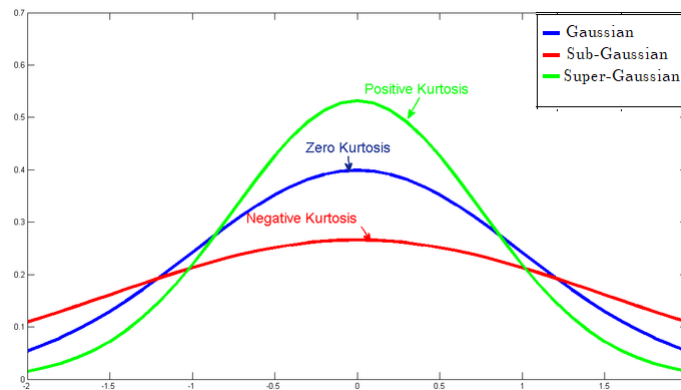


Figure 4.14: Kurtosis values and non-gaussianity

Kurtosis is a tool for approximating independence by means of non gaussianity which is computationally very efficient and the concept of non-gaussianity is used in this thesis to calculate the independent components after the whitening (PCA) procedure using the **Extended Infomax Algorithm**.

4.5.6 Extended Infomax Algorithm

ICA method decomposes a set of observed data into independent components by applying a first step of whitening and another one of approximating independence through the maximization/minimization of the aforementioned statistical metrics which is also known as learning procedure. Several algorithms exist to estimate these components such as Infomax [48] which maximizes the mutual information or fastICA [49] which tries to maximize the non-gaussianity. Extended Infomax [50] is an algorithm which, as the name suggests, extends Infomax and separates mixtures of sources from non-gaussian distributions. ICA's goal is to estimate a transformation of mixing matrix B as shown in (4.27). Extended Infomax uses a learning rule associated with Maximum Likelihood to estimate B . In order to derive the learning rule the p.d.f. of the observations x is required.

$$p(X) = |\det(B)|p(Z) \quad (4.34)$$

where $p(Z)$ is the distribution of the sources. The log-likelihood of the previous equation is expressed as:

$$L(Z, B) = \log|\det(B)| + \sum_i^N \log p_i(z_i) \quad (4.35)$$

The maximization of log-likelihood with respect to B sets up a learning rule for B :

$$\Delta B \propto [(B^T)^{-1} - \phi(Z)X^T] \quad (4.36)$$

where $\phi(Z)$ declares the non-linearity [51]. To maximize the log-likelihood natural gradient is being utilized according to the following equation:

$$\Delta B \propto \frac{\partial L(B, Z)}{\partial B} B^T B = [I - \phi(Z)Z^T]B \quad (4.37)$$

where I is the mutual information of the observed vector X . This learning rule is simplified by the $B^T B$ factor and it could be deduced to the simple Infomax Rule if the ϕ is selected as $\phi(Z) = 2\tanh(Z)$ where \tanh represents the hyperbolic tangent function.

$$\Delta B \propto [I - 2\tanh(Z)Z^T]B \quad (4.38)$$

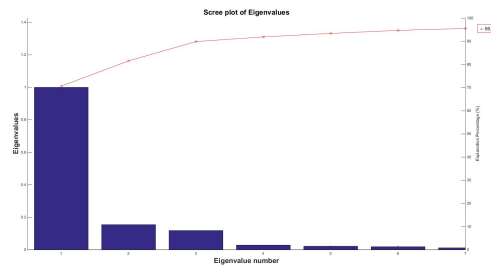
Extended infomax algorithm aims at separating sources with a variety of distributions given a fixed nonlinearity ϕ . However, we could claim that the distribution of the sources are generally either super or sub Gaussian having assumed first that they are not Gaussian. The extended infomax provided two learning rules for distinguishing the distribution type of the sources as follows:

$$\begin{aligned} \Delta B &\propto [I + \tanh(Z)Z^T - ZZ^T]B : \textit{subgaussian} \\ \Delta B &\propto [I - \tanh(Z)Z^T - ZZ^T]B : \textit{supergaussian} \end{aligned} \quad (4.39)$$

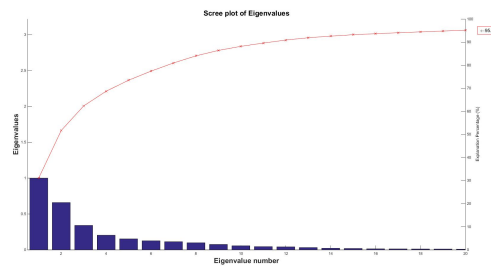
In the preceding learning rule one could observe that the only difference between the two non-gaussian distributions is the sign of the hyperbolic tangent. This sign could be defined either by employing kurtosis [52] or by stability criteria [50]

4.6 Artifact Detection

In a neurophysiological measurement there are several factors and components that contaminate the signal and thus distort the brain activity in which we want to focus for medical diagnosis and treatment purposes. In an EEG and MEG recording this interference stems from external or physiological sources as explained in the previous chapter. To reject such contamination we need to detect it and to classify its origin in order to decide whether or not we should eliminate it. In order to characterize a component as artifactual we firstly performed PCA to reduce the dimensionality of the data facilitating the smooth performance of the ICA. The redundance of the information was decreased by defining the PUI criterion at 95% and thus PCA retained only the most significant components the sum of which, contained information approximately equal to the desired percentage. An example of the retained components using PCA for one state recording is depicted in the [Figure: 4.15](#). In this figure the Principal Components are in order based on the percentage of information they contain. Henceforth, the first component embodies the most information, fact which confirms the validity of Principal Component Analysis that incorporates a step of eigenvalue sorting.



(a) PCA for EEG Data



(b) PCA for MEG Data

Figure 4.15: PCA on EEG/MEG data based on PUI criterion at 95%

The following part of the Component Analysis moves towards the ICA application on the Principal Components which reduced the dimension of mixing matrix thereby reducing the complexity of the ICA. This method was implemented taking advantage of FieldTrip's `ft_componentanalysis` defining as input parameters the number of the Principal Components, the `'runica'` and `'extended=30'` arguments which are equivalent with ICA and Extended Infomax correspondingly. Last but not least, the learning rule of this machine learning method is set by default on 512 iterations (steps).

The use of Component Analysis suggests a strong link between the Independent Components and the Artifact Detection plan which is depicted in the [Figure](#): 4.16. The following sections offer a detailed account of this plan. In a nutshell, the detection plan is comprised of 3 phases each of which involves the Independent Components (ICs) of both EEG and MEG data. Specifically, in the *Phase A* the ICs are being visualized and inspected in order to get a first insight on possible artifactual components. In addition, on *Phase B* for every IC the metrics **Kurtosis**, **Skewness**, **Entropy**, [53], which have typical values for artifacts (as will presented in the following sections), are calculated and according to some thresholds the components are characterized as suspicious contamination factors. Having discussed how to 'set some components in quarantine', the final phase (*Phase C*) of this plan addresses ways of correlation of the components with the channels that record non-brain activity such as Ocular (EOG) and Cardiac (ECG) channels. In other words the last step either correlates the whole component or segments of it with these channels. If the suspicious components of previous steps match the components of which the correlation values exceed a certain threshold then these components are marked as artifacts and based on which channel they have stronger link they are associated as cardiac, ocular or other type of artifacts.

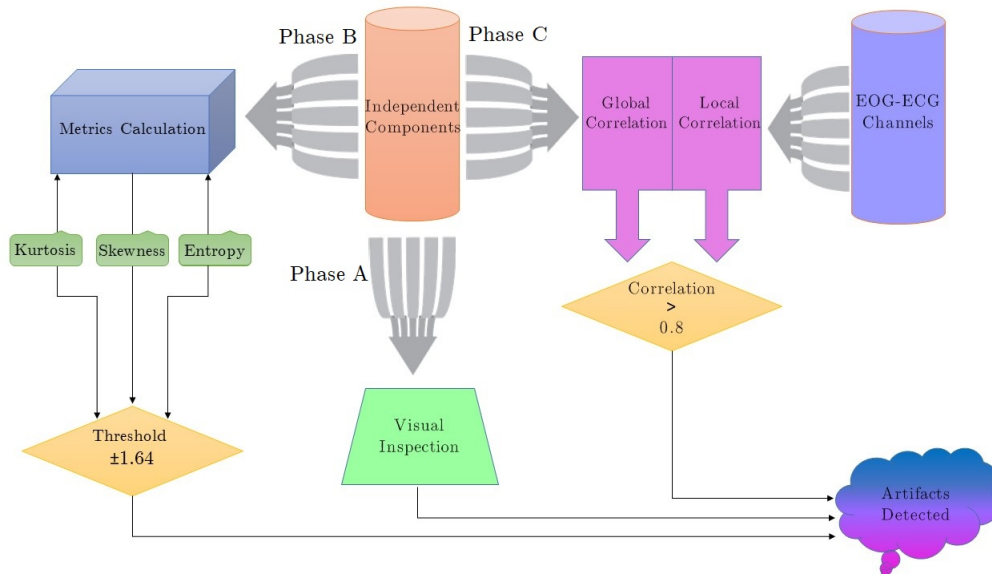


Figure 4.16: Artifact Detection Plan

4.6.1 Visual Inspection of Components

As previously stated, the first phase of artifact detection plan is the visual inspection of the Independent Components. In order to visualize the ICs the function `ft_topoplotIC` was used which takes as input the components and plots a topographic distribution of the IC on the 2D head at circular view observing from the top. Moreover the coefficients of mixing matrix A which represent the weights on the mixture of the signals are being visualized with a color map. The latter indicates the intensity of brain activity on a special region. In more details red color is equivalent with strong activity while yellow and orange are mild activity and blue is the activity with negative potential. The topographical representation of the ICs for both EEG and MEG at one state recording example are depicted below:

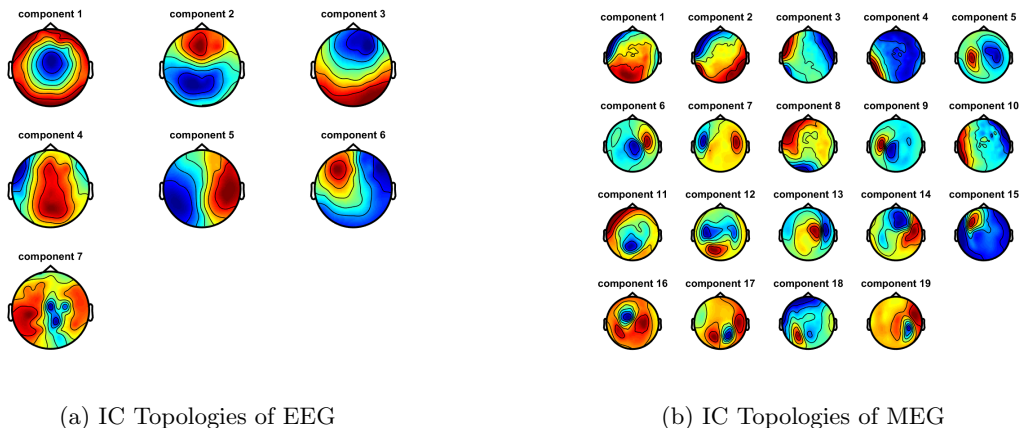


Figure 4.17: Topographic Distributions of Independent Components at 4th state run recording

The topologies of the Independent components could offer us an insight on the non-brain

activity by recognizing strong activity in areas that are associated with biological processes such as occipital lobe for vision or strong activity in the frontal lobe which might indicate that the frontal electrodes captured ocular movements and blinks. Another type of possible contamination might be the activation in the left hemisphere of the brain which is accredited to the cardiac activity and especially because of the position of the heart at left part of the body. Having said that we could estimate which components might be suspicious. On the EEG case **IC2** has strong activity on the frontal lobe which might be associated with eye movements and therefore may be an ocular artifact. On the other hand also **IC7** has activations on the left temporal lobe which could indicate cardiac activity. On MEG case **IC3, IC4, IC8 and IC11** might be suspicious for corresponding reasons. However the topographic distributions are not enough proof of artifactual interference and thus time waveforms of these components should be evaluated in order to complement our assertions.

Observing the timeseries of the ICs of both EEG and MEG some components marked as suspicious because of their morphology. Specifically the EEG ICs marked as suspicious were the following:

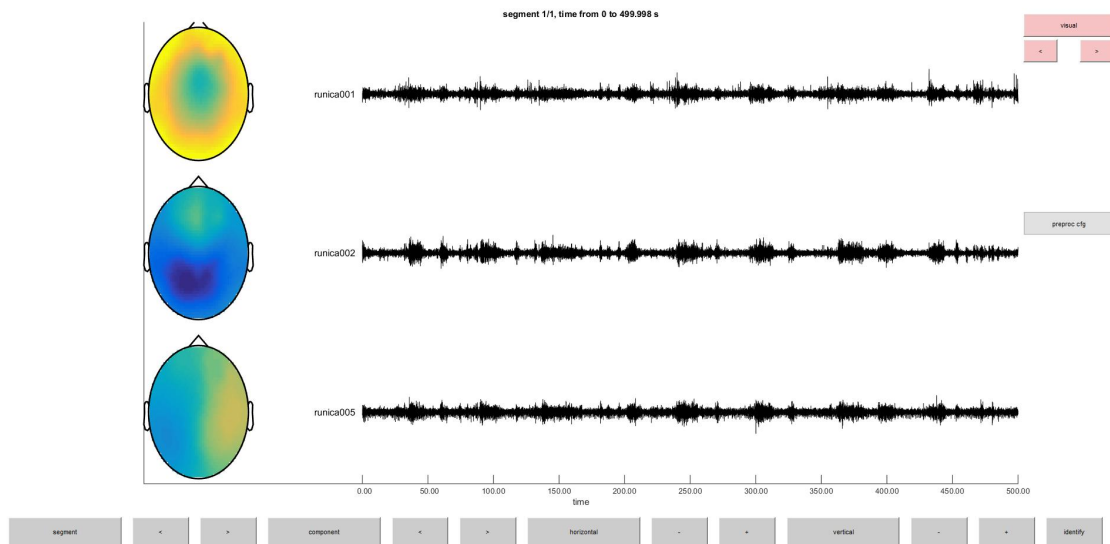


Figure 4.18: Suspicious EEG Independent Components

We could state that the first two components have sparse peaks which might be due to random eye blinks. In more details the IC2 confirms our claim since there is a strong activation on the frontal lobe. On the other hand, IC5 has high frequent noisy components which show the cardiac contamination even though that the activation is on the right temporal lobe. The latter consists the motivation to perform correlation with the channels that record the corresponding activity since in this way the identification of an artifactual component will be easier.

MEG Independent Components that considered as suspicious could be summarized in the following figures:

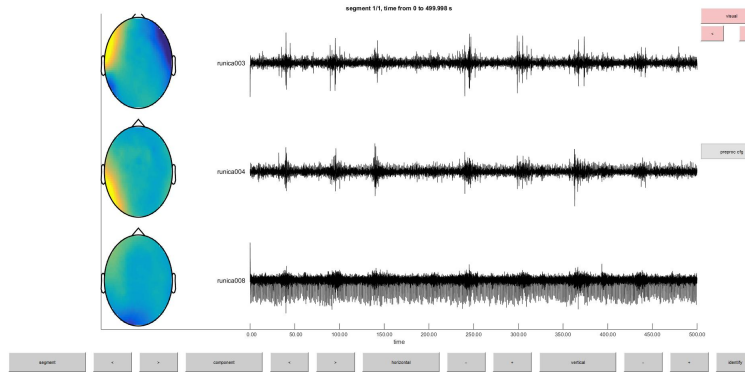


Figure 4.19: Suspicious MEG Independent Components

The MEG components are clearly more identifiable as artifactual since the time waveforms indicate the characteristics of the components that are generally known as ocular/cardiac artifacts. Specifically the first two components have apparent sparse peaks at random time points some of which match at both ICs. These components are considered as possible ocular artifacts fact which can be proven if we evaluate their waveform at smaller segments (Figure: 4.20). On the other hand, the last component resembles a lot to the heart pulse fact which is verified on the Figure: 4.21 that shows part of the QRS complex which possibly was decomposed by ICA and certainly comprises a Cardiac Artifact.

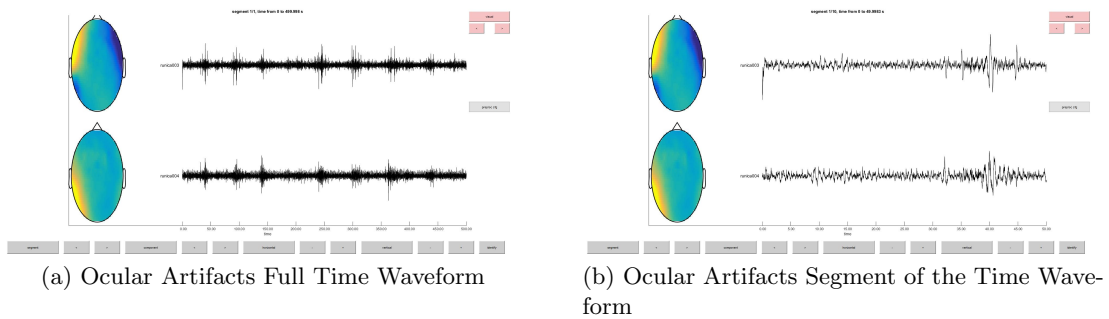


Figure 4.20: Possible Ocular Artifacts Time Waveform

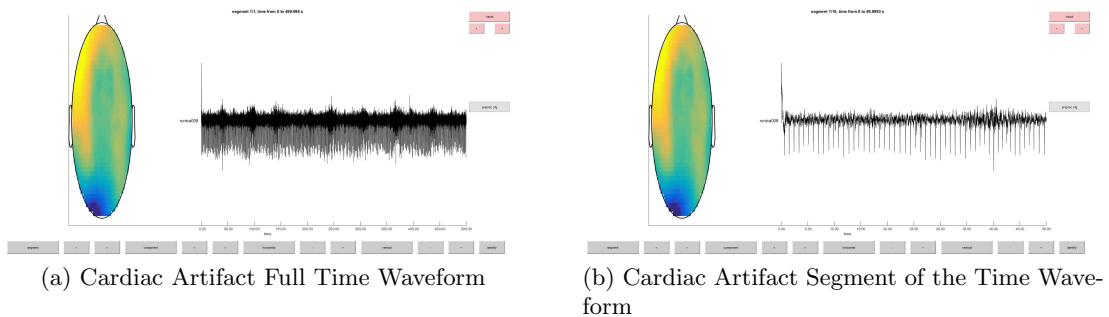


Figure 4.21: Possible Cardiac Artifact Time Waveform

4.6.2 Kurtosis, Entropy and Thresholding

The second approach for the artifact detection was a combination of metrics calculation on each component. The metrics chosen on this phase were **Kurtosis**, **Renyi Entropy** and **Skewness** [54]. Among various artifact detection techniques the aforementioned metrics show robustness and high percentages of successful marking [55]. Specifically, kurtosis is positive for distributions that show peaks, typical of eye blink and cardiac artifacts while it is negative for noisy distributions [53]. Renyi entropy is a measure of randomness and it contributes in identifying signals which are concentrated in small temporal regions which are likely to comprise an artifact. Last but not least, skewness is a third order statistic and measures the asymmetry. In an EEG or MEG recording the skewness takes non-zero values if an ocular artifact exists since it increases the asymmetry locally on a component's segment [56].

After taking into account the metrics to use for marking the artifacts, those markers were computed for each IC on the whole time-range (globally) and they were submitted a normalization process (zero-mean). To characterize a component as an artifact a thresholding approach was considered setting adequate values at ± 1.64 [53], [57]. The results of the metrics calculation on EEG and MEG ICs on fourth state run reording are summarized in the figures below:

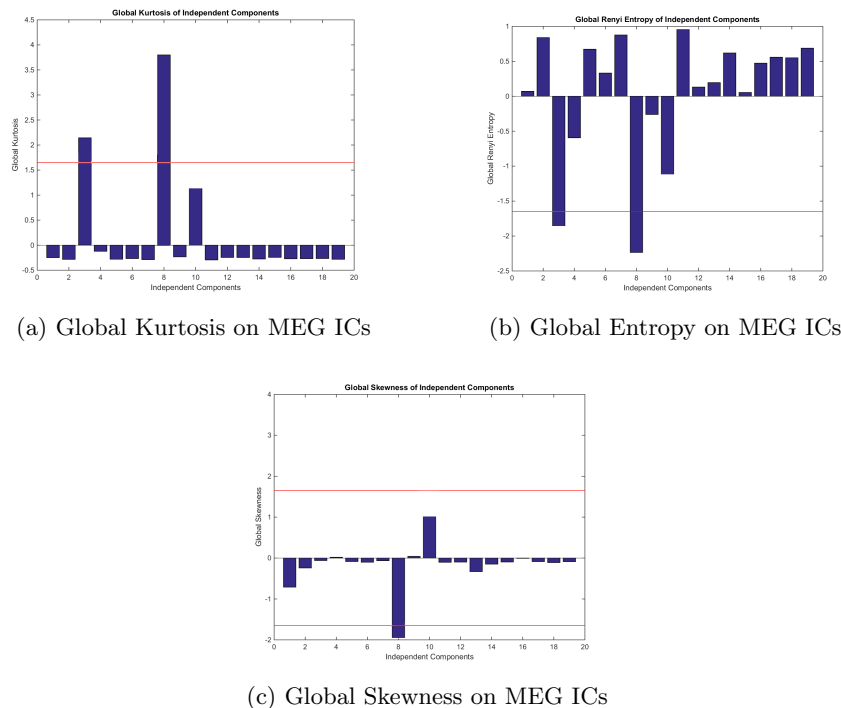
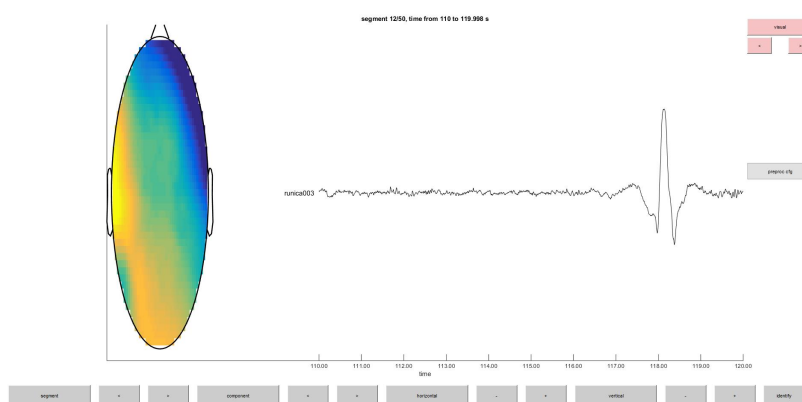


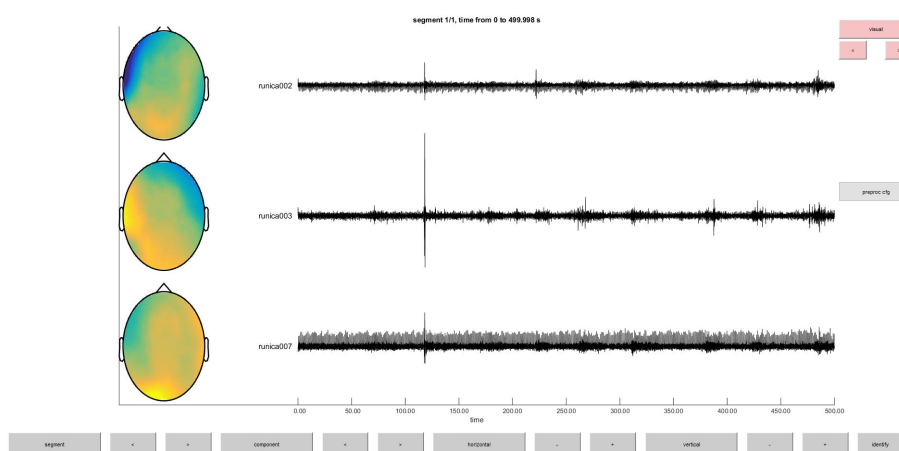
Figure 4.22: Artifact Metrics for MEG ICs that declare non-brain activity

The results on these metrics indicate that each metric complements the other and in this way taking a union of the information they provide we could mark a component as artifact. For example IC8 and IC3 has in all three metrics exceeded the thresholds and together with the visual inspection part we could claim that for sure these Independent Components have signs of artifactual behaviour. On the other hand, it is important to verify which type of

artifact they comprise in order to decide the correction plan of these component and thus the third step of detection technique classifies the type of the artifact according to the correlation with channels of non brain activity. Furthermore, there were also cases where this approach offered faulty results and this is the reason why the detection plan was constructed on a three step technique guaranteeing thus the robustness and the validity of our claims. For example on the sixth state run these metrics exceeded the threshold for a specific component which according to the visual inspection the marking was erroneous. The reason behind this decision is illustrated below:



(a) Time Waveform of Component Erroneously Assigned as Artifact



(b) Visual Inspection of Artifacts Marked by Metrics Approach

Figure 4.23: Application of Metrics Approach faulty case

Observing the [Figure](#): 4.23 one could state that there is a time segment in which there is an abnormal peak distribution. Furthermore one could claim that it might be an ocular artifact. However, at the same time point this peak is also discovered in all the components marked as artifacts. This strange decomposition by ICA might indicate that the amplitude of this time segment has different order of magnitude than the artifactual segments and it couldn't be separated. Moreover, the morphology of this distribution resembles to epileptic spike and for this reason this component wasn't marked as artifact. Last but not least, the reason why this component led to faulty metrics calculation was that it has same characteristics as an

ocular artifact and thus it creates local asymmetries while it also has non-gaussian properties. Henceforth, both skewness and kurtosis exceeded the corresponding thresholds.

4.6.3 Global and Local Correlation Approach

The last step of the artifact detection offers classification of the artifacts based on their source of origin. It incorporates two processes which validate the previous results and categorize the component. In more details, on this phase each component is submitted to a correlation with the channels which record non brain activity such as 'IO1' or 'ECG'. However, since we have 2 Dimensional signals the approach adopts the cross correlation as a metric of similarity between the two waveforms because this metric also takes into account the displacements of one compared to another. Cross correlation for continuous signals f, g is defined as follows:

$$(f \star g)(\tau) \triangleq \int_{-\infty}^{\infty} \overline{f(t)}g(t + \tau) dt \quad (4.40)$$

The cross correlation defines the similarity between the two signals by sliding the second one calculating the integral of their product at each position. The values range between -1 and 1 each of which indicate inverse or identical similarity relationship. Therefore in our case we perform a global correlation between ICs and EOGs and ECG channels in the whole waveform to detect possible similarities. Moreover, the ICs are divided into segments of 1 and 0.1 seconds and they are correlated with ECG and EOG correspondingly. The time segments were chosen according to the type of activity they are correlated. Specifically if the correlation is computed between IC and ECG the segments are of 1 second since the cardiac pulse has approximately the same duration. Similar approach was considered with the EOG in which the eye blink duration was taken into consideration for the correlation. As a consequence each segment of IC is correlated with the corresponding ones from the cardiac/ocular channel. In this way we secure the correct detection of either local or global similarities. In more details, the global approach is appropriate for marking cardiac artifacts which are characterized by the high frequency of the contamination whereas ocular artifacts which have low frequencies and short duration are more prone to be detected by the local (segment) approach since it is able to detect similarities in small time segments. The ICs are marked as artifacts if the correlation exceeds the value of 0.8 in the global approach or if 20% of the segments exceed the same threshold [57].

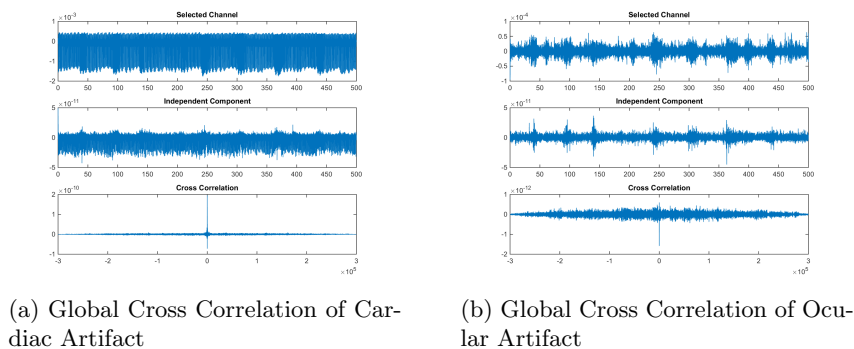


Figure 4.24: Global Cross Correlation Approach

On the previous figure, the top axis contains either the cardiac or ocular channel, the second one is the component with which the correlation is performed and the bottom one is the result of the computation. As illustrated above, on the cardiac artifact the cross correlation result shows a total match of the component with the ECG channel whereas on the ocular case it shows that there are also some similarities on slided versions of the IC and this is the reason why the segment approach identifies better the Ocular Artifacts. The local correlation approach is not visualized since the only computation performed was the calculation of cross correlation of each segment and the percentage of similar segments in order to compare them with the threshold.

4.7 Artifact Rejection and Correction

Having discussed how to identify artifactual components that contaminate the brain activity, the final section of this chapter addresses ways of correcting this interference. First of all, cardiac or muscular activity are typical forms of high duration signal corruption. As a consequence, these components are instantly rejected. In contrast, the ocular artifacts are components with short duration in which a rejection plan would be pernicious since along with the ocular artifacts a significant percentage of useful information would have also been rejected. To resolve such issue an artifact correction plan should be constructed. The idea is that ocular artifacts are comprised of low frequent components and therefore reconstructing such signals would result in a clean signal. To implement such correction the Empirical Mode Decomposition (EMD) algorithm will be utilized.

4.7.1 Empirical Mode Decomposition Algorithm

EMD, [58] is an one dimensional technique which decomposes a signal into basic functions called Intrinsic Mode Functions (IMFs) which have an instantaneous frequency. The IMFs are sequentially computed based on an iterative process which is described on the Figure: 4.25. The process is repeated until a convergence criterion is satisfied resulting in decreasing frequency functions.

```

Input: data sequence  $s[n]$ 
1. Identify all the local extrema
2. Separately connect all the maxima and minima with
   natural cubic spline lines to form the upper,  $u[n]$ , and
   lower,  $l[n]$ , envelopes
3. Find the mean of the envelopes as  $z[n] = [u[n] + l[n]]/2$ 
4. Take the difference between the data and the mean as the
   proto-IMF,  $h[n] = s[n] - z[n]$ 
5. Check the proto-IMF against the definition of IMF and the
   stoppage criterion to determine if it is an IMF
6. If the proto-IMF does not satisfy the definition, repeat
   step 1 to 5 on  $h[n]$  as many time as needed till it satisfies
   the definition
7. If the proto-IMF does satisfy the definition, assign the
   proto-IMF as an IMF component,  $c[n]$ 
8. Repeat the operation step 1 to 7 on the residue,
 $q[n] = s[n] - c[n]$ , as the data
9. The operation ends when the residue contains no more
   than one extremum

```

Figure 4.25: Empirical Mode Decomposition Process

Adapted from Md Kafiul Islam et. al 2016

The proposed correction plan for Ocular Artifacts involve the decomposition of the component based on EMD which leads in n number of IMFs. After extracting these function the goal is to find the total number of IMFs which represent the corrected signal. The optimal

number of IMFs is calculated based on an iterative procedure. Specifically, on each iteration the correlation coefficient of the initial component with the M summed IMFs. In other words on the first step the correlation coefficient (CC) between the first IMF and the contaminated component is computed while on the second one the CC is calculated taking into account the sum of the two IMFs. This process is repeated until a stopping criterion is satisfied. Particularly, if the CC is between 0.55 and 0.6 with a deviation of 10% the procedure stops [59]. The sum of the IMFs that satisfy the criterion is the artifact-free signal which replaces the contaminated one. An example of EMD application on an Ocular Artifact is shown below:

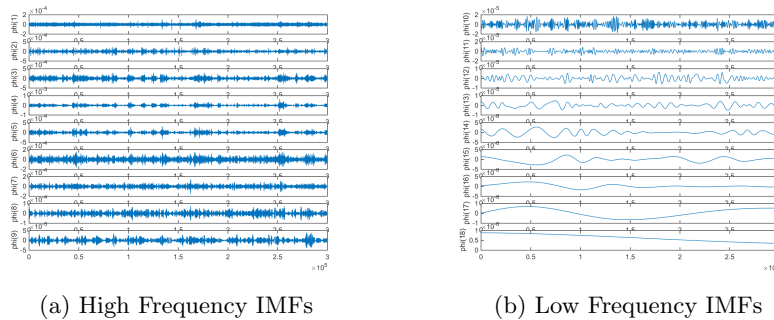


Figure 4.26: Intrinsic Mode Functions of an Ocular Artifact in a decreasing frequency order

The last step of the correction is to project the components back to the original space in a process called **backprojection**. Essentially, the original data are being reconstructed by the estimation mixing matrix and estimated sources of the ICA including also at the same time the corrected Independent Components. This process was implemented using the `ft_rejectcomponent` and at this point the efficiency of the correction plan could be evaluated by comparing two channels near the eyes before and after the reconstruction. The comparison was performed in both time and frequency domain and the results are summarized below:

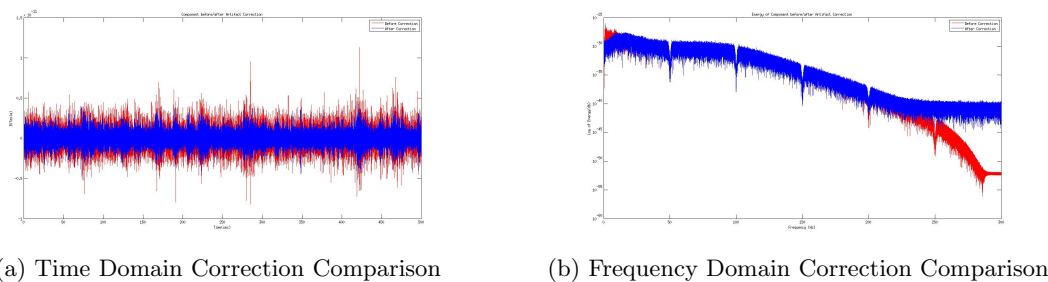


Figure 4.27: Signal/Spectrum of a channel before and after Ocular Artifacts Correction

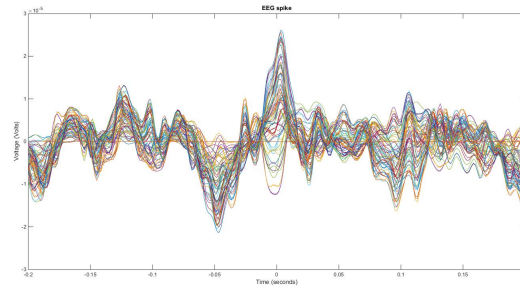
What stands out in this figure is that on time domain the peaks at random time points (eye blinks/movements) have been removed. However the most striking evidence of the correction efficiency is on frequency domain where it could be clearly seen a rapid attenuation on the delta frequency band (0.5, 4 Hz). The energy spectrum of corrected signal highlights the removal of ocular artifacts due to this attenuation which is strongly connected with the frequency band where the optical activity occurs.

Clustering of Epileptic Activity

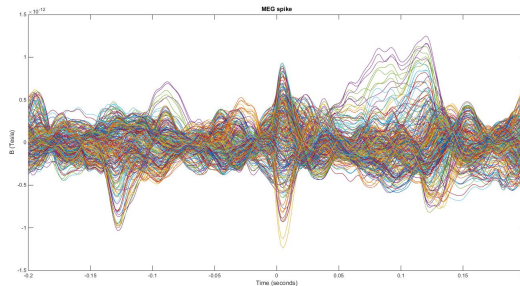
5.1 Spike Detection and Marking of Spike Activity

The previous chapter has described the methods used in the data cleaning aspects and it dealt with removal of unwanted components. In the chapter that follows the clean data are processed according to the disorder that is being investigated, namely epilepsy. Therefore, the focus on the brain activity for epilepsy required clean and preprocessed data. Beyond the diagnosis of the epilepsy, the spike detection could contribute in treatment as well. The motivation for this step of data analysis derives from the fact that multichannel recordings lead to activity mixture and thus focusing on several categories of neurons synchronization it may be advantageous for spotting abnormal states and regions of the brain. Specifically, the goal of this step is to group epileptic spikes based on some similarity indexes, known as **features**. The latter is known as **spike sorting or clustering** and it will provide optimal clue in disentangling the mixed recorded signals to detect the sources of the brain activations during various states, **inverse problem**.

So far the spike detection is a complicated procedure and there are attempts to automate it either by applying a simple amplitude thresholding function [60] or by creating Machine Learning Approaches which decide if a waveform contains an epileptic spike or not [61]. However, in this case the spikes were selected manually by an epileptologist by marking the time points around which an abnormal waveform was present. In the automated methods there is a trade off since the threshold approaches will lead to the capture of the spikes along with noisy events if the value is low or the opposite when the threshold is high. Furthermore the machine learning approaches are suitable if there are train data sets capable of discriminating objectively the spike waveforms. For this reason in our use case the spike marking by epileptologist was the best option. In this process he marked 66 spikes along the six state run recordings out of which 30 were MEG and 36 were EEG spikes. After the detection the spikes stored by selecting a time window of 0.4 seconds including the spike peak ([62]). The extracted spikes are visualized on the next figure in which there is a peaky distribution around zero. It is important to highlight that the spikes are aligned and thus each of which have similar behaviour around the zero time point. All of the spikes that marked are interictal and they are characterized by several features such as by the wave followed at the afterhyperpolarization state. Averaging of the amplitude of nearly simultaneously occurring spikes in different channels and of the time-shifts between their peaks can help to describe pathways of spike propagation.



(a) EEG Spike



(b) MEG Spike

Figure 5.1: Typical Spike Waveforms

5.2 Clustering of Epileptic Spikes

Turning now to the clustering of marked epileptic spikes, the motivation for grouping them according to some features stems from the various types of spike morphologies which could lead in inaccuracies when it comes to perform further analysis taking all of them into account. Henceforth, a spike sorting approach could bring out hidden information and reveal important connections/pathways between brain activity and epileptic semiology. From another perspective the ambition is to link each individual spike cluster with a single area which is considered as epileptic focus. The reason behind this would be beneficial for multifocal epileptic patients since in this way the different focal areas are separated and thus their detection becomes more feasible. In other words, a focal area may be characterized by weaker neuron synchronization than another and thus the spikes assigned to the strong area may prevail the ones of the other thereby leading to accurate detection of only one. The proposed spike sorting approach involves two layers of clustering as shown in [Figure: 5.2](#) incorporating two different algorithms, namely **Self Organized Map** and **K-Means**. The cluster analysis aims at finding clusters in multidimensional data set and classifies them based on those clusters [63]. All the cluster methods assume that the data derive from several independent classes which can be described by a model. Notwithstanding the efficiency of the clustering methods, the most challenging part of these techniques is to describe the data set with representative features with which the algorithm will perform the classification. This pre-clustering step is known as feature extraction in which few features for each spike are calculated with the goal to get rid of all dimensions dominated by noise and choose the best features.

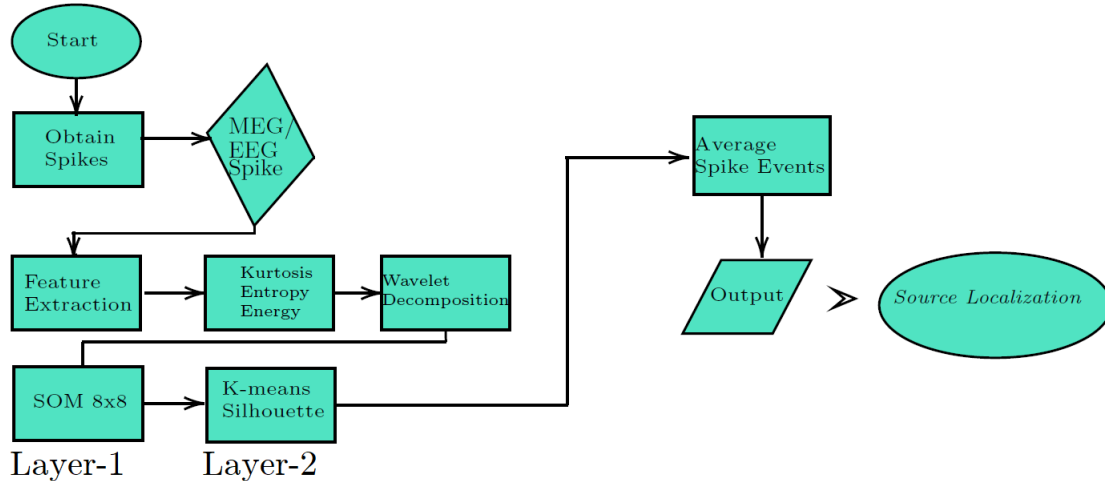


Figure 5.2: Clustering Step Flowchart

What follows in the next sections is a detailed account of the flow for clustering of the spikes. In a nutshell, after considering the spike detection scheme and the discrimination between EEG & MEG spikes, several features were selected as the most appropriate and calculated in each spike. As a consequence two feature vectors (EEG-Feature Vector, MEG-Feature Vector) were formed having as dimensions the **Number of spikes x Number of Features**. These vectors were given as input to the Self Organized Map which performs a 1st step of clustering by assigning each spike in a 2-Dimensional Grid reducing at the same time the dimensionality. The output of this assignment is fed into K-Means algorithm which forms the actual spike clusters taking into account the SOM-grid topology. Last but not least the spikes within each cluster are submitted to an average process which is utilized on the next chapter. Taking advantage of these signals Source Localization tries to disentangle the information from superpositioned activity into single sources that declare the area of the brain they originate.

5.3 Feature Extraction from Interictal Spikes

Before proceeding to examine the proposed feature extraction approach, it is important to highlight the goals and some of the previous related methods. Feature extraction aims at transforming the input data into a form that makes it easier for the clustering algorithm to identify the clusters. The first attempts to sort epileptic spikes was introduced with the implementation of a feature vector containing the amplitudes of the waveforms. However, nearby neurons can have same peak amplitude but different spike shape. As a consequence the feature vector start to be enriched using more geometry - shape characteristics. Some of the most common features which describe the spike shape are the width, the positive or negative peak of the first spike derivative and the waveform slope. Although these features offer

good discrimination between various spike types, they lack information about the distribution which could provide more efficient clustering since the features which they are describing it have more variations among different spikes. Typical metrics used in describing the spike distribution are kurtosis, energy, skewness or the inter-quartile range [64]. Last but not least, the aforementioned features are vulnerable to some use cases and thus another approach for feature selection is the transformation of the spike into several components that best describe its characteristics. Representative examples of such approach are the Principal Components [65] that account for almost the whole energy of the spike or the decomposition wavelet coefficients the selection of which is based on a criterion [66].

Taking into consideration all the features used in previous research works at the same domain the suggested approach incorporates the computation of a feature vector which combines some of these features. Specifically, the selected features were **Kurtosis**, **Energy**, **Entropy** and some **Wavelet Coefficients**, the number of which we selected is described below according to a statistical test. The reason behind this selection is established on the fact that by combining these features we offer the necessary information to the clustering algorithms to find discrete clusters. Moreover, PCA was rejected since it is vulnerable in inaccuracies in case there are more than two spike shapes in the dataset [67] and our spikes present variety in their shapes. The kurtosis and entropy were calculated in the same way as in the [Artifact Detection](#) section while entropy as defined in the equation (4.2) and all of those three were computed in the whole time range but represented as single value. Therefore each spike had three values which indicated its kurtosis, entropy and energy correspondingly.

Turning now to the **Wavelet Decomposition** to compute coefficients which will be used as features we performed a 4-level Wavelet Transform using 'Haar' wavelets in 2 dimensions [60]. Wavelet Transform was selected since it offers the optimal resolution in both time and frequency domain despite its computational complexity revealing hidden characteristics for the spikes. Wavelet transform is projecting the input signal in various instances for various frequency bands. These frequency bands are scaled versions of the original space and they are generated using scaled and shifted basis functions which are known as **mother wavelets**. The Wavelet transform for a continuous signal can be expressed from the following equation:

$$X_w(\tau, s) = \frac{1}{\sqrt{s}} \int_{-\infty}^{\infty} x(t) \psi^* \left(\frac{t - \tau}{s} \right) dt \quad (5.1)$$

where ψ^* is the conjugate of the mother wavelet. In our case the mother wavelet is a Haar wavelet and is described in the next figure:

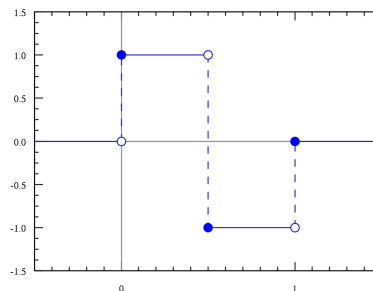


Figure 5.3: The Haar Wavelet

Adapted from Wikipedia

In more details, contracted versions of the wavelet function match the high-frequency components, while dilated versions match the low-frequency components. Then, by correlating the original signal with wavelet functions of different sizes, we can obtain details of the signal at several scales. To compute the wavelet coefficients the Wavelet Packet Decomposition (WPD) was followed in which the spikes were decomposed at both dimensions in 4 levels (Figure: 5.4). In each level the signal is passed through a **filterbank** which is either a Low pass filter or a High Pass Filter each of which downsamples the signal by a factor of 2 and computes four types of coefficients (Horizontal, Vertical, Diagonal and Approximation Coefficients). In a n -level decomposition we obtain 2^n coefficients which leads to 64 coefficients since we perform a 4-level, 2-dimensional decomposition which produces four types of coefficients or in other words 2^4 in each direction. It is worth mentioning that the approximation and detailed coefficients (Horizontal, Vertical, Diagonal) are decomposed in each level through a recursive algorithm in an invertible way but despite the downsampling the overall number of coefficients is the same with no redundancy.

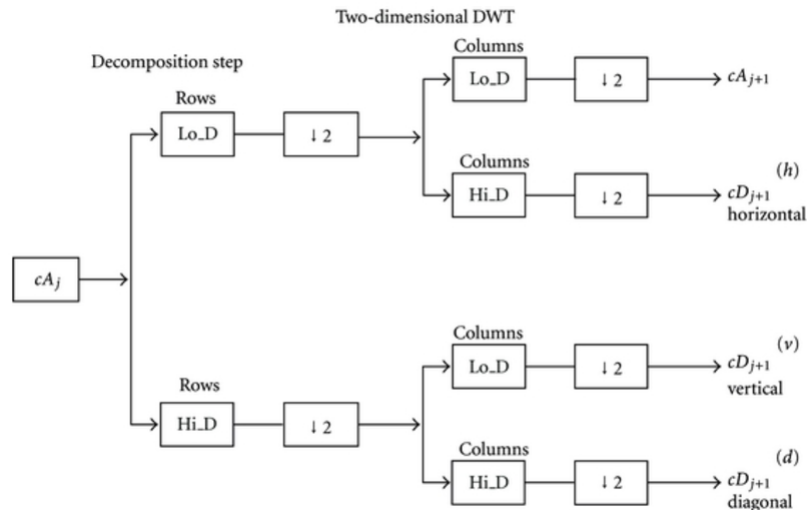


Figure 5.4: Wavelet Packet Decomposition

The question emerging after computing the coefficients is how many and which to use as features. The answer to this challenging selection was given by *Quiroga* [60] who claimed that the first 10 coefficients with the greatest deviation from normal distribution are the optimal selection. Anyone would wonder why the deviation from normality leads to better clustering efficiency. The answer was given again by the previously mentioned scientist who proved that if the data contains more than one unit, a wavelet coefficient that can separate the different spikes shapes should have a **multimodal distribution** [68],[69]. Considering the selection of coefficients which deviate from normality the Liliefors modification of Kolmogorov Smirnov Test was used. **Liliefors Test** is a statistical approach to test the normality which rejects or not the null hypothesis. In this way considering a set of data H_0 with normal distribution and H_a a set of data with non-normal distribution the test follows the next steps: First of all it computes the sample mean \bar{x} and standard deviation s as follows:

$$\bar{x} = \frac{1}{n} \sum_{i=1}^n x_i \quad (5.2)$$

$$s = \sqrt{\frac{1}{n-1} \sum_{i=1}^n (x_i - \bar{x})^2} \quad (5.3)$$

Then it finds the maximum discrepancy between cumulative distribution function of the normal distribution and the empirical distribution function. Specifically it calculates the normalized sample values Z_i which determine the empirical distribution function $S(x)$

$$Z_i = \frac{x_i - \bar{x}}{s} \quad (5.4)$$

The comparison between the two distributions is performed using the supremum of the absolute difference of the distributions $F^*(x)$ and $S(x)$:

$$T = \sup |F^*(x) - S(x)| \quad (5.5)$$

Finally it assesses if the maximum discrepancy is large enough to reject the null hypothesis by calculating a p-value which is a probability with scalar value in the range of (0,1) and determines if it is more extreme than observed value of null hypothesis. Values close to zero doubt the validity of the null hypothesis (Mathworks). Henceforth sorting the p-values of wavelet coefficients in ascending way we could choose the first 10 as the desired features.

Finally, the Feature Vector is comprised of 13 features for each spike and thus its dimensionality is 30x13 for the MEG spikes and 33x13 for the EEG spikes. Having constructed the feature vectors we have the necessary supplies for performing the spike clustering.

5.4 Self Organized Map Algorithm - SOM

Having discussed how to construct the Feature Vectors, the last step of the spike sorting is the cluster analysis addressing ways of forming groups of spikes with similar properties. To identify such clusters the **Self Organized Maps (SOM)** are being exploited [70]. The self-organizing map is a statistical data analysis method which belongs to the unsupervised learning category, whose goal is to determine the properties of input data without explicit feedback (R.Martin et. al. 2009). It is an abstract mathematical model of topographic mapping from the sensors to the cerebral cortex. The human brain is divided in specialized areas each of which responds to certain stimuli. Same kind stimuli activate a particular region of the brain. This idea is transposed to the Self Organized Map learning system where the input space (Feature Vector) is mapped in a small space. The characteristics of the small area that the assignment is performed are described by a principle which defines that similar individuals in the initial space will be projected into the same neuron or at least in neighboring ones. It is worth noting that SOM serves as dimensionality reduction, data visualization and cluster analysis tool.

Self Organized Maps may find its ancestors in the **Vector Quantization Method (VQ)**. In this approach, the space of input vector-data is partitioned into a finite number of contiguous regions each of which is represented by a model vector called **codebook vector**. If the input data is optimally partitioned, the codebook vectors have a minimized metric value (i.e minimum Euclidean distance) between the input value and the best matching codebook

vector. SOM defines an ordered mapping and a projection of the set of given data onto a 2-dimensional grid. Each grid node is comprised of models M based on which the input data point is assigned to a neuron taking into account its similarity (computation of a metric) with the model. Like the Vector Quantization the model is a weighted local average of the given data as the codebook in VQ. The models of nearby neurons have similar characteristics as shown in the [Figure: 5.5](#).

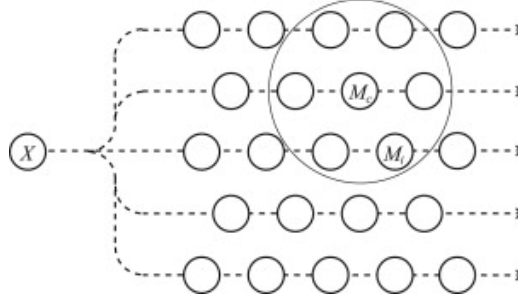


Figure 5.5: SOM Grid and Models of Grid neurons

Adapted from Kohonen 2013

After the assignment of the input data to the neuron that is represented by the model that best matches the input data point there is a process of modification/updating the model and a subset of the neighboring neurons [71]. In a nutshell, SOM is represented by a 2-D rectangular hexagonal grid to form a discrete topological mapping of input space $X \in R^n$. The algorithm starts with the initialization of the weights w_i that are associated to a neuron i and forms the model for this neuron. The next step of the algorithm is to repeat the steps 3 to 6 till the iterations of the learning procedure will reach the desired number or until the map converges.

Algorithm 1: Self-Organized-Map Algorithm

- 1 Each node's weight are initialized with small random numbers;
 - 2 **do**
 - 3 A vector is chosen randomly from the set of input data;
 - 4 Calculate the winning neuron/Best Matching Unit (BMU);
 - 5 The neighborhood of the BMU is calculated;
 - 6 Winning neuron is updated along with its neighborhood;
 - 7 **while** *Map Converges* || *N iterations reached*;
-

Let us denote now the w_i the weight of the neuron i and r_i the location vector of the same neuron. The winning neuron in each iteration is computed based on the following equation:

$$v(t) = \arg \min_{k \in \Omega} \|x(t)w_k(t)\| \quad (5.6)$$

The neighborhood $\eta(v, k, t)$ is computed in step 5 for each neuron, time and each BMU which belongs to the neuron indexes Ω

$$\eta(v, k, t) = e^{-\frac{\|r_v - r_k\|^2}{2\sigma(t)^2}} \quad (5.7)$$

with σ being the effective range of the neighborhood and is often decreasing over the time, while the update for the BMU and its neighbours is offered by the equation:

$$\Delta w_k(t) = a(t)\eta(v, k, t)[x(t) - w_v(t)] \quad (5.8)$$

After observing the algorithm an emerging/challenging issue is which is the convergence criterion or when the algorithms is stop processing. Often SOM takes as input an a-priori knowledge of maximum iteration steps or it takes into account stopping criteria that force it not to change weights after numerous iterations. The output of this algorithm is a codebook for each output node and is a visual representation of the weight distribution over the 2D grid. Another approach for convergence criterion is suggested by Vesanto [72] which claims that $SOM_{size} = 5\sqrt{N}$ is the best Grid Size with SOM_{size} expressing the product of the two grid-dimensions while N is the dataset size (rows x columns).

An important aspect of the SOM algorithm is the ability of an individual to interpret the output since the visualizations are complicated. Specifically, SOM produces an output codebook vector which visualizes the grid with the assigned dataset based on a color code. In this visualization, the color code enables the identification of areas with a high density of individuals. In other words areas which have same price range in the color representation are likely to form a cluster of the data with a specific pattern Figure: 5.6/(a). However, there are cases in which the price range of some neurons may be the same but it doesn't indicate similarities since they describe two different patterns Figure: 5.6/(b).

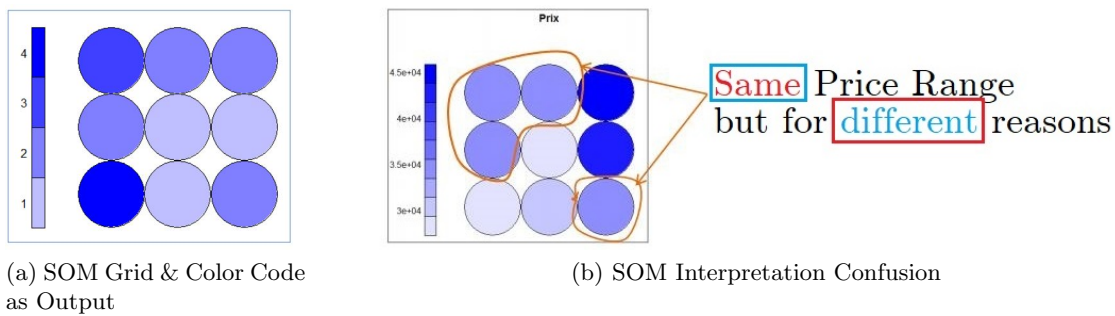


Figure 5.6: SOM Output Visualized

Moreover, for input dataset with a reasonable number of features SOM could provide also a visual representation of the grid and the assignments in each neuron based on each feature. To rephrase this, the Figure: 5.6 is produced for each feature showing thus, a heatmap of how the input is being distributed and projected onto the grid for a specific feature. In this way we can extract the information which indicates the patterns that are present in input space for a specific metric/feature. Thus far, this section has attempted to provide a brief summary of the Self Organizing Map Method relating to the cluster analysis showing that this technique could help in revealing patterns in the input data and assign these patterns in nearby regions. Then, these regions could be further analyzed by another clustering algorithm, such as K-Means to form the actual clusters.

5.5 K - Means Algorithm

K-Means [73] is an iterative procedure trying to place cluster centers in groups of data that are *unlabeled*. It is one of the simplest unsupervised learning methods whose main idea is to define K centroids $\mu_1, \mu_2, \dots, \mu_k$ one for each K-clusters, which are assumed a-priori . The centroids location should be considered smartly since different starting locations cause

different outputs and unstable results. So, the better choice is to place them as much as possible far away from each other. The next step is to take each point by selecting it randomly from the given set and associate it to the nearest centroid. The term nearest is determined by a specific distance metric $c_{(i)}$. At this point K new centroids are re-calculated μ_j as representatives of the clusters resulting from the previous step. After obtaining these K new centroids, a new binding has to be done between the same data set points and the nearest new centroid. This procedure is performed continuously as a loop until no more changes are done. In other words centroids do not move any more. Finally, this algorithm aims at minimizing an objective function, in this case a squared error function. The objective function is the following:

$$J = \sum_{j=1}^k \sum_{i=1}^n \|x^{(i)} - c_j\|^2 \quad (5.9)$$

The algorithm described before could be summarized below:

Algorithm 2: K-Means Algorithm

1 Initialize cluster centroids $\mu_1, \mu_2, ..\mu_k$;

2 **do**

3 For every i set:

$$c^{(i)} := \underset{j}{\operatorname{argmin}} \|x^{(i)} - \mu_j\|^2$$

 For each j set:

$$\mu_j := \frac{\sum_{i=1}^n \{c^{(i)} = j\} x^{(i)}}{\sum_{i=1}^n \{c^{(i)} = j\}}$$

4 **while** *Convergence is Achieved*;

Notwithstanding its clarity and its straightforward approach, K-Means has some limitations which need to get overcome. First of all, data containing **outliers** could lead in inefficient clustering and high squared errors that result in variations in the stability. Furthermore, another obstacle in K-means' performance could be the **empty clusters** which are formed in case during the assignment step no points are allocated to a cluster. Last but not least, determining the **number of clusters** in advance is a challenging and tricky task. Many times, this number is selected based on an individual's visual perception about existed classes in the dataset. The latter coupled with the previous constraints arise questions of validity examination and ways of tackling these effects.

Regarding the efficiency and validity of the clusters produced by K-means algorithm there are couple ways considering such topics. One method to validate the number of clusters is the **elbow method**. The idea of the elbow method is to run K-Means clustering on the dataset for a range of values of k (e.g, K from 2 to 5), and for each value of K calculate the sum of squared errors (SSE). Then by plotting these errors for each iteration of K-Means with different K we could claim that increasing the number of the clusters leads to reducing the distance between the data points and cluster centroid. This inverse relationship is continued to the extreme of reaching zero when K is equal to the number of the data points. One should choose therefore the number of clusters so that adding another cluster doesn't improve much better the within cluster square error which could be found in the point known as **elbow point** as shown in the figure below:

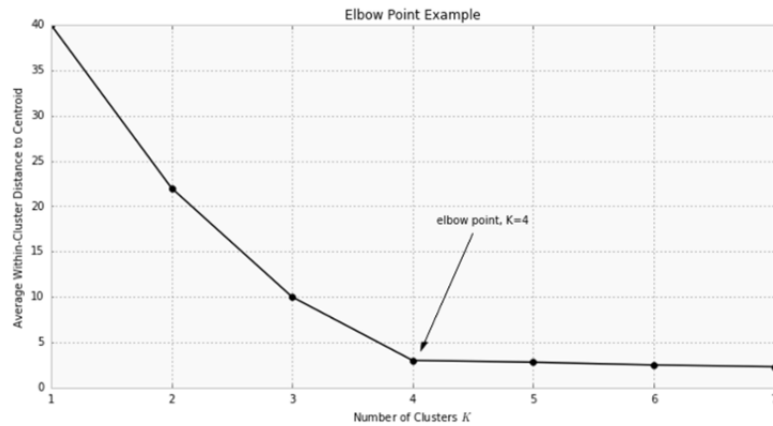


Figure 5.7: Elbow Point

The aforementioned evaluation method may not be applicable in all use cases since the curve might show monotonically decreasing properties and thus the elbow cannot always be unambiguously identified (Ketchen et. al. 1996). As a consequence of this another evaluation method is considered. **Silhouette Analysis** is preferable over elbow method for validation purposes since it doesn't use any representative of a cluster but is based on the full pairwise distance matrix over all data. In other words, it is a way of measuring how close each point in a cluster is to the points in its neighboring clusters. Silhouette values range from -1 to 1. Silhouette coefficients near 1 indicate that the sample is far away from the neighboring clusters. A value of 0 indicates that the sample is on or very close to the decision boundary between two neighboring clusters and negative values indicate that those samples might have been assigned to the wrong cluster.

Mathematically, for a single data point silhouette could be expressed as follows:

$$s(i) = \frac{b(i) - a(i)}{\max(a(i), b(i))} \quad (5.10)$$

where $a(i)$ is the distance of X_i to its own cluster, which is defined as the average distance of X_i to all the other data points in its own cluster. $b(i)$ is the distance of X_i to its closest neighbouring cluster, which is defined as the average distance of X_i to all the data points in its closest neighbouring cluster [74]. To decide which number K is the optimal for clustering one should consider the following points:

- Firstly, the mean value of silhouette values of all data point should be as closest to 1 as possible.
- Secondly, the plot of each cluster silhouette values should be above the mean value or at least the majority of its data points
- Last but not least, the width of each cluster silhouette plot should be as uniform as possible. In other words the cluster should contain approximately the same number of data elements.

The following figure illustrates the silhouette plots for 3 different K 's in which the red vertical line represents the mean silhouette value of all data points with x-axis declaring the silhouette Value S and y-axis the number of cluster K .

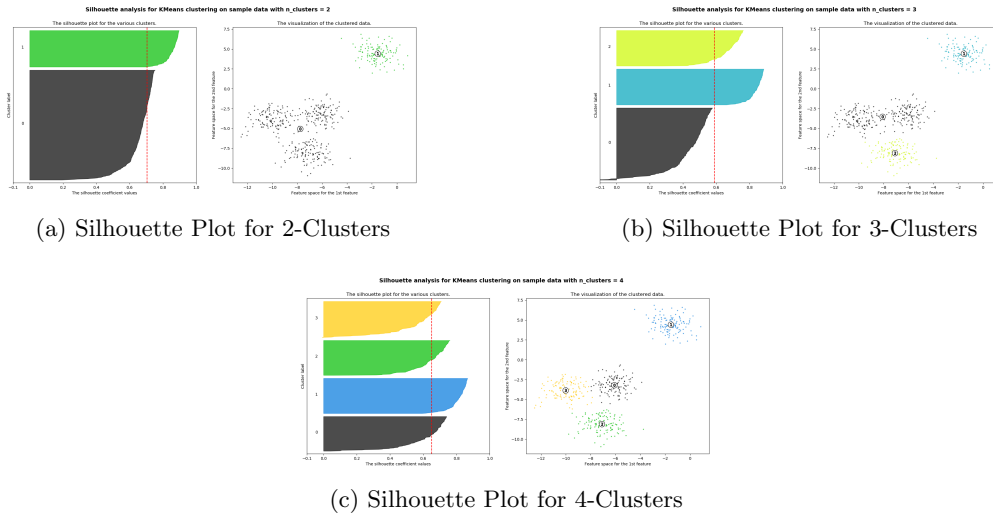


Figure 5.8: Silhouette Plot for a sample dataset example
Adapted from scikit K-Means tutorial

The silhouette plot when K is equal to 2, shows uneven distribution of data points resulting in different cluster sizes while at the same time on cluster 2 there are many elements which hardly reach the mean silhouette value. The same applies also in the case of 3 clusters. However when the K is equal to 4, all the plots are more or less of similar thickness and hence are of similar sizes as can be also verified from the labelled scatter plot on the right. Thus the $K = 4$ could be considered as the optimal number of clusters for this specific sample dataset.

With respect to tackling some of limitations and problems of K-means such as that randomization of centroids leads to unstable and different results if the test is repeated, the **combination of SOM and K-means** is considered as discussed in the following section. The reason behind this is that SOM Output is used as a-priori knowledge to the K-Means initialization and thus the robustness and efficiency of the latter are significantly increasing.

5.6 Combining SOM and K - Means

At this point, the combination of the two clustering methods is considered in a 2-level abstraction approach. Specifically, on the first abstraction layer the multidimensional Feature Vector is mapped onto 2-Dimensional SOM Grid. Multiple dimensions of the Feature vector are expressed in form of multiple columns describing the Input Dataset (multiple features). SOM produces a number of prototype vectors which is a compressed representation of the dataset (**codebook vectors**). However, it can be very difficult to attribute some units of the input to a given cluster given the Feature Vector. Therefore, the problem lies in cases where a clear distinction between two clusters is impossible. Henceforth, a second stage of clustering is applied to remove ambiguity and to validate SOM results [75]. By implementing clustering in two stages it was found that the computational complexity is eliminated since approaching clustering only with K-Means on multidimensional data generates more time complexity than the 2-level approach. Another benefit of this approach is the noise reduction as the SOM prototype vectors are local averages of the data and thus less sensitive to random variations than the original data. Also SOM tends to eagerly overwrite previously learned

data, especially in the initial stages. This is a main shortcoming, giving us further motivation for K-Means on the second level. Last but not least, by applying the SOM prior to the K-Means we reduce the unstable output phenomenon in which the clusters produced have variations if we repeat the algorithm. The scheme of this approach could be summarized below showing how the transition from multidimensional Feature Vector to 1-Dimensional Cluster Assignment information is performed.

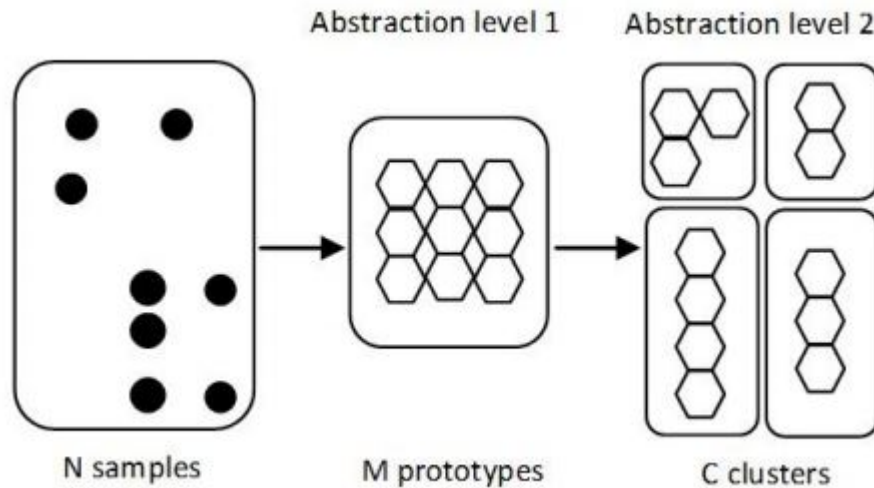


Figure 5.9: 2-Stage Clustering Approach

Adapted from [75]

The clustering procedure is starting by defining the SOM Grid Size as an 8x8 Grid following the rule from [72] and by testing various grid sizes empirically. The reason behind this selection is that Feature Vectors are 30x13 and 36x13 and according to the criterion the optimal size would be the 10x10. However when this size was tested there were huge variations and not clear mapping. The SOM clustering applied using the neural network Matlab toolbox `nctool`, Figure: 5.10 while the specified input was normalized before the process since in this way the comparison between input space and grid neurons' weights is more efficient with normalized values.

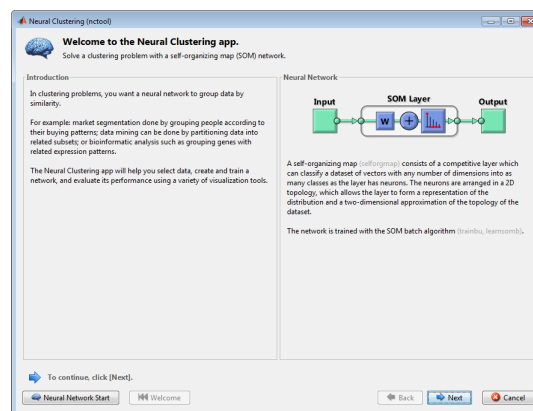


Figure 5.10: Neural Network Toolbox and SOM Architecture

Adapted from Mathworks

The SOM algorithm is being performed with a default number of iterations which was set by Matlab to 200 Iterations. The SOM Grid and the output of the SOM output weight positions for the EEG spikes Feature Vectors are shown in the next figure:

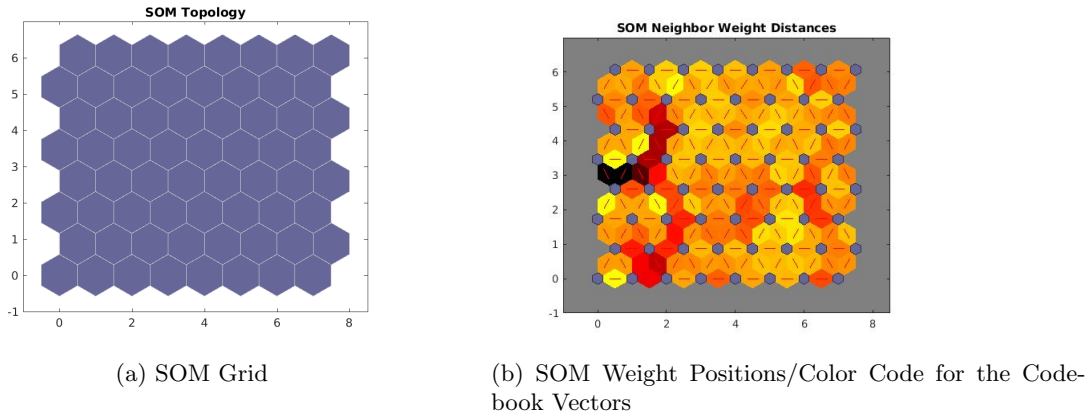


Figure 5.11: 8x8 SOM clustering

The output of the SOM is a color representation of the input points assigned to neurons based on weight comparison. Light colors between neurons mean that there is high percentage of similarity while dark colors show that the input points between dark areas have great differences. As a consequence we could say that regions with light colors could form a cluster while dark areas are the cluster separators. However as explained before the cluster discrimination is not an easy process and thus K-Means disentangles this information into a more human-comprehensible way. To evaluate SOM efficiency we observed the weight adaptation plot [Figure: 5.12](#) in which we could see how the Neurons' Weights adapts well into the N-input-samples.

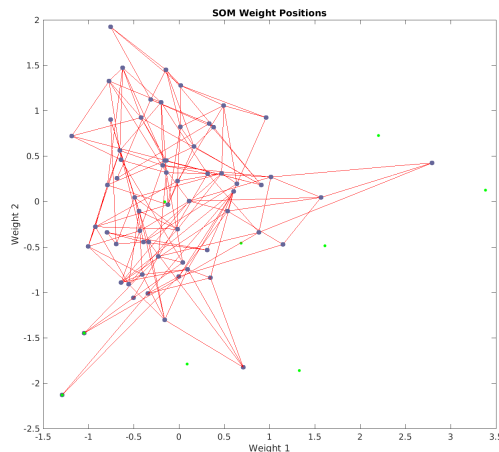


Figure 5.12: SOM Weight Adaptation Plot

SOM offers additional information of the assignment by producing figures of the input assignment to the neurons for each Feature. Therefore we could examine which feature provides strong cluster formation and which are helping in cluster separation. From the figure below it is clearly seen that inputs 4-13 shape light areas on the grid with good discrimination

from the rest and thus these features are aiding the cluster formation. On the other hand inputs 1-3 are producing dark grid areas which could be translated in variations of these values among the spikes and hence they are good cluster discriminators. The 3 first inputs are kurtosis, entropy and energy while the rest are the wavelet coefficients. In this way we could claim that there are many different spike types in the input dataset since their first three features have many variations while in the time-frequency domain present similarities based on which we could classify them.

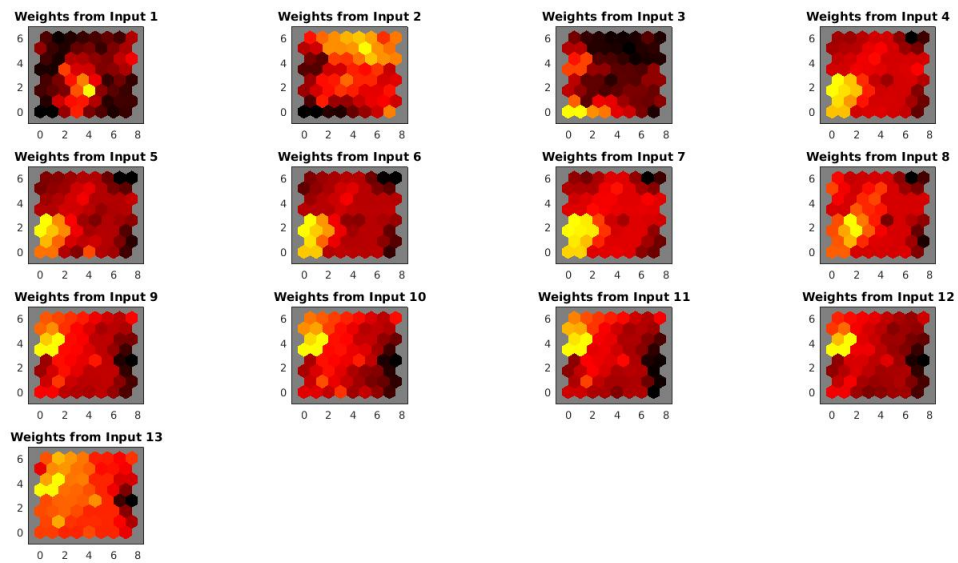


Figure 5.13: Weights Distribution for each Feature

In the Matlab Workspace SOM produces a vector which stores the information of the assignment. Specifically, in this vector the assignment of each spike to grid’s neurons is included. This output is fed to the K-means algorithm which was tested for various K between 2 and 10 but also for all the possible distance metrics. The results from the different iterations of the K-Means are depicted in the figures below which were evaluated by the silhouette index.

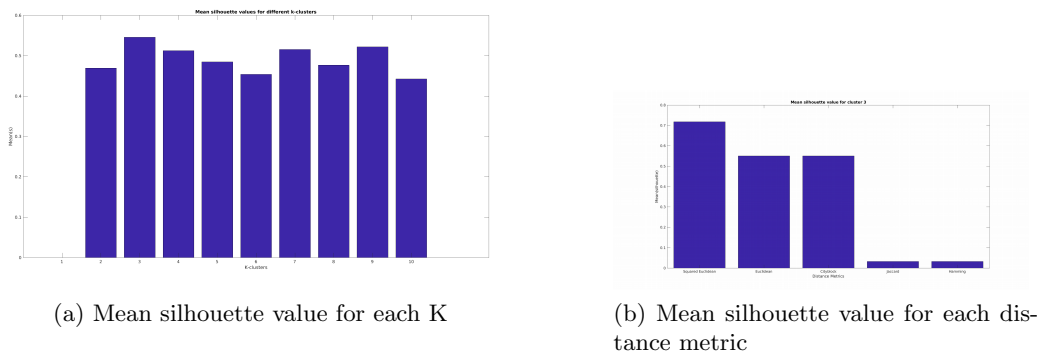


Figure 5.14: K-Means clustering for different K’s and distance metrics

What stands out in the previous figure is that for $K = 3$ the higher mean silhouette value is achieved giving us an insight of the optimal K while the best distance metric seems to be the Euclidean distance. However to confirm that 3 is the best number of clusters we observe the silhouette value for each cluster point. In the next figure the silhouette index for 3 and 4 clusters is being evaluated.

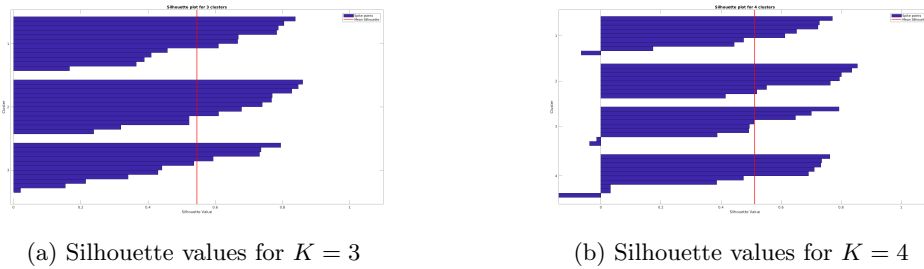


Figure 5.15: Silhouette index for two sample K 's

In this figure the silhouette values for each cluster point was calculated and was depicted as a bar plot while the red vertical line indicates the mean silhouette value. According to the criteria for choosing the best K described in the previous section we could state that $K = 3$ is the optimal number of clusters. This stems from the fact that it seems that the clusters have almost equal number of spikes (almost equal width), the majority of each cluster's point silhouette exceeds the threshold of the mean silhouette value and the values approximate the 1 which is the best fit. On the contrary, in the case of 4 clusters there are many points with negative values indicating wrong assignment, fact which comprise enough proof for rejecting this K . The aforementioned results are for the EEG clustering while for the MEG the same pipeline was followed and the K was selected accordingly and was also set to 3. K-Means labels the data by assigning them to a cluster which is characterized by a centroid. The output of this labelling procedure is shown in the figure below for both EEG & MEG clustering. The scatterplots below are a coloured representation of the cluster with X indicating the clusters centroids whereas the 3 different coloured points are the different clusters.

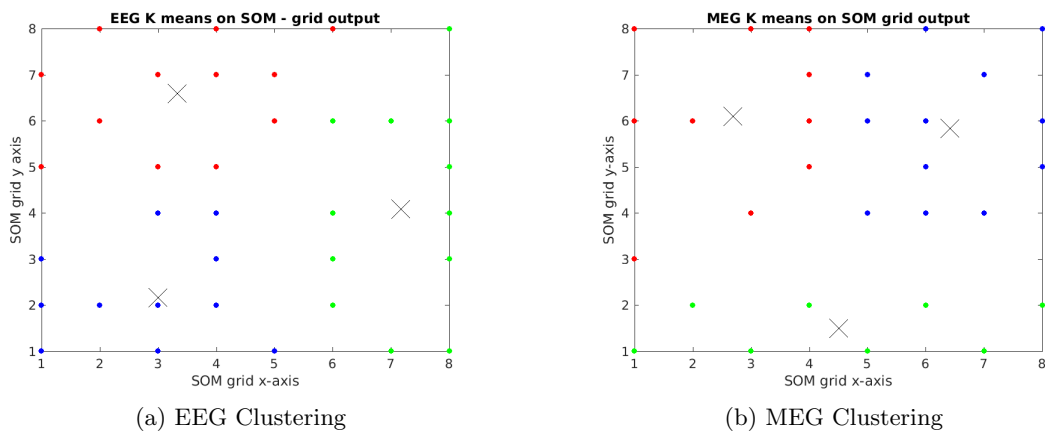
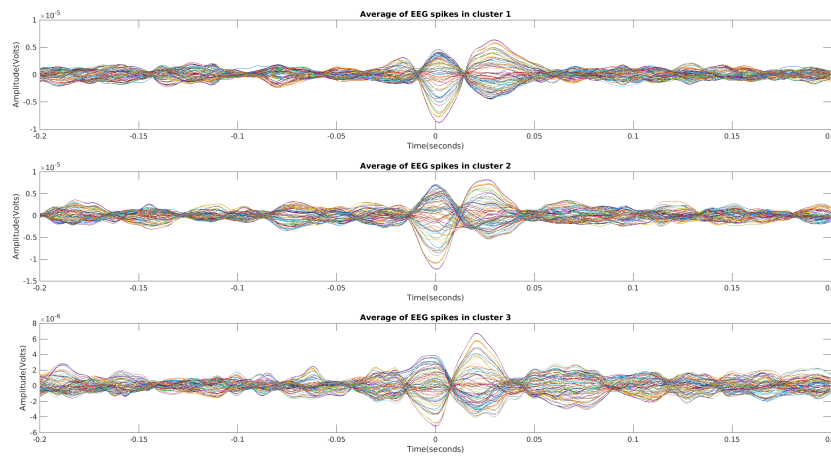


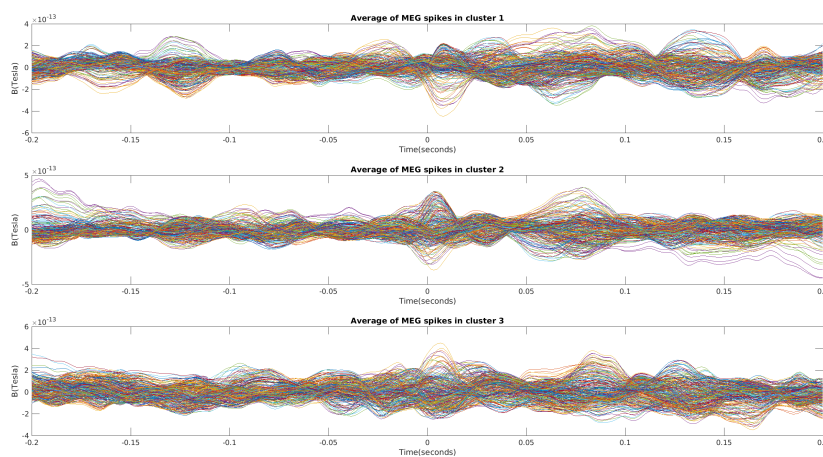
Figure 5.16: Clustering of spikes after the 2-level approach

5.7 Clustering and Source Localization

One of the main reasons why we followed a spike clustering pipeline was to give prominence to phenomena that possibly would not have been noticed in the further analysis (source reconstruction). The question arising is what is the way to achieve that. The main aim of this thesis is to identify the abnormal regions which cause the epileptogenesis. In order to accomplish that we need signals with spike waveforms and epileptic patterns. As will be explained in the following chapter, the source localization method requires time-locked /average data. It had been shown that computation of subaverages of similar spikes (spikes within a cluster) enhances the signal to noise ration of spike maps and thus the efficiency of accurate reconstruction is optimized [76]. Consequently, the subaverage of spikes in each cluster was computed and the results are summarized below with the EEG case being first re-referenced:



(a) Average in EEG Clusters



(b) Average in MEG Clusters

Figure 5.17: Average of spikes in each EEG & MEG clusters

Source Localization

6.1 Forward and Inverse Problem

A significant percentage of neuroscientists have focused on the study of the underlying neuronal activity which is not measured and is manifested prior to the recording. In this way they might reveal explanations for possible abnormal or not brain states while various disorders may be reconsidered. Neural current sources produce both electric potentials and magnetic fields which are recorded by the EEG & MEG modalities. The current fields can be divided into two components, the primary and the secondary current terms which represent the microscopic passive cellular currents and the macroscopic electric field respectively [77]. The development of the recording systems allow to estimate these primary currents. To estimate such currents or also known as sources a 2-stage approach is required. First of all, it is imperative to formulate a model of the recorded potentials at the sensors potentials given active neurons/ sources in the head [78]. This problem is commonly known as **Forward Problem**.

On the other hand, the next step is the attempt to find the primary source which generates the recorded brain signal. The latter is recognized in the literacy with the name of the **Inverse Problem**. It is worth highlighting that the Forward Problem solution is indispensable ingredient for the solution of the Inverse Problem.

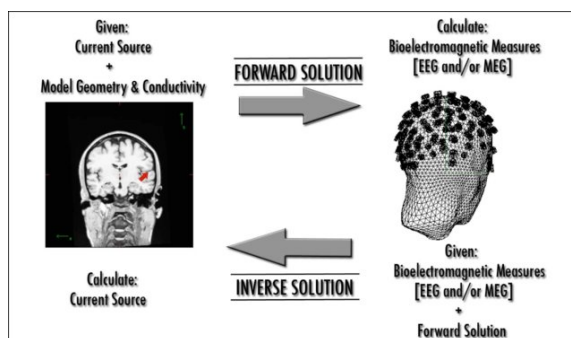


Figure 6.1: Forward and Inverse Problem Correlation

Adapted from: Bangera, 2008

Both the Forward and the Inverse Problem are formulated within the framework of a certain mathematical model, wherein the underlying physiological assumptions are precisely

formulated. In the case of epilepsy there are small zones inside the brain that give major contribution in the generation of the electric field. Neurologists have been interested in determining the location of the epileptogenic zones from the measured potential on the scalp in order to avoid invasive techniques and to diagnose/treat and evaluate the specific type of epilepsy. In order to solve these complex mathematic problems there is the need for some factors which are known such as the geometry and the electrical properties of the head, as shown in the previous figure. A more detailed account of these problems' formulation and solution is presented in the following sections.

6.2 Forward Problem

The Forward Problem (FP) of EEG addresses the calculation of the electric potential V on the scalp for a known configuration of sources, provided that the physical properties of the head tissues (conductivities) are also known. One should take into account that the same forward model of the EEG can be used for the MEG as well, since the magnetic field can be calculated from the potential V by simple integration [79]. An accurate solution of the forward problem is a necessary prerequisite for solving the inverse problem, and is extremely important to take maximum benefit from the EEG and the costly MEG, which have the advantages of noninvasiveness and excellent time resolution but they have lack of spatial resolution. To precisely determine the solution of the forward problem there is the need for two models that describe the physics and the physiology of the problem. The first one is a physical model of the neural sources while the second one is a model which describe how the sources generate electromagnetic fields on the outer surface of the head [80].

In order to construct models able to resolve the forward problem and consequently the inverse one should take into account the physics of the EEG signal and its generators. Thus, to build a macroscopic model of the underlying processes which depict the variations of the scalp potentials either spatially or temporally. As discussed extensively in the [Chapter 2-Brain Physiology and Epilepsy](#) the sources of the measured EEG signal are the pyramidal cells. All the processes involve either excitatory or inhibitory activity are described by primary currents. However, the potential distribution on the surface of the head is being evaluated with secondary currents and is based on the principle of some fundamental equations of Maxwell which are investigated further on the next sections. Generally, the amount of current flowing in and out of an activated neuron is microscopically the same [81]. From a microscopic field of view the modelling of this kind of electrical activity is difficult to be composed but from a distant electrode this field could be approximated by a **dipole field**. Since the activated area of the cerebral cortex may be larger, it can be modeled by a layer of dipoles. Therefore, in the case of synchronous activation of a number of pyramidal cells the electrodes capture macroscopically this electrical activity (or better they are sensitive to a portion of neural activity). The macroscopic recording of such activity is performed by observing the sources as an **Equivalent Current Dipole (ECD)**.

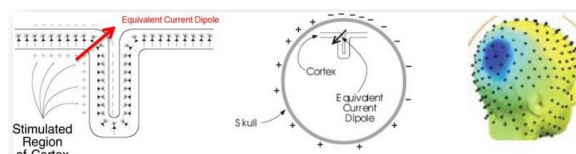


Figure 6.2: Equivalent Current Dipole

The most important characteristic of the ECD is its orientation. However, to fully describe a current dipole one should consider its position and its moment as well. One of the simplest current configurations is to approximate it as a wire between two points which are a source and a sink of the current. From a physiological point of view the dendrite exhibits an increase in the positive ions due to an excitatory synapse and thereby a source is formed there and a sink at the soma. However, when these two are close each other there is a current dipole. The position of the dipole could be considered as the unified position of sink and the source whereas the moment is vector pointing from the source to the sink and its amplitude is correlated proportionally with the distance [82] as explained in the equation below. The equivalent current dipole is defined by Q which could be considered as the strength of the source at the location r_Q or as the concentration of the current density to a single point due to primary currents $J^p(r)$ [38]. Therefore the concentration is expressed as follows:

$$J^p(r) = Q\delta(r - r_Q) \quad (6.1)$$

where δ is the Dirac function to model the locality of the point. The concentration term has units A/m^2 . To offer a more detailed representation of the current dipole let us consider a current I traversing a wire with length Δs in the direction \hat{x} .

$$J^s = \hat{x}I\Delta s \left[\frac{u(x + \frac{\Delta s}{2}) - u(x - \frac{\Delta s}{2})}{\Delta s} \right] \delta(y)\delta(z) \quad (6.2)$$

where $u(x)$ is the unit step function. Considering a wire much smaller than the location r ($\Delta s \rightarrow ds$) the current converges to a single point.

$$J^s = \hat{x}Ids\delta(x)\delta(y)\delta(z) \quad (6.3)$$

The current dipole could be oriented in any direction and thus the I becomes a vector \mathbf{I} while the term $\mathbf{I}ds$ prevails in the current density equation. As a consequence one could claim that the dipole moment is defined as:

$$Q = \mathbf{I}ds \quad (6.4)$$

and thus the source current density is expressed as:

$$J^s = Q\delta(x)\delta(y)\delta(z) \quad (6.5)$$

The dipole moment has A/m as units while each delta function has m^{-1} and for this reason the current density has units A/m^2 .

6.2.1 Source Model

The source model refers to the mathematical model used to approximate the source current density. The source model most often used is the equivalent electric dipole model, which approximates the primary current density within a patch or volume as a point source. To compute the source model one should choose an interface from a segmented MRI image of the subject. Usually the interface chosen is the white or gray matter. Then for this interface the positions of the dipole are estimated taking into account the sensor locations as well. A realistic source model consists of a dipole layer, representing an activated part of the cortex. When the dipoles are oriented perpendicularly to the layer and the dipole density is

homogeneous, it appears that the electrical potential and magnetic field caused by the dipole layer only depends on the outer contour of the layer. Therefore, in terms of potential, a flat layer and the curved layer exactly generate the same potential distribution (*Wolters et. al 2012*).

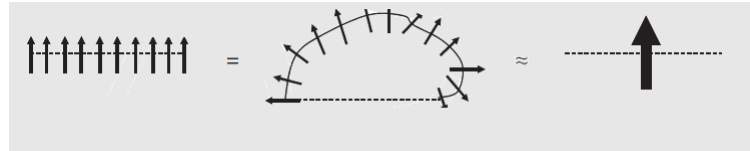


Figure 6.3: Source Model as dipole layer and single dipole

Adapted from EEG - MEG Forward Modelling, Wolters et. al 2012

6.2.2 Head Model

Another important element for going one step closer to solving the forward problem is the **Head Model**. It is responsible for modelling the potential distribution on the scalp due to a dipole from the source model. It further aims at defining the geometry and electrical/magnetic properties of the head. It is needed in order to account for the environment in which the source is placed and the way this assignment affects the potential distribution at a specific distance from the source. The first historical head model was the **single uniform sphere model** which was expanded later to **three-layer model** including the brain, skull and scalp as concentric spheres. Nowadays, there are many attempts to model the head geometry with realistic shapes (**Realistic Head Models**) incorporating also the conductivity properties of a single layer and in the interface between two layers as well. The importance of the correct head modelling could be depicted in the forward problem solution. In other words an inaccurate head model leads to high localization errors and to wrong propagation effects.

The shape of the head is particularly important since it varies from subject to subject and thus a precise representation should take into consideration. Otherwise using universal head models for all the patients we would neglect possible injuries or malformations that are strongly connected with the localization of the sources thereby leading to incorrect results. A most common strategy to extract a subject-based head geometry is to use the MRI-scan which offers 3D image of the head describing all the layers and parts of the brain such as white & gray matter, skull, scalp, CSF but also some bones between these interfaces.

Another aspect of the head modelling which should be taken into account is the conductivity properties of the different compartments. Modelling the conductivity one could understand the propagation of the electromagnetic fields and the attenuation they are subjected to prior to the recording by the outer-sensors. At this point there are two basic conductivity properties that need to be highlighted, the homogeneity and the anisotropy. The former describes the conductivity within a compartment stating that it is constant while the latter is expressing the conductivity values in various directions. Specifically if a compartment is called anisotropic it means that its conductivity is not equal in every direction. It is worth noted that realistic head models are able to specify this property which represents accurately the head characteristics. To build an anatomical model of the head an MRI scan must be obtained from each individual subject. Usually T1,T2 scans aid in the segmentation of the various compartments and often they achieve that complementarily. Then these surfaces are tessellated and they are projected into the 3 Dimensional space in a process called **meshing**. However, another step we need to bear in mind is the coordination between sensor locations

and the dipole locations. In other words they must be expressed in the same coordinate system (e.g CTF) and this is achieved by translating, rotating and scaling based on fiducial points which are placed on specific points of the head during the MRI test. The last prerequisite involves another element that need to be evaluated in the forward modelling which is the sensor locations. Sensor locations can be measured with the MEG or EEG devices but they could be also approximated by templates which is to be avoided since they introduce errors.

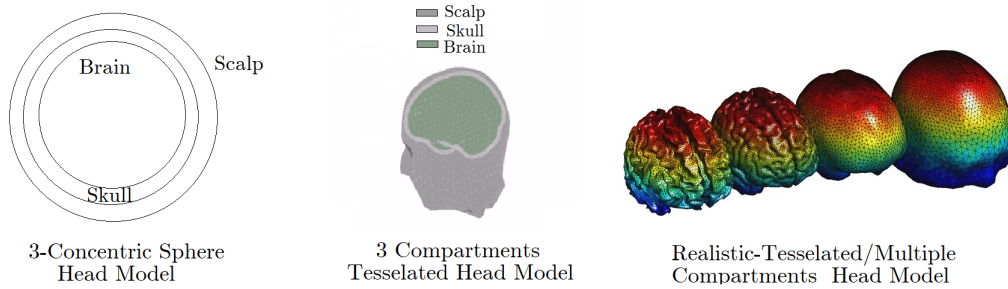


Figure 6.4: The progress of head-modelling

6.2.3 Maxwell Equations

On the question of the mathematical formulation of the Forward Problem one should firstly consider that the solution of the FP could be found by modelling both the primary and secondary current density which are the sources of the Electro Magnetic signals. This modelling is performed throughout the head volume conductor which has inhomogeneous and anisotropic properties that ideally need to be incorporated for accuracy and efficiency. The electric sources inside the brain produce electric and magnetic fields that can be modeled by the Maxwell Equations.

$$\begin{aligned}
 \nabla \cdot \mathbf{E} &= \frac{\rho}{\epsilon_0} \\
 \nabla \cdot \mathbf{B} &= 0 \\
 \nabla \times \mathbf{E} &= -\frac{\partial \mathbf{B}}{\partial t} \\
 \nabla \times \mathbf{B} &= \mu_0 \left(\mathbf{J} + \epsilon_0 \frac{\partial \mathbf{E}}{\partial t} \right)
 \end{aligned}
 \tag{6.6}$$

where \mathbf{E} is the electric field, \mathbf{B} is the magnetic field, \mathbf{J} is the current density, ρ is the total electric charge density, ϵ_0 is the permittivity of free space and μ_0 is the permeability of free space. The nabla symbol ∇ denotes the 3D gradient operator while the $\nabla \cdot$ and $\nabla \times$ represent the divergence and curl vector operators respectively. When studying brain activity and its electromagnetic properties these equations could reveal the underlying behaviour. However their complexity is high and at the same time requires attention in the interpretation. Notwithstanding their complexity, due to the specific neurons' behaviour and the recording process these equations could be simplified by the **quasi-static approach**. Specifically, the potential fields of the synaptic currents at different dendrites of neurons van cancel each other out [83]. Also at one time instance all fields are triggered by the active source or in other

words no time delays are introduced. This is because of the proximity of the MEG/EEG sensors to the brain with respect to the frequency range of neural sources (up to 1 kHz) [80]. Last but not least, the permeability of the tissue in head is considered equal to that of free space [38]. Therefore a time-independent Maxwell equation ($\frac{\partial B}{\partial t} = 0$, $\frac{\partial E}{\partial t} = 0$) may be used to model the FP (formulate a relationship between Electric Potential and Impressed Current). It is althoug useful to first divide the current density J into two components, the primary current J_i and the passive or return current:

$$J(x) = \sigma(x)E(x) + J_i(x) \quad (6.7)$$

where σE represents the return current flowing through the extracellular space and it satisfies the **Ohm's law** with σ being the conductivity sensor, *EEG and MEG forward modelling, Wolters et al. 2012.*

6.2.4 Poisson Equation

Exploiting the quasi-static approximation the electric field can be expressed with a scalar potential:

$$E = -\nabla V \quad (6.8)$$

The FP is formulated using the Poisson equation which correlates the potentials at any position in a volume conductor with the applied current sources. The derivation of this equation results from the following equations:

The current source density is expressed by the divergence of current density:

$$\nabla \cdot J = -I_m \quad (6.9)$$

Using the source model in which the sources investigated and modeled are those that represent the removal or the injection of positively charged ions at the apical dendrite and at the cell body of the pyramidal cell respectively the (6.9) is transformed to:

$$\nabla \cdot J = I\delta(r - r_2) - I\delta(r - r_1) \quad (6.10)$$

where the r_1 and r_2 are the locations of the current sources that represent the ions variation. Taking into account the (6.9), Ohm's law ($J = \sigma E$) and (6.8) the **Poisson's equation** is obtained:

$$\nabla \cdot (\sigma \nabla V) = \nabla \cdot J = -I_m \quad (6.11)$$

Generally, the EEG Forward Problem is rephrased to the problem of finding the scalp potential $g(r, r_{dip}, q)$ on an electrode at a specific position r due to a dipole r_d with a moment q . This could be achieved by solving the Poisson's equation by finding the scalp potentials for all different sensors. The latter can be expressed by a set of linear equations for N electrodes and z dipoles as follows:

$$V = \begin{bmatrix} V(r_1) \\ \vdots \\ V(r_N) \end{bmatrix} = \begin{bmatrix} g(r_1, r_{dip_1}, q_1) & \cdots & g(r_1, r_{dip_z}, q_z) \\ \vdots & \ddots & \vdots \\ g(r_N, r_{dip_1}, q_1) & \cdots & g(r_N, r_{dip_z}, q_z) \end{bmatrix} \begin{bmatrix} q_1 \\ \vdots \\ q_z \end{bmatrix} \quad (6.12)$$

$$V = GQ \quad (6.13)$$

with V being the matrix of the observations, G is the gain matrix or also known as **leadfield matrix** and Q is the matrix with the dipole magnitudes.

When it comes to solving the Forward Problem, behaviour between two interfaces play a crucial role and pose some conditions that need to be taken into consideration. First of all, no charge can be accumulated in the boundary between two compartments and thus a charge should enter the other interface. This could be translated into transition from one conductivity layer σ_1 to another σ_2 . The boundary conditions were developed by **Neumann** and could be summarized below:

Between two interfaces a component e_n is traversing the two interfaces boundary without piling up charge there.

$$(\sigma_1 \nabla \cdot V_1) e_n = (\sigma_2 \nabla \cdot V_2) e_n \quad (6.14)$$

Regarding the outer interface of the head with the air no current can be injected into the air due to its low conductivity:

$$(\sigma_1 \nabla \cdot V_1) e_n = 0 \quad (6.15)$$

Last but not least, according to **Dirichlet boundary condition** the potential cannot have discontinuities when crossing two interfaces [83]:

$$V_1 = V_2 \quad (6.16)$$

As explained previously the solution of EEG forward problem, calculation of scalp potentials, lead also to the solution of MEG forward problem which refers to calculation of the magnetic field $B(r)$ from a given current distribution $J^p(r')$ within the brain [38]:

$$B(r) = \frac{\mu_0}{4\pi} \int \frac{J(r') \times R}{R^3} dv' \quad (6.17)$$

with r being the point in which the field is computed while the r' refers to the source region.

6.2.5 Solving Forward Problem

The problem of forward modelling could be unfolded in two ways either by **analytical** or **numerical** approaches which will be discussed in this section. With respect to the MEG FP analytic solutions can be computed if the volume conductor is approximated by an isotropic **sphere** or by **overlapping spheres**. Similarly, in EEG the analytical solutions are based on volume conductors with **concentric spherical layers** with different isotropic conductivities. On the contrary, head shape and its properties are more complicated and thus geometry, inhomogeneity and anisotropy should be incorporated in the modelling and in process of finding the FP solution. Such methods are the **Boundary Element Method** and **Finite Element Method**.

Analytical Solutions: The first attempts towards forward modelling were characterized by using simplified head geometry which was represented by a homogeneous sphere or a set of concentric spheres. The former was soon rejected since the conductivity values of different compartments of the head varies and thus a set of multilayer concentric spheres described more accurately this property. In other words each layer/sphere is a compartment. The more common approach is a 3-layer headmodel in which the outer sphere is the scalp, the intermediate is the skull and the inner one represents the brain each of which has different

conductivities. Of particular interest is the use of these headmodels in the MEG Forward Problem since sources in both of these generate the same MEG fields. The latter stems from the fact that different conductivity layers affects only the secondary currents which are impressed by the primary ones. Henceforth both conductivity and radius of each sphere/layer doesn't influence MEG FP whereas this doesn't apply for the EEG FP. For the concentric sphere geometry a semi-analytical solution exists which is formulated below:

$$V = \frac{1}{4\pi SR^2} \sum_{i=1}^{\infty} \frac{X(2i+1)^3}{g(i+1)i} b^{i-1} [i d_r P_i \cos\theta + d_t P_i^1 \cos\theta] \quad (6.18)$$

with \mathbf{S} denoting the conductivity of the layers, \mathbf{R} the radius of the outer shell, \mathbf{X} is the ratio between the skull and soft tissue, \mathbf{b} is the relative distance of the dipole from the center, θ is the polar angle of the surface point and P_i express some Legendre Polynomials. Last but not least g_i represents the various source points in different layers [83]. It is worth noted that geometrical registration of head model to the an individual's MRI improves the fitting and helps in finding the scalp potentials for an arbitrary dipole. Another observation from this solution is that due to spherical symmetry radially currents don't generate magnetic fields thereby MEG fields by radial sources are attenuated with respect to perpendicular ones. Therefore a useful conclusion is examined which is connected with the fact that magnetic fields decrease faster than electric potentials leading in claiming that MEG is less sensitive to **deeper** brain structures [80].

Numerical Solutions: The spheroidal head models are the most important and common source of localization errors and miscalculations of electric, magnetic potentials and fields. Despite their computational efficiency and optimal time complexity they lack proper representation of the head shape and accurate modelling of the conductivity properties thereby inducing important errors. As a consequence more realistic approaches are adopted. The head is not spherical and its geometry is modelled using realistic surfaces while the varying tissue conductivities are assumed to consist a set of contiguous anisotropic regions. This model is taken into account in the numerical approach known as **Boundary Element Method (BEM)**. This specific method is computationally efficient despite the fact that restricts the model in homogeneous volume conductor with isotropic conductivities. The head model is built from surfaces which encapsulate a particular tissue while the solution lays its foundations in investigating the tissues inspecting them by small boundary elements which tessellate the interface (See Figure 6.5). Most common interfaces used in BEM are **scalp, skull & brain**. BEM is based on integral equations involving unknowns on the interfaces. The latter consists the advantage of this method since it reduces the number of unknowns requiring only surface meshes instead of volume meshes. BEM digitizes each interface S_j with N_{S_j} triangles and calculates the potentials in the center of each triangle. The potential in each surface is expressed as the summation of integrals over the triangles.

$$V = \frac{2\sigma_0}{\sigma_k^- + \sigma_k^+} V_0(r) + \frac{1}{2\pi} \sum_{i=1}^R \frac{\sigma_j^- - \sigma_j^+}{\sigma_k^- + \sigma_k^+} \int_{r' \in S_j} V(r') \frac{r' - r}{||r' - r||^3} \quad (6.19)$$

where σ_0 denotes the medium in which is the dipole located and $V_0(r)$ the potential at r at this specific medium. σ_j^- and σ_j^+ represent the conductivities of the inner and outer compartments which are divided by interface S_j . However, the solution for the integral element is not feasible and thus an approximation is defined using linear combination of simple basis functions for each triangular element [83].

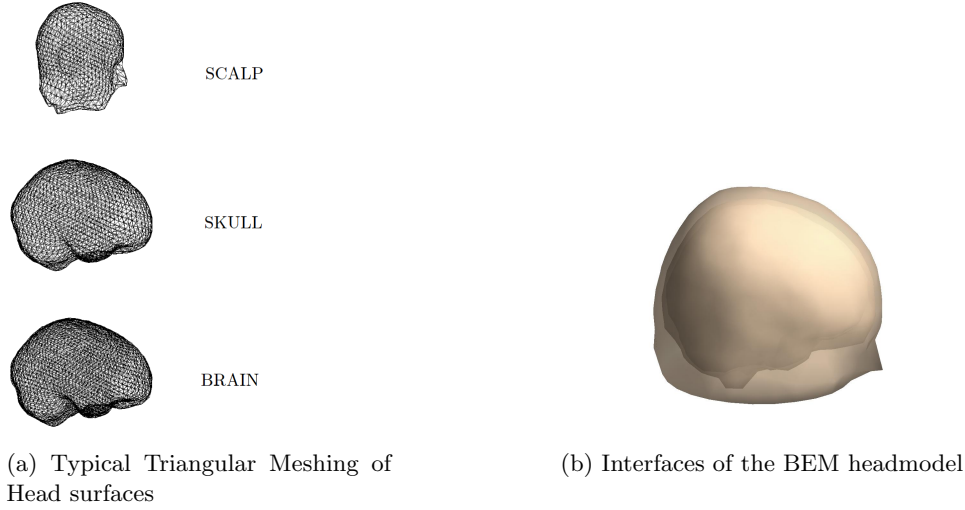


Figure 6.5: BEM headmodel geometry tessellation

The solution of the forward problem that BEM offers demand the calculation of the potential in every mesh node which leads to computational complexity escalation. Moreover, the localization accuracy is not the optimal since the solution depends directly from the depth of the underlying source for which the potential is calculated. The aforementioned limitations are depicted when the precision of calculation drops for sources that their distance from the sensor is comparable to the triangle in the mesh. Last but not least, BEM idealizes somehow the head geometry but also the conductivity properties. In other words it simulates brain as one surface rather than multiple layers which have different electrical properties and at the same time it cannot model the anisotropic properties of the head.

Boundary Element Method may have been an important factor in solving the Forward Problem with an acceptable amount of computer resources. However there exist several restrictions which described previously thereby forging directions towards more realistic and accurate solutions. A modern and widely used approach is the **Finite Element Method** which offers the mathematical tool for solving complex equations which incorporate realistic physics and geometrical properties. Similarly with BEM the FEM utilizes a number of layers/compartments of which the most common are: **scalp, compacta & spongiosa bones, gray & white matter and CSF**. In the FEM the solution domain can be discretized in a number of uniform or not finite connected elements. Each location is approximated with a variable and changes of this are expressed by an interpolation function. In the case of the boundary problem integral formulations are used which embed the interpolate functions. The Finite Element Approximation is utilizing the Galerkin method:

$$(\sigma \nabla \Phi, \nabla \bar{\Phi}) = (-I_v, \bar{\Phi}) \quad (6.20)$$

where $\bar{\Phi}$ is a test function. Exploiting this method the Forward Problem is formulated firstly with a weak equation:

$$\int_G \nabla \phi \cdot (\sigma \nabla V) dG = \int_G \phi I_m dG \quad (6.21)$$

At this point FEM transforms the problem from continuous to discrete since it creates a finite dimensional subspace, defines parameters of the test function at every node points and

creates basis functions as linear functions able to represent the test function $\bar{\Phi}$. In this way the entire 3D volume model is divided into small elements which contains n computational points for which there are test functions that help to find the unknown potentials. However, these test functions are limited only to adjacent elements and they are equal to the unity thereby leading to a equivalent system of equations which is sparse.

$$V(x, y, z) = \sum_{i=1}^n V_i \phi_i(x, y, z) \quad (6.22)$$

where ϕ_i expresses the set of the test/basis functions. The tessellation that FEM produces is usually achieved with tetrahedrals or hexahedrals. One of its main advantage over BEM is the anisotropy modelling for the white matter which has different conductivity values according to the direction of the diffusion of the water but also for the skull in which there are layers of different abrasiveness that either allow the smooth or not flow of ionized particles. FEM achieves the modelling of these properties by utilizing **Diffusion Tensor Imaging (DTI)** information [20].

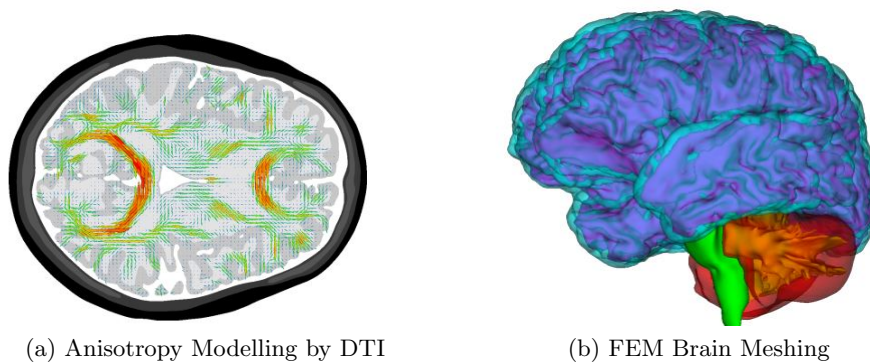


Figure 6.6: FEM model for the forward problem

Adapted from Felix Lucka, Carsten Wolters et.al. 2012

All the methods for solving the FP which were described are chosen according to the nature of the problem. In our use case the geometry and boundary problem need to be investigated and as a consequence a realistic geometry is important to approximate our solution. Moreover, the head consists of layers that are highly heterogeneous and present features that are described more precisely with the FEM. Henceforth, the selected method is the Finite Element method despite its complexity in developing and interpretation. It is worth noted although that there is a method in the vicinity of the FEM. The **Finite Difference Method (FDM)** which utilizes differential equations and cubes for geometry were not considered as a solution to our problem since its computational points are strictly defined for both isotropic and anisotropic properties and thus they can represent irregular interfaces that optimally as FEM.

What described through these mathematical solutions is how to find the scalp potentials due to a specific underlying source (EEG FP). In our use case we also want to solve MEG FP for which we want to implement a source localization to detect the epileptic sources. The MEG FP is quite straightforward once EEG FP is solved and scalp potentials V on each surface are obtained. The magnetic field B in a sensor with location r is described with the

following equation [38]:

$$B(r) = B_0(r) + \frac{\mu_0}{4\pi} \sum_{j=1}^m (\sigma_j^- - \sigma_j^+) \sum_{k=1}^{n_j} \int_{\Delta^{kj}} V(r') \frac{R}{R^3} \times dS'_j \quad (6.23)$$

6.3 Inverse Problem

The **Inverse Problem (IP)** aims at estimating the locations and magnitudes of the current sources that generate the measured Electro-Magnetic data. Sometimes it is also referred as Neural Source Imaging problem (NSI) and is considered as a means of providing detailed spatial-temporal analysis of the brain activity for different functions. An accurate solution of NSI could contribute to understanding the underlying brain mechanisms and to pinpointing abnormal regions that might indicate tissue damages. Another benefit from solving the IP is the localization of various neurological disorders origin by detecting the sources of abnormal EEG/MEG waveforms. A fundamental difficulty with the Inverse Problem is that there is an infinite number of different current distributions that can explain the recorded data. The reason behind this problem is that there are **silent sources** that produce not observable electromagnetic fields and they could be added to a solution without affecting the data fit. According to *Hadamard* definition for well-posed problems there are three conditions satisfied by their definition one of which is the uniqueness of the solution. The latter doesn't hold in IP's definition and therefore the Inverse problem is called **Ill-Posed Problem**. To tackle this difficulty we incorporate **a-priori assumptions** about the nature of the sources by setting anatomical/neurophysiological constraints or number of underlying sources. As a consequence the validity of the solution domain is depending to the correctness of the assumptions adopted. Usually, one or several number of dipole sources are assumed and their positions and orientation is estimated by an iterative process in order to fit with the recorded data. The accuracy with which a source can be located is affected by a number of factors including head-modelling errors, source-modelling errors and noise[78].

Extensive research has been done to accurately solve the Inverse Problem. Essentially the solution is the estimation of the dipole parameters that are considered as current sources that contribute to the scalp potentials and magnetic fields. These parameters are six of which the three are correlated with the location in the 3D space, two dipole axis angles and the dipole moment. The calculation of the solution is a nonlinear problem and is usually obtained by an iterative process where the assumed source is moved in the head model and its parameters change till the best fit is acquired. Another solution is to first divide the brain into a large number of cells and then assign a dipole to each cell while the search is performed again for the optimal fitting. It is evident that unique solution is obtained only if the source and the head model is assumed. Some of the methods that they are extensively described in the next sections involve regularization techniques and the most common ones are the standardized Low-Resolution Electromagnetic Tomography Activity (**sLORETA**), Minimum Norm Estimate (**MNE**) or **eLORETA**. Furthermore, according to Bayesian estimation one has to assume prior probability distribution that describes the likelihood of possible states of the system. Other classical techniques rely on the utilization of sparsity to derive an optimal solution or maximization of entropy on the mean. These approaches assume quasi-static approximation to formulate the mathematical correlation of the sources with the recorded data and they are mapped through the leadfield matrix.

6.3.1 Assumptions of the Inverse Problem

As indicated previously given that the solution to the Inverse Problem is not unique one should first consider a set of assumptions. In general, the generation of the signal should be reasonable and thus assumptions related to this impose constraints that reduce the solution domain. Therefore, it is important to assume that the EEG signal measured on the scalp derives by the pyramidal neurons which are perpendicular to the cortical surface. Since the dendrites of the pyramidal neurons are all parallel the EPSP should ideally sum across space and time and could be approximated by a current dipole. Moreover, since currents in a conductor typically form a closed loop, it is assumed that there are also return currents, that close the loop. This return current is assumed to arise because the cerebrospinal fluid and the tissues covering the brain such as the dura, skull and scalp all conduct electric currents *Narayan P Subramaniam, 2018*. Additionally, several dipole localization methods work under two major assumptions. The first one is that the number of sources is constant in time while the second is that the source locations are fixed. Moreover, many source localization methods incorporate noise in their mathematical framework for which they assume that it is Gaussian, additive and homogeneous for all the sensors but also uncorrelated between every pair of sensors.

6.3.2 Mathematical Formulation

According to the mathematical formulation of forward problem of subsection 6.2.4 we could express the mathematical framework of the inverse problem. Specifically, in the FP the solution is on the domain of searching for the electrode potentials V in a scalp location r given the dipole sources with various configurations (different locations, angles, moments). From the (6.12) it is assumed that the orientation and the magnitude of the dipoles are unknown. However, dipoles are constrained to have a normal orientation to the surface according to the assumption about the signals generation on the apical dendrites. As a consequence only the magnitude vary and therefore the formulatin is transformed :

$$V = GQ + n \quad (6.24)$$

where now Q is a matrix of dipole magnitudes at different time instances and n is a noise matrix added to the recorded data. From this equation we could state that the Inverse Problem's goal is to estimate the dipole magnitude matrix \hat{Q} given the electrode positions and scalp potentials or the magnetic fields.

6.4 Algorithms for the Inverse Solution

Regarding the solution of the Inverse Problem there are several algorithms/methods which are classified according to their assumptions and to their constraints. There are two main approaches for the inverse solution: non-parametric and parametric methods [78]. In the **Non-parametric** models several dipole sources with fixed locations and (possibly) fixed orientations are used on the cortical surface. Under the assumption for the neurophysiological basis of the recorded data the orientations are fixed and there is a following process in which the amplitudes of these dipole sources are then estimated. The dipole locations are fixed and therefore the problem is classified as a linear one. On the other hand, in the **Parametric** algorithms there is a standard number of few dipoles whose location and orientation are

unknown.

A second type of classification concerns the way different inverse methods treat the temporal dependence of the data. Indeed, due to the high temporal resolution of MEG/EEG data the data tend to be smooth, and the underlying currents exhibit a similar degree of smoothness in the temporal variable. The first methods tended to solve the inverse problem at different time instances due to the limited computer resources by neglecting in this way the temporal dependency. These methods are also called as static methods. However, modern methods incorporate the temporal properties in their models and thus they reduce the ill-posedness. These methods are known as dynamic methods and their solution domain embed the temporal dependency of the primary current sources. The next sections focus on the Inverse Methods used in our use case for which the solution domain is summarized along with their mathematical approach for the localization of the underlying sources.

Some of the parametric methods are quite straightforward since given the Poisson's equations with boundary conditions as explained in (6.11) and (6.15) one could clearly claim that there is no trivial solution but it could be restricted based on the assumptions. Using the (6.24) the Inverse methods try to estimate the Q but in order to do so they need the inverse matrix of LeadField which in term is non invertible. Hence, regularization techniques are employed to solve the IP. The minimization criterion is given by the

$$\min \|V - GQ\| \tag{6.25}$$

In regularization theory the solution is found by minimizing a functional that combines the fit with the data and a penalty term:

$$\hat{Q} = \operatorname{argmin}(\|V - GQ\|_2^2 + \lambda P(q)) \tag{6.26}$$

where λ is a regularization parameter and $P(q)$ the penalty term. Essentially in this framework there is an attempt to rather than solving the Inverse Problem one aims at quantifying the amount of information that is available on the unknown underlying neural currents. This information is called prior and it helps in quantifying the posterior distribution given the measured data (conditional density of sources given the measured data). The posterior distribution is expressed using the Bayes rule:

$$p(q|v) = \frac{p(v|q)p(q)}{p(v)} \tag{6.27}$$

Therefore we could state that there is a connection between posterior distribution and the solution of (6.26) under Gaussian assumptions:

$$p(q|v) \propto \exp(-\|V - GQ\|_2^2) \tag{6.28}$$

Non-Parametric Methods try to minimize this penalty term and to properly choose the regularisation parameter while the Parametric Methods search for solutions which represent the best dipole positions and orientations. To achieve that they compute the global minimum of the residual energy but in order to do that they perform a non-linear minimization of the cost function: $\|V - G(r_i, r_{dip_i})Q\|$ over all parameters.

6.4.1 Dipole Scanning

One example of parametric inverse method is the **Dipole Scanning**. In this method a single point or small number of points that explain the maximal amount of topographical variance is assumed. In other words it assumes that the source of brain activity is one or a small number of dipoles. This method performs a grid search (for each location of the source space) based on the assumed dipole(s) either for a time window or a time point and identifies the dipole model parameter that minimize the error between simulated and measured distribution as explained before [84]. The resulting Equivalent dipole model is interpreted as the source of cortical activity. The drawback of this approach is that it is not appropriate for distributed cortical activity or simultaneous activity in different regions.

6.4.2 Beamforming

Another renowned parametric method is the **Beamforming Approach**. Beamformers design spatial filters W^T that pass signal at a specific location and suppress the others [85]. In this way they represent the neuronal activity of each dipole d in a time t as: $V(t) = W^T q(t)$ (\star). These filters suppress the activity of the other locations by the filters W^T that satisfy the following for dipole location r_{dip} .

$$W^T(r_{dip})G(r) = \begin{cases} I & \|r - r_{dip}\| \leq \delta \\ 0 & \|r - r_{dip}\| \geq \delta \end{cases} \quad (6.29)$$

where G is the forward matrix and δ is a small distance [78]. These filters are being optimized by data covariance. Their advantage is that they don't assume in advance the number of sources while at the same time they are robust since the environmental noise can be filtered out. However there is one assumption that they use. Beamformers assume uncorrelated sources and this could influence the localization with errors for correlated sources. There are several types of beamformers of which one common is the Linearly Constrained Minimum Variance Beamformers (LCMV). This specific type of beamformers minimize the covariance of the neuronal activity representation (\star) in order to suppress the activity from other locations:

$$\min(\text{Tr}(C_y)) \rightarrow W^T(r_{dip})G(r_{dip}) = I \quad (6.30)$$

with C_y being the covariance of the matrix $W^T C_m W$ while C_m is the covariance of the estimated signal from the available data. In other words beamforming minimizes the output energy assuming that only one dipole is active at a time. Minimizing the variance we achieve optimization of the stopband and applying the spatial filter W we estimate the dipole moment at r_{dip} while the location is estimated by an approximation of variance as function of location. The assumption of this approach is that the sources are weighted combinations of dipoles.

6.4.3 Minimum Norm Estimate (MNE)

The Minimum Norm Estimate Method [86] is classified as non-parametric method since it does not have an inclusion of a-priori restrictions that allow approximating a solution closer to the actual physical behavior in the brain from the set of possible solutions [87]. MNE is used to reconstruct the neural source resulting from the activity at the surface as well as within the brain volume. This method is suitable for reconstruction of the activity on the cortical surface. Furthermore, its solution domain is based on a search for the minimum power

and correspond to the Tikhonov regularization. It corresponds to solving a simplified version of (6.26) where each point is treated independently and with Penalty function defined as $P(q) = \|q\|_2^2$. The advantage of this approach is that analytical calculation is feasible, thanks to the relatively small size of the matrices involved:

$$S_{MNE}^{\hat{}} = [G^T G + \lambda I]^{-1} G^T V \quad (6.31)$$

where $S_{MNE}^{\hat{}}$ denotes the estimated sources, λ is the regularisation parameter and I the identity matrix. It is worth noted that the value of λ is evaluated through the L-curve algorithm in which the maximum value of the parametric plot indicates the optimal value. MNE is although prone to over smoothing the estimates of the neural currents and to create a bias towards superficial sources because they are closer to the sensors and therefore weaker signals encouraged by the l^2 norm. To overcome MNE's tendency to favour weak and surface sources a **weighted Minimum Norm Estimate** (wMNE) was proposed in the literarcy. The latter compensates the MNE's drawback by introducing a weighting matrix into the penalty term $P(q) = \|Wq\|_2^2$ or using a l^1 norm $P(q) = \|q\|_1$

6.4.4 sLORETA

MNE localization approach presented drawbacks related to the magnitude and depth of the sources. Therefore, a motivation for a new method was arisen. With the introduction of **low resolution brain electromagnetic tomography (LORETA)** the problem of extensively large errors seemed to be resolved. This method has good accuracy in localization of the sources even when they are deep. Its solution combines the Lead Field normalization with the Laplacian operator thereby compensating the smoothly distributes sources problem. However all methods proposed till then contained localization error. A new method was designed by Pasqual-Marqui (**Standardized Low Resolution Brain Electromagnetic Tomography (sLORETA)**) [88] which sounds like a modification of the previous LORETA approach but it tends to resemble more to the MNE. This method has zero localization error and is based on images of standardized current density. Specifically it standardizes the $S_{MNE}^{\hat{}}$ by using its variance and variation due to noise $S_{noise} = \lambda I$. The potential variance is given by :

$$S_V = G S_Q G^T + S_{noise} \quad (6.32)$$

where S_Q is the variance of the sources while the estimated current density is obtained as follows:

$$S_{\hat{Q}} = T S_{noise} T^T = G^T [G G^T + \lambda I]^{-1} G \quad (6.33)$$

where T is the inverse operator resulting from MNE solution $T = G^T [G G^T + \lambda I]^{-1}$. The estimation of standardized current density is produced by sLORETA as:

$$S_{MNE}^{T\hat{}} [S_{\hat{Q}}]_l^{-1} S_{MNE}^{\hat{}} \quad (6.34)$$

where $[S_{\hat{Q}}]_l^{-1}$ is the current density estimate of the sources S_V at the l -th diagonal block of the estimated current density [78]. One of the main benefits of this method is that it can detect deep sources accurately outperforming MNE and it has exact zero localization error in noise free simulations .

6.4.5 eLORETA

Exact Low Resolution Brain Electromagnetic Tomography (eLORETA) is a particular form of weighted MNE which achieves exact localization with zero-error [89]. Similar to sLORETA the estimated current density is given by the following equation incorporating the weight matrix W :

$$S_{\hat{Q}} = W^{-1}G^T[GW^{-1}G^T + \lambda I]^{-1}V \quad (6.35)$$

The weight matrix is zero except for the diagonal subblocks while the l -th voxel of eLORETA for the sources $S_{\hat{Q}}$ is computed as:

$$[S_{\hat{Q}}]_l = w_l^{-1}G_l^T[GW^{-1}G^T]^{-1}V \quad (6.36)$$

with w_l being the eloreta weights obtained by a symmetric square root matrix. An advantage of the eLORETA over sLORETA is the ability of suppressing less significant sources but also performs in a better way for localizing the sources [90]. However, the low spatial resolution of LORETA methods is undesirable in some cases such as feature extraction of spatio-temporal pattern recognition where high resolution is needed. In these cases, high resolution subspace based approaches (such as MUSIC, RAP-MUSIC etc.) by using dipole approach can provide results with higher accuracy and low localization errors.

6.5 Source Localization on Clustered Data

The following part of this thesis focuses on the results obtained during the source localization of epileptic clusters which were obtained according to the methods discussed in **Chapter 5**. A first attempt towards this field was performed using the FieldTrip Toolbox which divides the Forward and Inverse Problem in a quite straightforward process comprised of some steps to construct all the required elements to solve these problems. Regarding the forward problem we need to construct a head model, a source space but also to exploit the sensor information as shown in the Figure below. The process is depicted in the Figure: 6.7(b) and is composed of some steps.

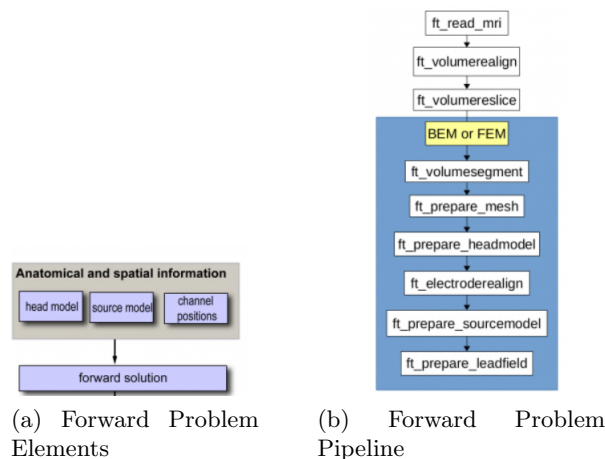


Figure 6.7: Forward Problem using the FieldTrip Toolbox

As a consequence the first step towards solving the forward problem is to prepare a headmodel. In order to do that we firstly tried to model it through a template MRI by the FieldTrip Toolbox. After aligning this MRI with the sensor locations through some fiducial markers interactively a segmentation process followed. For both the EEG and MEG it was decided to use a three-compartments headmodel using the BEM analysis (despite the fact that even simple sphere would work also for MEG). Hence, the three compartments segmented were the **scalp, skull & brain** as shown in the Figure: 6.8(a). The segmented parts were then projected in the 3-Dimensional space using the meshing process to create a 3D geometrical representation (Figure: 6.8(b)) and the volume conductor head model was prepared by defining homogeneous and isotropic values for conductivities ([0.4 0.01 0.4] respectively for [scalp skull brain] which were typical values for these compartments). Last but not least, a source space was computed assuming sources only inside the brain for EEG for a high grid resolution search. The last step of the Forward Problem was to compute the Gain/Leadfield Matrix for each location of the source space.

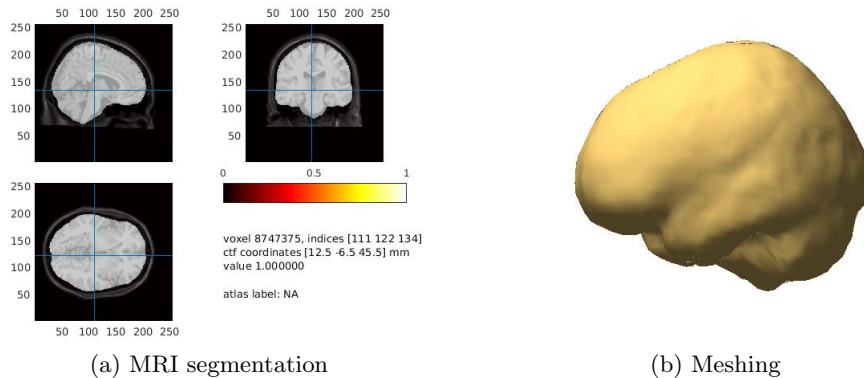


Figure 6.8: Brain Segmentation and Meshing

Having solved the Forward Problem (calculation of the LeadField Matrix-Potential/Magnetic Field Distribution) the Inverse Problem was decided to be solved using the Minimum Norm Estimate both for EEG & MEG data. The reason behind this is that it could detect sources which expand in an area and it is extremely useful in our use case since our patient is suffering from multi-focal epilepsy which means that we are searching for more than one activated epileptic regions. To find the solution of Inverse Problem we will need some elements such as the Functional Data (Averaged Signals obtained from clusters, which are a pattern of epileptic predisposition between seizures), the Forward Problem solution, the time instance(s) we would like to check and the parameters of the method. Based on the average of the signals we computed the covariance matrices in a window of the [-100 ms 100ms] which represented the spikes peak area. The focus is on this area since it could give us insight on the underlying epileptic sources. Then, we selected a time window of [-5ms 10ms] for which we performed our localization. The reason behind this selection was that the rising flanks of the spikes were located in this area (the spike peak was a bit shifted from the 0ms, in the case of EEG). Last but not least, MNE requires a regularization parameter λ which was set by default to three according to FieldTrip tutorials. The results obtained for the three EEG clusters and the 3 MEG clusters visualized in the 3 slices of MRI are summarized below:

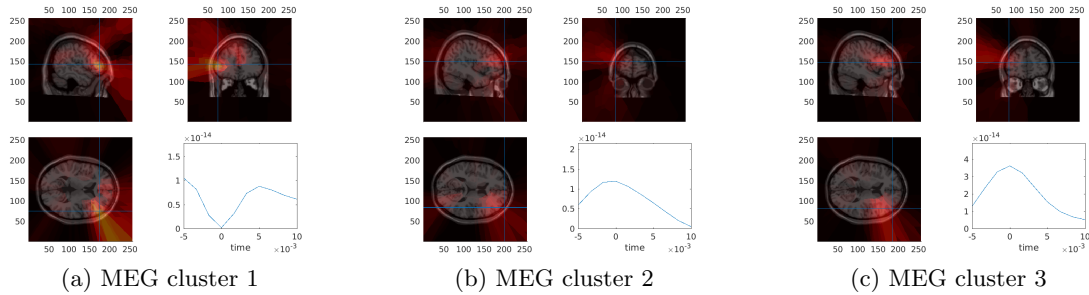


Figure 6.9: Minimum Norm Estimate for MEG clusters

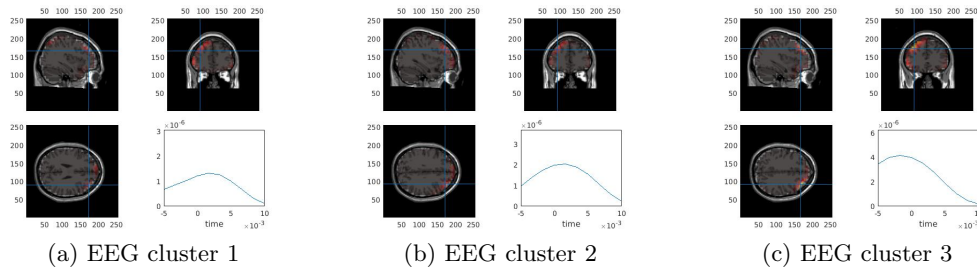


Figure 6.10: Minimum Norm Estimate for EEG clusters

From the visualizations above we could clearly see some activations in different areas. However there are some errors regarding the visualization process which might be due to the MRI template and due to the brain consideration as one compartment. Another visualization was to interpolate these points and to project them to the 3D mesh selecting a specific time point Power as color map. The results are shown below:

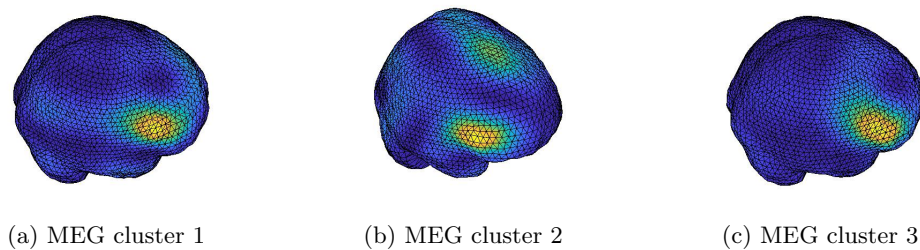


Figure 6.11: Minimum Norm Estimate for MEG clusters visualized in the Brain Mesh

Observing the figures above we could state that the result obtained from the Figure: 6.11(b) clearly shows two activations in right frontal area and one in the left fronto-central which could be highly correlated with the results obtained from [20] for the same patient in which the left fronto-central area was responsible for the symptomatology of the patient. However, in the EEG case the results are discouraging since the power of the activated areas were lower compared to the MEG and they couldn't be visualized similarly. The reason behind this might be the **low SNR's**, the **template MRI** instead of the subject's MRI but

also either the method itself or the covariance window which was more extended with respect to the time window inspected.

After performing **experimental attempts** for source localization we could claim that is of utmost importance to construct a head model according to a subject-based methodology incorporating the **realistic properties** in both geometrical and physiological aspects [6]. As a consequence, it was decided to construct a headmodel by the acquired MRI of the subject utilizing the **FEM** analysis for solving the Forward Problem defining thus more accurately the Forward Solution. The head model was built using information from both T1w- and T2w- MRI (MAGNETOM Prisma 3.0 T, Release D13, Siemens Medical Solutions, Erlangen, Germany) in a 6-compartment approach (skin, skull compacta, skull spongiosa, CSF, gray and white matter), Figure: 6.12 using MATLAB and SPM12 [40], [20], [91]. Geometry was adapted from hexahedral meshes including white matter anisotropy by the DTI information. The source modelling using FEM simulations and Venant principle was performed using the SimBio and the corresponding pipeline [92]. The inverse problem was solved by investigating the methods: Dipole Scanning, Beamforming, sLORETA, eLORETA and MNE. The motivation for this comparison stems from the fact that we desired to understand which method offers the best fit for the specific use case. A more detailed account of the application of these methods is explained below along with their parameters and the rationale behind their values definition.

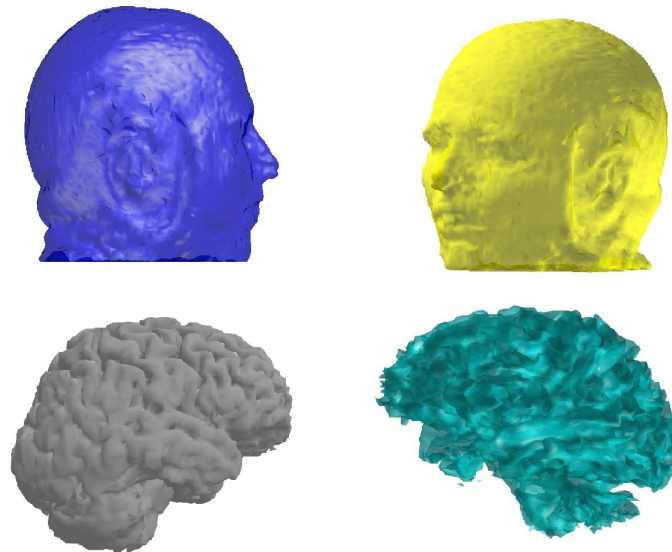


Figure 6.12: FEM headmodel various meshes (top: scalp, bottom: gray and white matter)

For the source localization methods it is worth mentioned that the covariance matrix was recalculated in a narrower window, namely $[-20 \text{ ms}, -5 \text{ ms}]$. The reason behind this rationale is that we want to focus on the rising flank of the spike to detect the epileptic area. In other words the abnormal functionality could be detected prior to the peak of the spike at 0 ms. The noise simulated as Gaussian diagonal while the methods applied for all single EEG or MEG clusters at specific time instances. Those instances were: -23 ms , -17 ms , -13 ms , -10 ms , -8 ms , -5 ms , -3.3 ms and 0 ms . Those timepoints selected accordingly in order to take insight on propagation phenomena for the epileptic abnormal behaviour and according to other related works such as [20], [18]. The results from each method are summarized below.

It is worth underlined that the combinations of possible source localizations could not be attached here since they are numerous but the most representative results are depicted in the next figures.

Dipole Scanning:

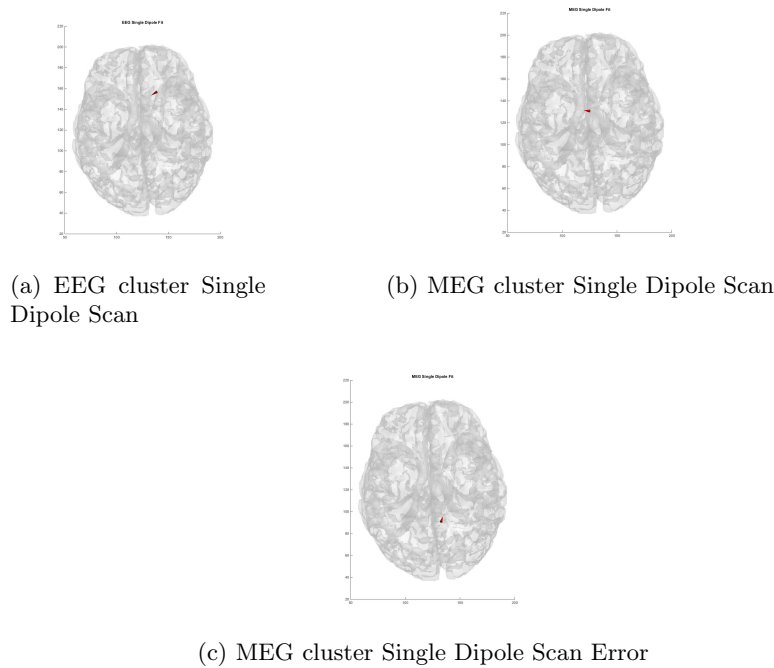


Figure 6.13: Single Dipole Scan for EEG/MEG clusters

The figure above is illustrating the results from some of the single dipole scanning for the clusters. It is clearly shown that this method places a single dipole as active source at the specific time point while at the same time it is not optimal for multiple and/or simultaneous activations at different areas. In order to further understand this a comparison of these results was performed with those of the [20] which were for the same subject. As a consequence we could claim that the dipole in both EEG & MEG is placed somewhere inbetween the distance of the two focal epileptic areas. Specifically, it was found according to [20] that the epileptic focus is strongly connected with two Focal Cortical Dysplacias (FCD), namely one in the right frontal area and one in left fronto central/ premotor cortex. Henceforth, the Dipole Scanning method is not well suited for our use case assuming one dipole activated because it erroneously places the dipole inbetween the distance of the two FCDs or even it has significant source localization errors as depicted in 6.13 (c). Moreover even if the assumption was for 2 dipoles it would clearly produce a wrong output because the activations are in an area and not discrete single sources.

Minimum Norm Estimate (MNE):

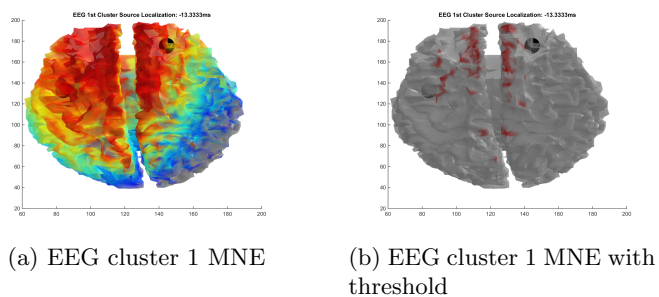


Figure 6.14: MNE on EEG Cluster 1

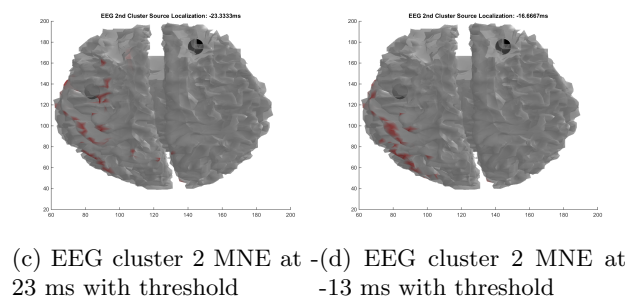
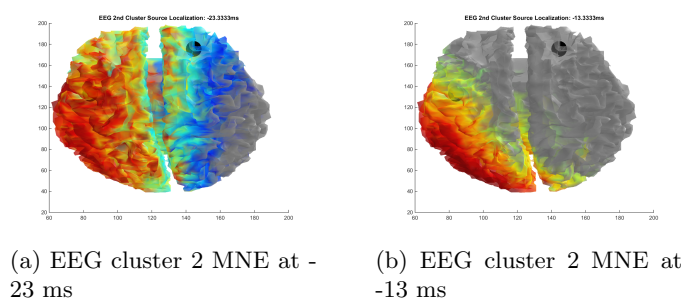


Figure 6.15: MNE on EEG Cluster 2

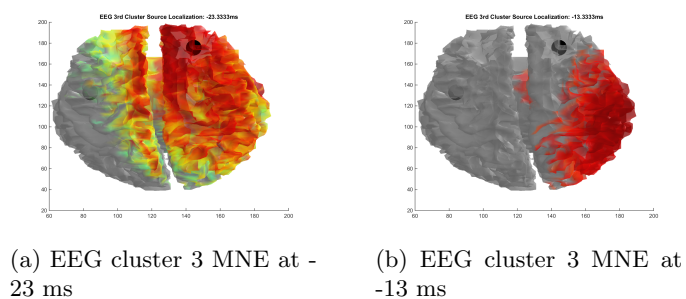


Figure 6.16: MNE on EEG Cluster 3

The figures for the MNE (with $\lambda = 25$, empirically defined) applied in EEG clusters depict the output visualized on the white matter mesh either with a threshold of 85% to retain the most significant sources or without it. Furthermore the two black spheres indicate the locations of the two FCDs extracted from [20] in order to evaluate our results accurately. On the thresholded outputs we could claim that the active sources represent a small portion of the cortex resulting in high accuracy. However, the results seem to approach the FCDs but not that efficiently. Specifically, on the 1st cluster the active zone is close to right FCD but it is far from total match. Additionally, there are active areas which doesn't suit with the FCDs and therefore they consist localization errors as shown in 6.16 (b). Regarding the non-thresholded results it seems that the FCDs are active but the area is much wider than the expected activations. Examples of these areas are shown in Figures: 6.15 (a) & 6.16 (a). A possible explanation could be that MNE detects sources close to cortical surface and therefore it is vulnerable to localization of more spreaded regions rather than narrow deeper sources.

On the other hand, MNE on MEG clusters seems to behave more accurately since it is able to detect either one or both FCDs as shown in 6.17 (a) and 6.17 (b) respectively. However, there also the same issues since the active areas are wide and there are also localization errors as clearly depicted in 6.17 (c). Consequently, this method lacks accurate definition of the seizure onset zone since it detects wide areas. The importance of describing the seizure onset zone is contributing to optimal resection of the abnormal tissues. Therefore, results like these are not medically approved and they need further investigation in order to decide whether or not a brain area needs resection.

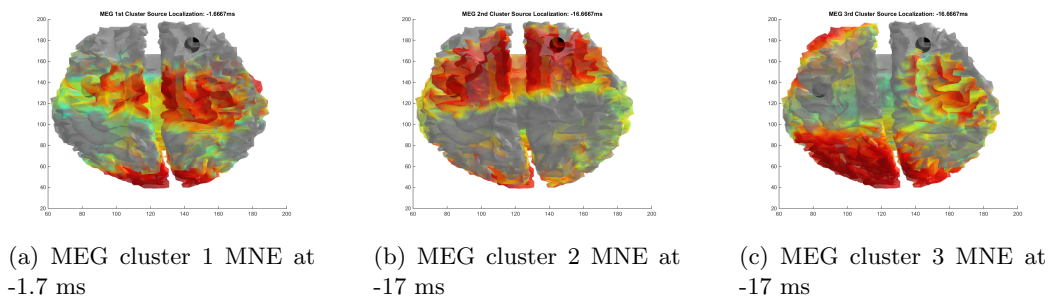


Figure 6.17: MNE on MEG Clusters

sLORETA

Turning now to the sLORETA inverse method there are a number of important differences compared to the previous results. Initially, the former tends to improve the localization area since it detects sources in narrow regions close to the FCDs. As shown in 6.18 (a) it clearly identifies an area which matched the right FCD while in EEG cluster 3 it is able to match the left FCD with a really high percentage of fitting. Provided that, sLORETA outperforms MNE in terms of accuracy while at the same time identifies the FCDs in separate clusters and at different time instances. Under those circumstances the spike clustering approach performed efficiently since it classified spikes responsible for the epileptic areas in different clusters. Consequently one important observation is that the spikes responsible for one FCD are expressed with different features than those of the other one. In this way the localization achieves high percentage of accuracy.

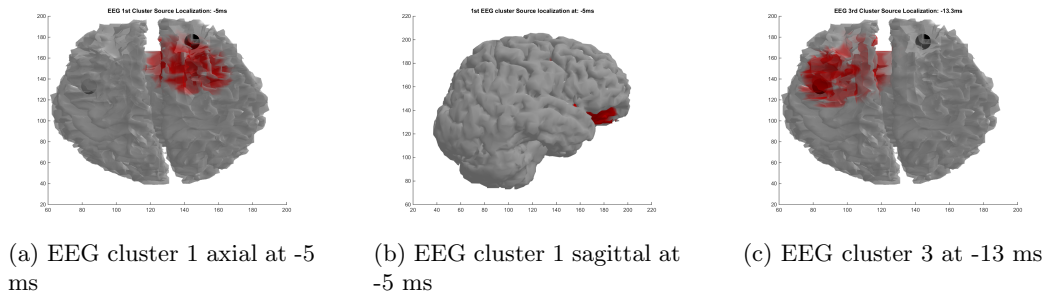


Figure 6.18: sLORETA on EEG Clusters (a): visualized in white matter, (b): visualized in gray matter

Another important remark is illustrated below when the method applied in the 2nd EEG cluster. In particular a propagation effect was found over the time domain. To put it another way, performing a source localization on the different time points, a transition of the activation from left FCD to right FCD was observed. The figure below portrays this transition which could be translated as a functional connectivity between these areas. From a medical point of view it is a critical conclusion which correlates the epileptic areas and signals that the neurons activation of the left FCD fire the nearby neurons creating a pathway for the right FCD. Above all, this outcome could clarify the surgical plan for this patient along with decoding the coupling of symptomatology with functional abnormalities.

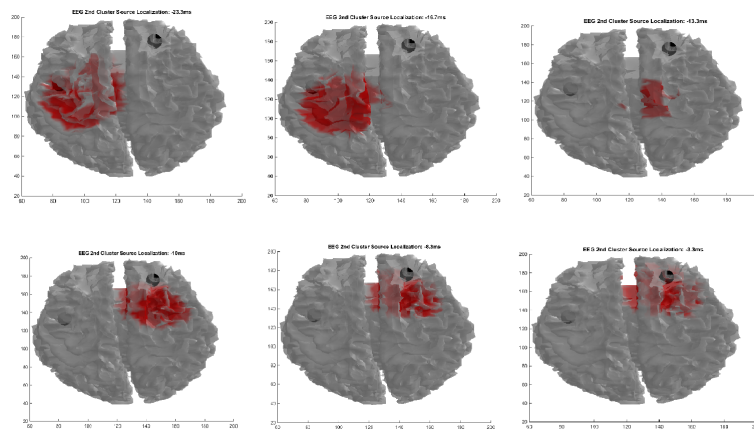


Figure 6.19: sLORETA on EEG cluster 2 - Propagation Phenomenon

Finally yet importantly, on MEG clusters the method performed rather well since it detected activity in the vicinity of the right FCD at -10ms on 2nd MEG cluster within a small area. On the other hand there are also localization errors such as in 1st cluster at -10ms that might indicate low SNR of the corresponding signal. It is worth noting that MEG cluster localization misses the activity of the left fronto-central area despite the fact that achieves high accuracy on the other one. Taking into account that EEG detects both sources we could consider a motivation for combining the two modalities to implement a multi-modality source localization.

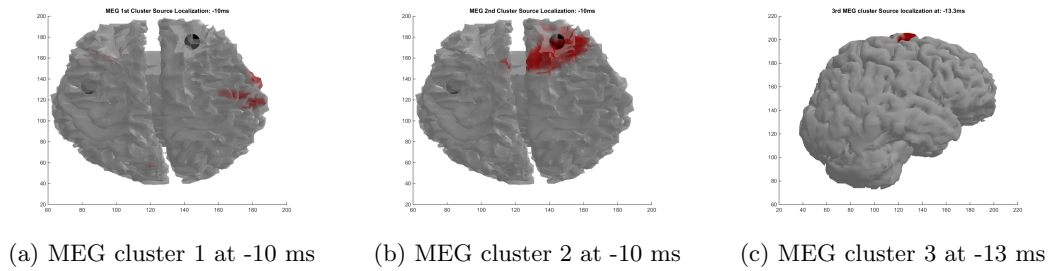


Figure 6.20: sLORETA on MEG Clusters

eLORETA:

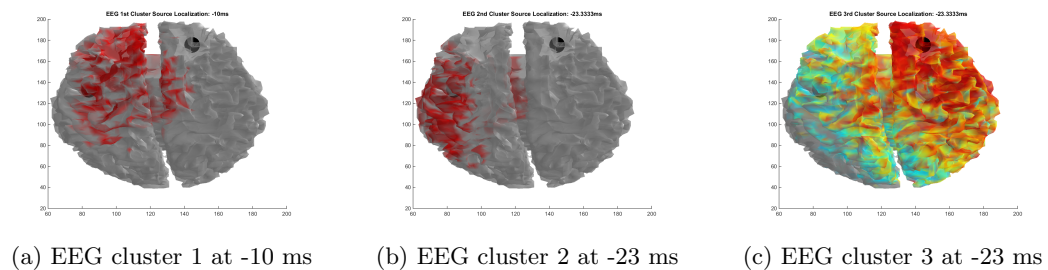


Figure 6.21: eLORETA on EEG Clusters

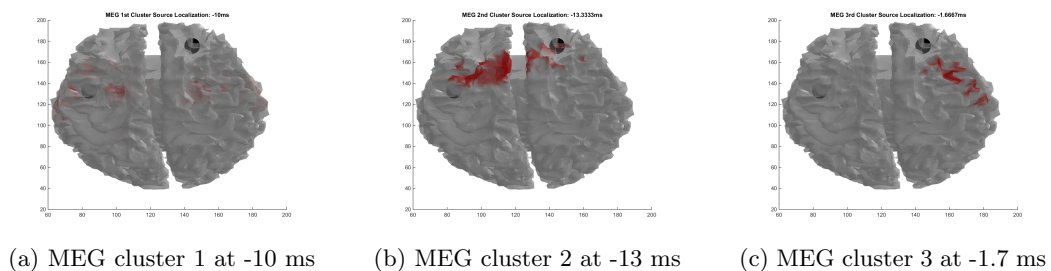


Figure 6.22: eLORETA on MEG Clusters

The process repeated again for eLORETA which is a similar method to sLORETA and MNE and it theoretically operates with less errors. However in this specific use case for both EEG & MEG the localization accuracy deteriorates compared to the sLORETA. Specifically in EEG it achieves a localization in the neighborhood of the FCDs (right FCD 3rd cluster, left FCD 1st cluster) but it spreads the area inducing significant noise and errors misplacing in this way the onset zone. With respect to the MEG the range of localization/activation decreases but the detection accuracy is also poor while at the same time it barely separates the activations of the two FCDs. Above all, sLORETA is still superior.

Beamforming:

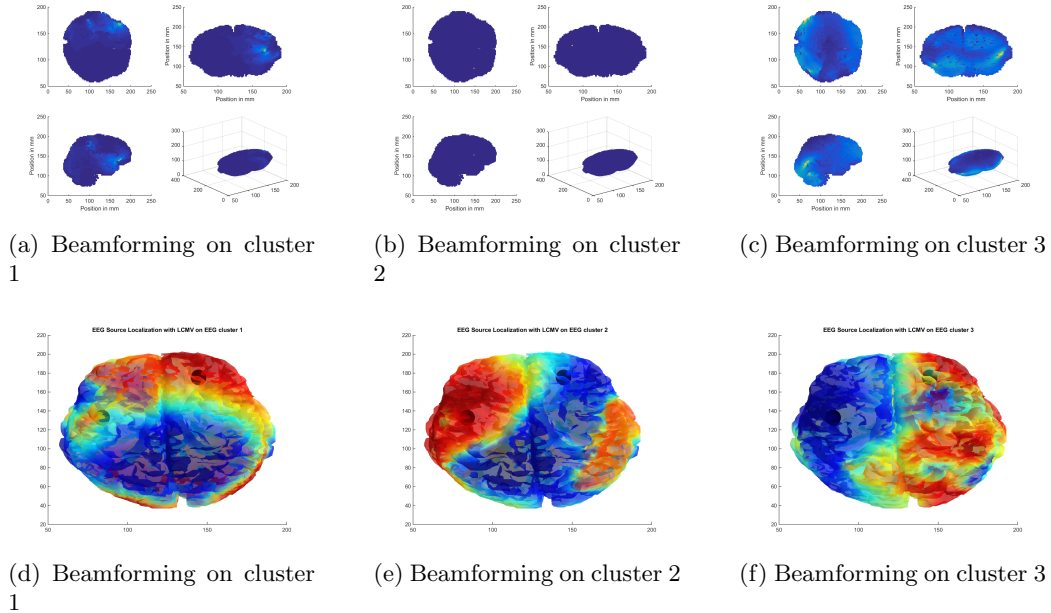


Figure 6.23: Beamforming on EEG clusters top row: source space visualization, bottom row: visualization on white matter mesh

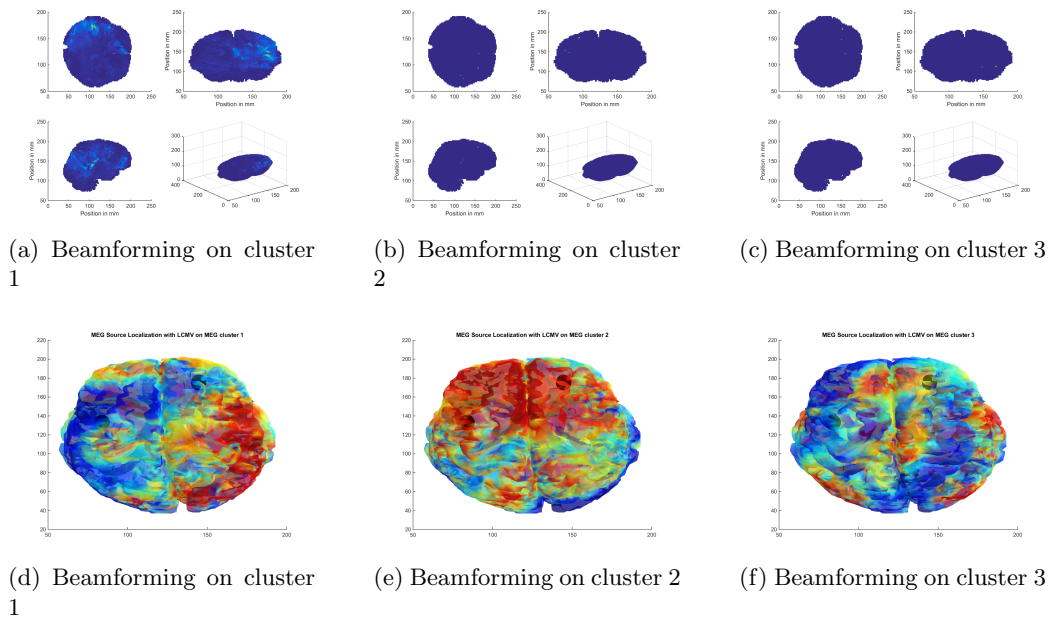


Figure 6.24: Beamforming on MEG clusters top row: source space visualization, bottom row: visualization on white matter mesh

The last approach applied in the clustering source localization was the beamforming.

In this method the covariance matrix used is the same with the previous algorithms (same covariance window) but in a regularized form. We used maximum variance beamformers with unit array gain. For the noise this method is a normalized variant of LCMV beamformer. Overall, the output of this localization complements the previous results since in the EEG clusters detects the two FCDs but the suppression of the rest of the activity is not optimal. The latter results in distortion by noise. Specifically in both 1st and 2nd clusters the activations are in vicinity of the two FCDs but there is noise introduced in the right temporal lobe and in occipital lobe while the 3rd cluster produces high localization errors. In the case of MEG beamforming the results are not satisfactory and the outputs visualized on the white matter mesh have poor goodness of fit.

Overall, the source localization for spike clusters applied with five different methods on specific time instances in order to detect the epileptogenic area(s). The patient's data evaluated led to detection of two abnormal areas of which the left one corresponds precisely to the seizure semiology (right limbs convulsions). Of all methods we could claim with certainty that dipole scanning is not the appropriate for this use case because it approximates the underlying activation with a single dipole idealizing in this way the brain mechanisms. Regarding the rest methods sLORETA functioned exceptionally in terms of goodness of fit since it achieved the localization of both FCDs in different clusters but also revealed propagation pathways bringing light to new scientific research for this subject. It is worth mentioned that sLORETA produces the output with the least errors and could guide the epileptologists for the surgical plan while its accuracy seems to achieve a maximum ceiling in MEG localization restricting the area significantly. The latter is important for the presurgical evaluation and at the same time consists motivation for the next step of this thesis which is to combine the two modalities in order to obtain more accurate results. The complementary information of EEG & MEG might offer us more accurate localizations and reveal hidden pathways of activations [20]. MNE and eLORETA detect activations within wide areas and therefore they are not suggested in this study while beamforming leads to erroneous localizations in MEG clusters. As a consequence we decided to continue with combined EEG/MEG localization using the sLORETA in all possible combination of the clusters.

6.6 Source Localization and Combined EEG/MEG

In contrast to the previous methods/techniques adapted to either the EEG or MEG clusters the source localization extends to the implementation of a multi-modality combination which yields accurate localization. [18], [20], [93]. For the epileptic studies modern studies incorporate the simultaneous recording of EEG & MEG, which is also the case for our subject, in order to exploit to the fullest the complementarity of these modalities. Despite the fact that both of them operate exceptionally temporally, when it comes to the spatial accuracy they both have drawbacks. Specifically, the EEG is sensitive to the quasi-radial, quasi-tangential sources while MEG only to the tangential sources fact which underlines the spatial resolution deficiency. On the other hand the conductivity properties of the head have stronger impact to the EEG. Moreover, the signal topologies are almost orthogonal between the two modalities as shown in the Figure: 6.25 (between (a)&(b) and (c)&(d)). Additionally, the simultaneous reconstruction could help in the robustness of the detection and to the stabilization of the results. Finally yet importantly, both modalities are affected by anisotropic properties thereby urging the use of a realistic head model

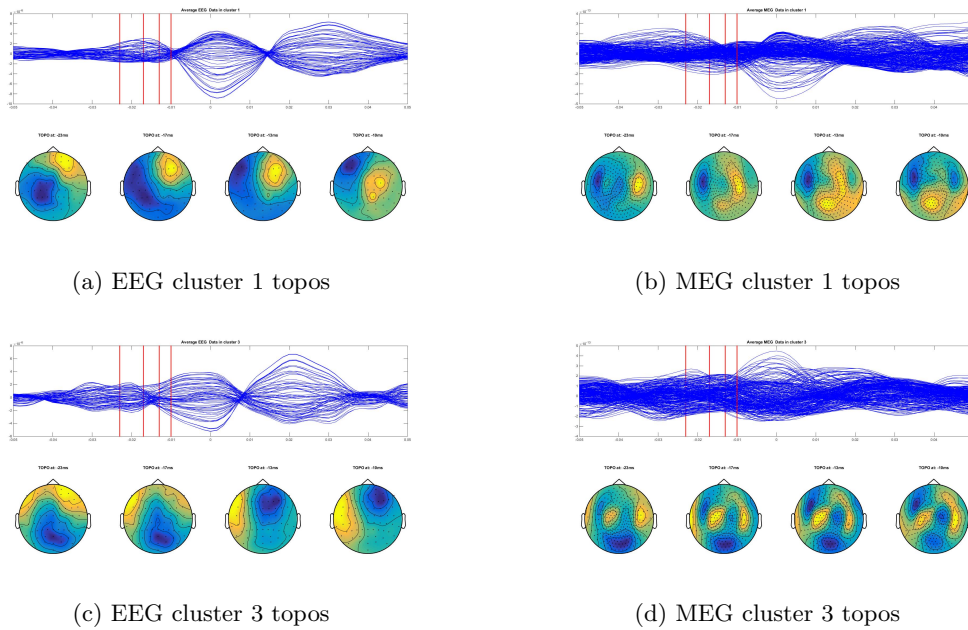


Figure 6.25: Signal topographies orthogonality for EEG & MEG clusters

Having said that, we performed a combined EEG/MEG source reconstruction (EMEG) using sLORETA with regularization parameter $\lambda = 25$. The headmodel used is the same utilized for the single modality reconstructions, namely a 6 compartment FEM headmodel with anisotropic white matter and skull compacta. The source space has 40468×3 dimensions while the leadfield used for the reconstruction is a concatenated form of the EEG leadfield (for 72 channels) and MEG leadfield (for 275 channels). The algorithm applied to all possible combinations of EEG and MEG clusters (3 EEG clusters, 3 MEG clusters \rightarrow 9 combinations) for time instances close to the spike onset (the same as the single modality reconstructions, 8 points).

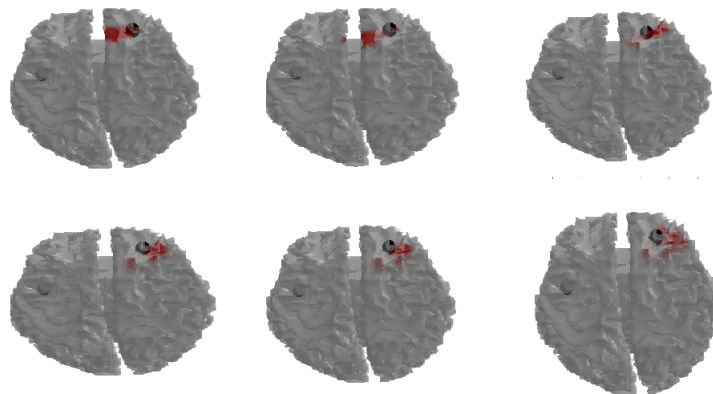


Figure 6.26: sLORETA EMEG Source Reconstruction for 2nd EEG and 2nd MEG cluster for 6 different time instances

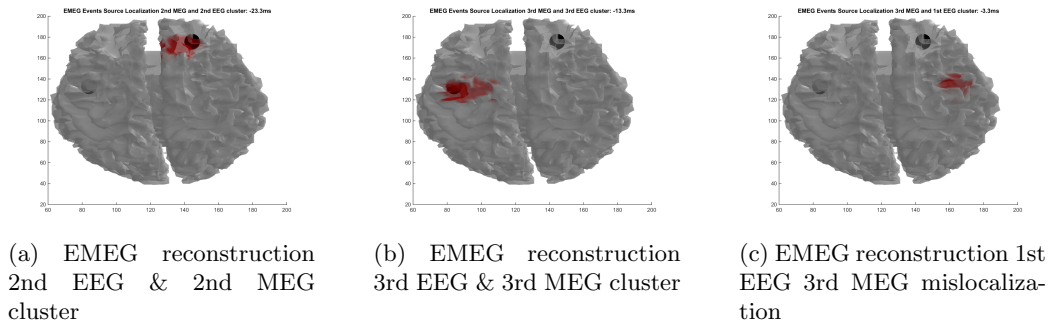


Figure 6.27: EMEG reconstruction leads to FCDs detection

The previous figures reveals three main aspects of the Combined EEG/MEG reconstruction. First and foremost from the Figure: 6.26 the specific combination produces a robust and stabilized reconstruction which matches accurately the right FCD in all the time instances visualized. Coupled with this the activation area is narrower compared to the previous sLORETA localizations in single clusters. In this way the epileptogenic area is detected with higher certainty. Another significant aspect of EMEG is shown in the Figure: 6.27 which is confirming our initial motivation for attempting this method. In other words both 6.27 (a) & 6.27 (b) reconstructions led to detection of the two FCDs in the closest vicinity of the two black spheres with regards to the other previous algorithms. Henceforth, these results are more than encouraging from a medical point of view since the neurophysiologists and epileptologists could plan their next steps taking into account the outcome of such methodology. Particularly, the activations of these small areas are an insight of abnormal epileptic behaviour which could lead in resection of some tissues helping the patient to be soothed by multiple seizures. However, the doctors need to evaluate further the results and to confirm our findings with further examinations since we produced also localization errors from some combination of the clusters as shown in 6.27 (c). Despite though these inaccuracies the majority of the combinations led to detection of at least one FCD. Consequentially, the combined EMEG reconstruction outperforms the single modality reconstruction and we could easily claim that the complementarity of the information from these two modalities is the one which offers robust, stabilized, accurate and encouraging results.

Summarizing this chapter has described the methods used in the investigation of underlying sources detection and it has shown that this field of research assists the Medical society by mitigating the effect of limited knowledge of brain mechanisms during a neurological disorder. As a consequence source reconstruction is significantly important for alleviating the treatment of an epileptic patient since it establishes conclusions which benefit the non-invasive diagnosis, treatment and post-treatment stages. From a technical point of view sLORETA was the optimal inverse method for our multifocal case in terms of Goodness of Fit (GOF) while the combined EMEG is increasing the accuracy which has important clinical implications and it is to be considered especially when there are available simultaneous EEG and MEG recordings.

Conclusions

7.1 Conclusions

Nowadays epileptic phenomena are more and more manifested many of which demonstrate pharmaco-resistant properties making the life of a patient devastating. The main purpose of this thesis was to contribute in the presurgical epileptic diagnosis in a non-invasive way utilizing EEG & MEG analysis in order to soothe patients and to improve early diagnosis and treatment. After the data preprocessing step which embodies complicated Decomposition Techniques, an Adaptive and Sophisticated combination of clustering techniques was implemented according to epileptic spikes similarities. The latter led to a robust method because it stabilizes the classification by eliminating the K-means random initializations. In this way we achieved accurate source reconstructions with complementary information both between clusters of data but also between modalities. According to the spike sorting techniques we were able to detect precisely the epileptogenic areas that assists doctors for the surgical plan. Last but not least through the Inverse Methods Comparison we evaluated their efficiency which could be valuable for future research studies.

7.2 Future Work

As for the future work we could evaluate more Inverse methods than the proposed ones especially those that take into account the Frequency Domain of the signals or to incorporate Deep Learning Approaches for the solution of Forward & Inverse Problem. Another important future step could be the Connectivity Analysis of the detected sources in order to find the propagation pathways of the sources which in term could lead to further understanding of the brain mechanisms and of the neurological disorder. The motivation for this step stems from the outcome produced by sLORETA which revealed a template of propagation pathway between the two FCDs. In the source reconstruction step another brainstorm is to apply the methods on each spike to obtain an entire view of the underlying sources and to focus to those which contribute the most for the recording of the corresponding spike. Moreover, the clustering efficiency and veracity could be upgraded by expansion of the Feature Vector and with the use of supervised learning techniques such as Deep Neural Networks. Last but not least, the data preprocessing pipeline would be simplified and improved if some of the detection and corrections steps are replaced by Machine Learning approaches.

Bibliography

- [1] Ivan Soltesz and Kevin Staley. *Computational Neuroscience in Epilepsy*. Academic Press, 2008.
- [2] David C. Steratt, Bruce P. Graham, Andrew J. Gillies, and David J. Willshaw. *Principles Of Computational Modelling in Neuroscience*. Cambridge University Press, 2011.
- [3] Eric R. Kandel, James H. Schwartz, Thomas M. Jessell, Steven A. Siegelbaum, and A.J. Hudspeth. *Principles of Neural Science*. MCGRAW-HILL Higher Education, 2012.
- [4] Mahmood Q, Shirvany Y, Mehnert A, Chodorowski A, Gellermann J, Edelvik F, Hedstrom A, and Persson M. On the fully automatic construction of a realistic head model for eeg source localization. 2013.
- [5] Federica Vatta, Fabio Meneghini, Fabrizio Esposito, Stefano Mininel, and Francesco Di Salle. Realistic and spherical head modeling for eeg forward problem solution: a comparative cortex-based analysis. *Computational intelligence and neuroscience*, 2010.
- [6] Johannes Vorwerk, Jae-Hyun Cho, Stefan Rampp, Hajo Hamer, Thomas R. Knsche, and Carsten H. Wolters. A guideline for head volume conductor modeling in eeg and meg. *NeuroImage*, 2014.
- [7] Fabrice Wendling. Computational models of epileptic activity: a bridge between observation and pathophysiological interpretation. *Expert Review of Neurotherapeutics*, 2008.
- [8] Roxana A. Stefanescu, R.G. Shivakeshavan, and Sachin S. Talathi. Computational models of epilepsy. *Seizure*, 2012.
- [9] William W. Lytton. Computer modelling of epilepsy. *Nature Reviews Neuroscience*, 2008.
- [10] Bassett D. S and Gazzaniga M. S. Understanding complexity in the human brain. trends in cognitive sciences. *Trends in Cognitive Science*, 2011.
- [11] Abbott LF and Regehr WG. Synaptic computation. *Nature*, 2004.
- [12] Nobukazu Nakasato, Michael F. Levesque, Daniel S. Barth, Christoph Baumgartner, Robert L. Rogers, and William S. Sutherling. Comparisons of meg, eeg, and ecog source localization in neocortical partial epilepsy in humans. 1994.

- [13] Fujiwara H, Greiner HM, Hemasilpin N, Lee KH, Holland-Bouley K, Arthur T, Morita D, Jain SV, Mangano FT, Degrauw T, and Rose DF. Ictal meg onset source localization compared to intracranial eeg and outcome: improved epilepsy presurgical evaluation in pediatrics. 2012.
- [14] Dinh C., Strohmeier D., M. Luessi, Gllmar D., Baumgarten D., Haueisen J., and Hmlinen M. S. Real-time meg source localization using regional clustering. 2015.
- [15] Seeck M, Lazeyras F, Michel CM, Blanke O, Gericke CA, Ives J, Delavelle J, Golay X, Haenggeli CA, de Tribolet N, and Landis T. Non-invasive epileptic focus localization using eeg-triggered functional mri and electromagnetic tomography. 1998.
- [16] Roberta Grech, Tracey Cassar, Joseph Muscat, Kenneth P Camilleri, Simon G Fabri, Michalis Zervakis, Petros Xanthopoulos, Vangelis Sakkalis, and Bart Vanrumste. Review on solving the inverse problem in eeg source analysis. 2008.
- [17] Van 't Ent D1, Manshanden I, Ossenblok P, Velis DN, de Munck JC, Verbunt JP, and Lopes da Silva FH. Spike cluster analysis in neocortical localization related epilepsy yields clinically significant equivalent source localization results in magnetoencephalogram (meg). *Clinical Neurophysiology*, 2003.
- [18] Aydin, Ümit, Johannes Vorwerk, Matthias Dmpelmann, Philipp Kpper, Harald Kugel, Marcel Heers, Jrg Wellmer, Christoph Kellinghaus, Jens Haueisen, Stefan Rampp, Hermann Stefan, and Carsten H. Wolters. Combined eeg/meg can outperform single modality eeg or meg source reconstruction in presurgical epilepsy diagnosis. *PLOS ONE*, 2015.
- [19] Marios Antonakakis, Sophie Schrader, Jens Haueisen, and Carsten Wolters. Combined eeg/meg source reconstruction of electric, haptic-tactile and pneumato-tactile somatosensory stimulation using realistic head volume conductor modeling. 08 2017.
- [20] Aydin Ü, Rampp, Wollbrink, Kugel, Cho J, Grova C Knösche TR6, Wellmer J, and Wolters CH. Zoomed mri guided by combined eeg/meg source analysis: A multimodal approach for optimizing presurgical epilepsy work-up and its application in a multi-focal epilepsy patient case study. *Brain Topography*, 2017.
- [21] Wolters CH, Kuhn M, Anwander A, and Reitzinger S. A parallel algebraic multigrid solver for finite element method based source localization in the human brain. 2002.
- [22] Wolters CH, Anwander A, Tricoche X, Weinstein D, Koch MA, and MacLeod RS. Influence of tissue conductivity anisotropy on eeg/meg field and return current computation in a realistic head model: a simulation and visualization study using high-resolution finite element modeling. 2006.
- [23] Zeynep Akalin Acar and Scott Makeig. Effects of forward model errors on eeg source localization. 2002.
- [24] Laurie Kelly Mc Corry. *Essentials of Human Physiology for Pharmacy*. CRC Press, 2011.
- [25] Herschel Raff and Michael Levitzky. *Medical Physiology - A systems approach*. Mc Graw Hill, 2011.

- [26] Rodney A Rhoades and David R. Bell. *Medical Physiology: Principles for Clinical Medicine*. Wolters Kluwer, 2013.
- [27] Jonathan D. Kibble and Colby R. Halsey. *Medical Physiology*. Mc Graw Hill, 2009.
- [28] James Bowman, Edward Dudek, and Mark Spitz. *Epilepsy*. 2001.
- [29] Jerome Engel and Timothy A. Pedley. *Epilepsy: A Comprehensive Textbook*. Solution, 2008.
- [30] Bromfield EB, Cavazos JE, and Sirven JI. *An introduction to Epilepsy*. West Hartford, 2006.
- [31] I. Sherwin. Interictal-ictal transition in the feline penicillin epileptogenic focus. *Electroencephalography and Clinical Neurophysiology*, 1978.
- [32] Liu G., Slater. N, and Perkins A. Epilepsy treatment options. *Am Fam Physician*, 2017.
- [33] *Wiley Encyclopedia of Biomedical Engineering*, chapter Electroencephalography. 2006.
- [34] Vittorio Pizzella, Laura Marzetti, Stefania Della Penna, Francesco de Pasquale, Filippo Zappasodi, and Gian Luca Romani. Magnetoencephalography in the study of brain dynamics. *Functional Neurology*, 2017.
- [35] Saeid Sanei and J.A Chambers. *EEG Signal Processing*. Wiley, 2007.
- [36] A.GuruvaReddy and Srilatha Narava. Artifact removal from eeg signals. *International Journal of Computer Applications*, 2013.
- [37] Mainak Jas, Denis A. Engemann, Yousra Bekhti, Federico Raimondo, and Alexandre Gramfort. Autoreject: Automated artifact rejection for meg and eeg data. 2017.
- [38] Matti Hämäläinen, Riitta Hari, Risto Ilmoniemi, Jukka Knuutila, and Olli V Lounarsma. *Magnetoencephalography-theory instrumentation and applications to noninvasive studies of the working human brain*. Reviews of Modern Physics, 1993.
- [39] A. Fujimoto, T Akiyama, and H Otsubo. *MEG in Epilepsy*, chapter 158. Springer, 2009.
- [40] Oostenveld Robert, FriesPascal, Maris Eric, and Schoffelen Jan-Mathijs. Fieldtrip: Open source software for advanced analysis of meg, eeg, and invasive electrophysiological data. *Computational Intelligence and Neuroscience*, 2010.
- [41] D. Gajic, Z. Djurovic, S. Di Gennaro, and Fredrik Gustafsson. Classification of eeg signals for detection of epileptic seizures based on wavelets and statistical pattern recognition. *Biomedical Engineering: Applications, Basis and Communications*, 2014.
- [42] Fiorenzo Artoni, Arnaud Delorme, and Scott Makeig. Applying dimension reduction to eeg data by principal component analysis reduces the quality of its subsequent independent component decomposition. *NeuroImage*, 2018.
- [43] Herve Abdi and Lynne J. Williams. Principal component analysis. 2010.

- [44] Marios Antonakakis, Giorgos Giannakakis, Manolis Tsiknakis, Micheloyannis Sifis, and Michalis Zervakis. Synchronization coupling investigation using ica cluster analysis in resting meg signals in reading difficulties. pages 1–5, 11 2013.
- [45] Athanasios Koutras and Evangelos Dermatas. Blind speech separation for solving the cocktail party problem in real room environments. 2002.
- [46] Aapo Hyvärinen, Jula Karhunen, and Erkki Oja. *Independent Component Analysis*. John Wiley & Sons Inc., 2001.
- [47] Simon Haykin and Zhe Chen. The cocktail party problem. *Neural Computation*, 2005.
- [48] Anthony J Bell and Terrence J Sejnow. An information maximisation approach to blind separation and blind deconvolution. *Neural Computation*, 1995.
- [49] Aapo Hyvärinen and Erkki Oja. A fast fixed-point algorithm for independent component analysis. *Neural Computation*, 1997.
- [50] Te-Won Lee, Mark Girolami, and Terrence J. Sejnowski. Independent component analysis using an extended infomax algorithm for mixed subgaussian and supergaussian sources. *Neural Computation*, 1999.
- [51] Pezoulas Vasileios. Dynamic analysis of brain activity from magnetoencephalographic data, 2015.
- [52] M.Girolami. Symmetric adaptive maximum likelihood estimation for noise cancellation and signal separation. *Electronics Letters*, 1997.
- [53] Antonino Greco, Nadia Mammone, Francesco Carlo Morabito, and Mario Versaci. Kurtosis, rnyis entropy and independent component scalp maps for the automatic artifact rejection from eeg data. *Electronics Letters*, 2008.
- [54] Jose Antonio Urigüen and Begoña Garcia-Zapirain. Eeg artifact removal state-of-the-art and guidelines. 2015.
- [55] A. Delorme, S. Makeig, and T. Sejnowski. Automatic artifact rejection for eeg data using high-order statistics and independent component analysis. *Proceedings of the 3rd International Workshop on ICA*, 2001.
- [56] Leor Shoker, Saeid Sanen, and Jonathon Chambers. Artifact removal from electroencephalograms using a hybrid bss-svm algorithm. *IEEE Signal Processing Letters*, 2005.
- [57] Giulia Barbati, Camillo Porcaro, Filippo Zappasodib, Paolo Maria Rossini, and Franca Tecchio. Optimization of an independent component analysis approach for artifact identification and removal in magnetoencephalographic signal. *Electronics Letters*, 2008.
- [58] Nord en E. Huang. The empirical mode decomposition and the hilbert spectrum for nonlinear and non-stationary time series analysis. Technical report, NASA, 1998.
- [59] Job P. Lindsen and Joydeep Bhattacharya. Correction of blink artifacts using independent component analysis and empirical mode decomposition. *Psychophysiology*, 2010.

- [60] R. Quian Quiroga, Z. Nadasdy, and Y. Ben-Shau. Unsupervised spike detection and sorting with wavelets and superparamagnetic clustering. *Neural Computation*, 2004.
- [61] Le Thanh Xuyen, Le Trung Thanh, Dinh Van Viet, Tran Quoc Long, Nguyen Linh Trung, and Nguyen Duc Thuan. Deep learning for epileptic spike detection. *VNU Journal of Science*, 2017.
- [62] Hernan Gonzalo Rey, Carlos Pedreira, and Rodrigo Quian Quiroga. Past, present and future of spike sorting techniques. *Brain Research Bulletin*, 2015.
- [63] Michael Lewicki. A review of methods for spike sorting: the detection and classification of neural action potentials. *Computational Neural Systems*, 1998.
- [64] Carmen Roco Caro-Martn, Agns Gruart Jos M. Delgado-Garca, and R. Snchez-Campusano. Spike sorting based on shape, phase, and distribution features, and k-tops clustering with validity and error indices. *Nature*, 2018.
- [65] Pu-Ming Zhang Jin-Yong Wu, Yi Zhou, Pei-Ji Liang, and Jingqi Yuan. Spike sorting based on automatic template reconstruction with a partial solution to the overlapping problem. *Journal of Neuroscience Methods*, 2004.
- [66] E. Hulata, R. Segev, and E. Ben-Jacob. A method for spike sorting and detection based on wavelet packets and shannon’s mutual information. *Journal of Neuroscience Methods*, 2002.
- [67] Robert Bestel, Andreas W.Daus, and Christiane Thielemann. A novel automated spike sorting algorithm with adaptable feature extraction. *Journal of Neuroscience Methods*, 2012.
- [68] R. Quian Quiroga. Spike sorting. *Scholarpedia*, 2007.
- [69] Hernan Gonzalo Rey, Carlos Pedreira, and R. Quian Quiroga. Past, present and future of spike sorting techniques. *Brain Research Bulletin*, 2015.
- [70] Teuvo Kohonen. Self-organized formation of topologically correct feature maps. *Biological Cybernetics*, 1982.
- [71] Teuvo Kohonen. Essentials of the self-organizing map. *Neural Network*, 2013.
- [72] Ignacio Rojas, Gonzalo Joya, and Andreu Catala. *Advances in Computational Intelligence*. Springer, 2015.
- [73] J.Mac QUEEN. *Some Methods For Classification and Analysis of Multivariate Observations*. Fifth Berkeley Symposium, 1967.
- [74] Fei Wang, Hector-Hugo Franco-Penya, John D. Kelleher, John Pugh, and Robert Ross. An analysis of the application of simplified silhouette to the evaluation of k-means clustering validity. 2017.
- [75] Khadir M. Tarek, Khdairia Sofiane, and Benabbas Farouk. Kohonen maps combined to k-means in a two level strategy for time series clustering application to meteorological and electricity load data. 2009.

- [76] D. Van t Ent, I. Manshanden, P. Ossenblok, D.N. Velis, J.C. de Munck, J.P.A. Verbunt, and F.H. Lopes da Silva. Spike cluster analysis in neocortical localization related epilepsy yields clinically significant equivalent source localization results in magnetoencephalogram (meg). 2003.
- [77] John C. Mosher, Richard M. Leahy, and Paul S. Lewis. Eeg and meg: Forward solutions for inverse methods. 1999.
- [78] Roberta Grech, Tracey Cassar, Joseph Muscat and Kenneth P Camilleri, Simon G Fabri, Michalis Zervakis, Petros Xanthopoulos, Vangelis Sakkalis, , and Bart Vanrumste. Review on solving the inverse problem in eeg source analysis. 2008.
- [79] Geoffray Adde, Maureen Clerc, Olivier Faugeras, Renaud Keriven, Jan Kybic, and Theodore Papadopoulo. Symmetric bem formulation for the m/eeg forward problem.
- [80] Sylvain Baillet. Forward and inverse problems of meg/eeg. 2014.
- [81] Michael Scherg. Fundamentals of dipole source potential analysis. 1990.
- [82] Sylvain VALLAGHÉ. *EEG and MEG forward modeling : computation and calibration*. PhD thesis, Graduate School of Information and Communication Sciences, University of Nice-Sophia Antipolis, 2008.
- [83] Hallez H, Vanrumste B, and et al Grech R. Review on solving the forward problem in eeg source analysis. 2007.
- [84] Lee C, Oostenveld R, Lee SH, Kim LH, Sung H, and Choi JH. Dipole source localization of mouse electroencephalogram using the fieldtrip toolbox. 2013.
- [85] Neugebauer F, Mddel G, Rampp S, Burger M, and Wolters CH. The effect of head model simplification on beamformer source localization. 2017.
- [86] Pasqual-Marqui. Review of methods for solving the eeg inverse problem. 1999.
- [87] Alejandro Lopez Rincon and Shingo Shimoda. The inverse problem in electroencephalography using the bidomain model of electrical activity. *Journal of Neuroscience Methods*, 274:94 – 105, 2016.
- [88] Pasqual-Marqui. Standardized low resolution brain electromagnetic tomography (sloreta):technical details. 2002.
- [89] Pasqual-Marqui. Discrete, 3d distributed linear imaging methods of electric neuronal activity. part 1: exact, zero error localization. 2007.
- [90] Munsif Ali Jatoi, Nidal Kamel, Aamir Saeed Malik, and Ibrahima Faye. Eeg based brain source localization comparison of sloreta and eloreta. 2014.
- [91] S. Wagner, M. Burger, and C. H. Wolters. An optimization approach for well-targeted transcranial direct current stimulation. 2016.
- [92] Vorwerk J, Oostenveld R., Piastra M.C, L Magyari, and Wolters C.H. The fieldtrip-simbio pipeline for eeg forward solutions. 2018.
- [93] Sharon D, Hamalainen Matti S, Tootell RB, Halgren E, and Belliveau JW. The advantage of combining meg and eeg: comparison to fmri in focally stimulated visual cortex. 2007.